AD-782 339

DEEP OCEAN OPTICAL MEASUREMENT (DOOM) REPORT ON NORTH ATLANTIC, CARIBBEAN, AND MEDITERRANEAN CRUISES

Donald E. Matlack

Naval Ordnance Laboratory
White Oak, Maryland

5 April 1974

UNCLASSIFIED

SECURITY CLASSIFICATION OF THIS PAGE (When Data Entered)

REPORT DOCUMENTATION PAGE		READ INSTRUCTIONS BEFORE COMPLETING FORM
1. REPORT NUMBER NOLTR 74-42	2. GOVT ACCESSION NO.	3. RECIPIENT'S CATALOG NUMBER AD-782 339
4. TITLE (and Subtitle) DEEP OCEAN OPTICAL MEASUREMENT (DOOM) REPORT ON NORTH ATLANTIC, CARIBBEAN, AND MEDITERRANEAN CRUISES		5. TYPE OF REPORT & PERIOD COVERED Final 6. PERFORMING ORG. REPORT NUMBER
7. AUTHOR(s) Donald E. Matlack		8. CONTRACT OR GRANT NUMBER(s)
9. PERFORMING ORGANIZATION NAME AND ADDRESS Naval Ordnance Laboratory White Oak, Silver Spring, Maryland 20910		10. PROGRAM ELEMENT, PROJECT, TASK AREA & WORK UNIT NUMBERS Task No. ORD 03C-001/ UF52-522-103
11. CONTROLLING OFFICE NAME AND ADDRESS Naval Ordnance Systems Command NORD-03C (J. Ropek) Washington, D. C. 20360		12. REPORT DATE 5 April 1974 13. NUMBER OF PAGES 128
14. MONITORING AGENCY NAME & ADDRESS(if different from Controlling Office)		15. SECURITY CLASS. (of this report) Unclassified 15a. DECLASSIFICATION/DOWNGRADING SCHEDULE

16. DISTRIBUTION STATEMENT (of this Report)

Approved for public release; distribution unlimited

17. DISTRIBUTION STATEMENT (of the abstract entered in Block 20, if different from Report)

18. SUPPLEMENTARY NOTES

19. KEY WORDS (Continue on reverse side if necessary and identify by block number)

Spectral attenuation measurement of ocean water
Light scattering measurements of ocean water
In-situ optical measurements
Deep ocean optical measurements

20. ABSTRACT (Continue on reverse side if necessary and identify by block number)

Optical attenuation data collected during four Deep Ocean Optical Measurement (DOOM) program cruises from September 1968 to April 1972 are presented. Locales of operation included tracks in the North Atlantic about 450 nautical miles off the middle Atlantic coast of the United States and along the trough north of the Greater Antilles between the Bahamas and Puerto Rico, in

DD FORM 1 JAN 73 1473 EDITION OF 1 NOV 65 IS OBSOLETE
S/N 0102-014-6601 |

UNCLASSIFIED

SECURITY CLASSIFICATION OF THIS PAGE (When Data Entered)

19. KEY WORDS (Cont.)

Underwater light transmission
Optical Oceanography

20. ABSTRACT (Cont.)

the Caribbean Sea from the Cayman trench south of Cuba through the Yucatan Strait into the Gulf of Mexico, and in the Mediterranean Sea from Greece to Gibraltar. Optical parameters, which are measured in-situ to all depths, are spectral attenuation coefficients at visible wavelengths in the transmission window and the volume scattering function also in the visible at 436 nanometers.

5 April 1974

NOLTR 74-42

DEEP OCEAN OPTICAL MEASUREMENT (DOOM) REPORT ON NORTH ATLANTIC, CARIBBEAN, AND MEDITERRANEAN CRUISES

The in-situ optical measurements of ocean water described in this report were made by the Radiation Physics Division of the Applied Physics Department. Data were obtained during oceanographic cruises aboard U.S. Naval Ships of the AGOR class which are under the operational control of the Research Ship Branch of the Naval Oceanographic Office. This work was performed for the Naval Ordnance Systems Command under Task Number ORD-03C-001/UF52-522-103.

ROBERT WILLIAMSON II
Captain, USN
Commander

W. W. Scanlon

W. W. SCANLON
By direction

CONTENTS

ILLUSTRATIONS

ILLUSTRATIONS (cont.)

ILLUSTRATIONS (cont.)

TABLES

I INTRODUCTION

This is the third in a series of reports on the Deep Ocean Optical Measurement (DOOM) program initiated at the Naval Ordnance Laboratory in 1967 for the purpose of investigating the optical parameters within the ocean which restrict the underwater transmission of light. Instrumentation was developed for the quantitative, in-situ measurement of two inherent optical properties of sea water; (1) the total attenuation coefficients $\alpha(\lambda)$ at near ultraviolet and visible wavelengths and (2) the volume scattering coefficient $s(\lambda)$ at a wavelength of 436 nanometers. Data are collected at sea during scheduled cruises aboard oceanographic vessels provided by the Oceanographer of the Navy for support of marine research programs at the various Navy laboratories. Equipment and operations are fully described in the initial DOOM report, NOLTR 70-165.[1]

The field program was conducted between December 1967 and June 1972 and consisted of nine measurement cruises to various areas of the North Atlantic Ocean and the Mediterranean and Carribbean Seas. Although instrumental problems and operational failures at sea have hampered the program, a large quantity of data has been collected from diverse geographical ocean areas under a variety of oceanographic and climatic conditions. This data represents an adequate statistical sampling of Atlantic waters and completes the present measurement phase of the program.

The nine separate cruises have been denoted in chronological sequence by successive letters of the alphabet, and thus are identified as Cruises A through I. Data collected during Cruises A and C were unreliable due to system error or malfunction and therefore cannot be reported. Results from Cruises D and E have been presented in detail in NOLTR 72-284.[2] Data from the remaining cruises have been included only as sample illustrations in a general survey paper.[3] This report will present in full the optical measurement data from Cruises B, F, and I. Also included as Appendix A are attenuation data from Cruise G which are presented in abbreviated form in order to expedite its release.

II CRUISE B NARRATIVE

Cruise B was scheduled to depart Norfolk, Virginia, on 13 October 1968 aboard the USNS Gilliss T-AGOR-4, steam on an eastwardly track for about 450 nautical miles, and then on 19 October turn north and proceed to an area east of Cape Cod. A total of 12 measurement drops were scheduled prior to returning to port on 27 October at Bayonne, New Jersey. A week prior to the scheduled departure, the port of embarkation was switched from Norfolk to Bayonne. Since clearances for sub-surface operations had already been granted for a cruise track from Norfolk and since securing confirmation for a revised track at this late date would be questionable it was decided to steam south from Bayonne and pick up the original track at a point east of Norfolk.

Departure from Bayonne was delayed until the afternoon of 15 October, first due to temporary loss of DOOM equipment in shipment and then on 14 October due to a main engine casualty which failed while attempting to leave port. Necessary repairs were completed in time for an afternoon departure on 15 October. Inclement weather and high seas prevented operations until the night of 20 October when measurements were commenced at a station about 450 nautical miles east of Cape Charles. Nightly drops were conducted through 25 October as the ship steamed north to a final station some 400 miles east of Atlantic City, New Jersey. The cruise track and station locations are shown in Figure 1. Pertinent data on the six drops are presented in Table I.

Initial DOOM sea trials during Cruise A in December 1967 had been beset by numerous equipment difficulties which had both limited and degraded the data. Even more discouraging was the subsequent discovery which was revealed during data analysis of instability and non-linearity in signal processing electronics. Thus meaningful reduction of Cruise A data was impossible. Fortunately over six months were available before Cruise B to remedy these problems and to modify equipment. However, a short term priority project preempted manpower so little effort could be devoted to correcting the DOOM deficiencies until late summer. Then the necessary minor repairs were made, but the major tasks of re-working the electronics and completing the scattering measurement section could not be completed in the scheduled time frame.

The non-linear electronics problem appeared in the data as an apparent "hysteresis effect" in which the signals recorded while retrieving the package would not retrace those recorded during lowering but rather would slowly increase and thus progressively deviate from the "down" signal with time. Although the general structure of the two signatures including the various peaks and valleys would repeat, the level was continuously biased as a function of time throughout the drop. In the processed attenuation profile of α, the "up" trace would diverge and fall below that of the "down" trace. We theorized that this non-linear effect was caused by thermal

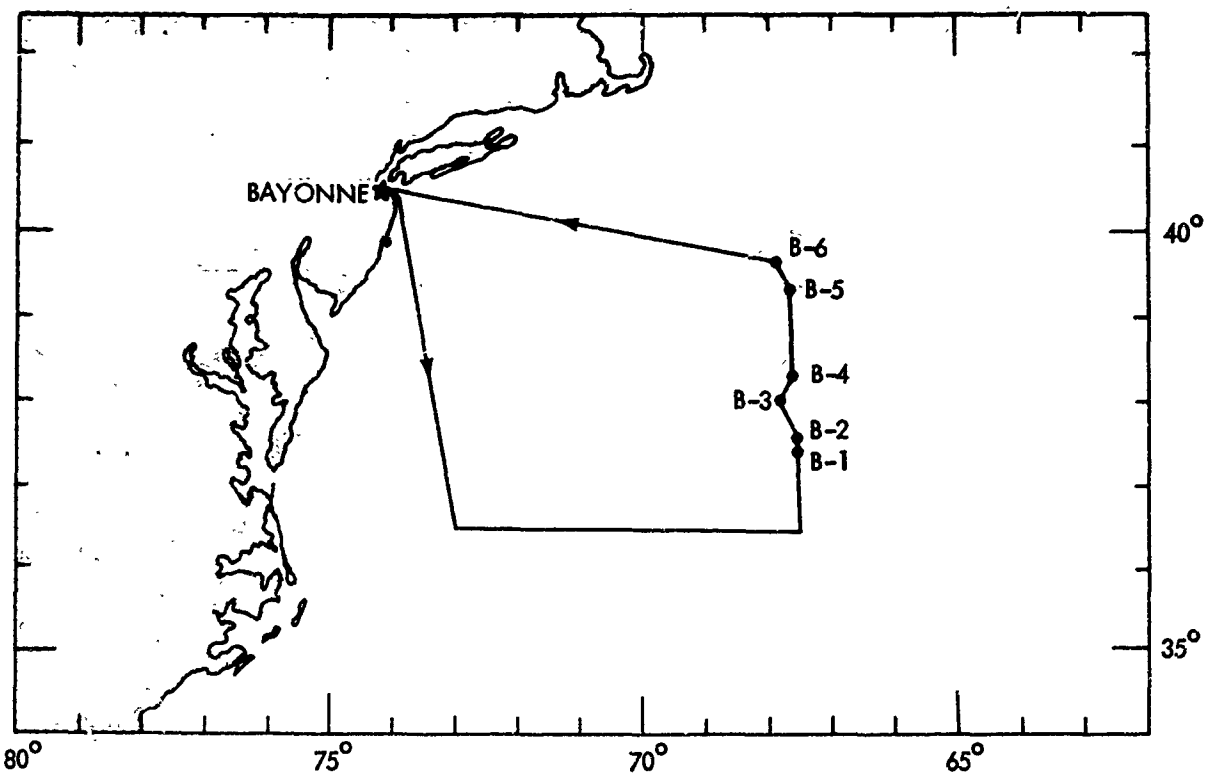

FIG. 1 TRACK CHART OF CRUISE B

TABLE I. PERTINENT DATA ON CRUISE B STATIONS

Drop #	Date	Time	Latitude North	Longitude West	Depth (m)	Measurement Depth (m)
B-1	10-20-68	1935	37° 25'	67° 30'	4650	300
B-2	10-21-68	1932	37° 30'	67° 30'	4740	1000
B-3	10-22-68	1914	38° 06'	67° 45'	4325	3003
B-4	10-23-68	2038	38° 14'	67° 37'	4353	565
B-5	10-24-68	1844	39° 21'	67° 37'	3410	200
B-6	10-25-68	1855	39° 37'	67° 57'	2880	2880

instability of the operational amplifiers which were exposed to temperatures ranging from about 25°C on deck to near freezing in the cold waters of the deep ocean. Error in recorded in-situ signals would vary as component temperature deviated from the temperature at the time of the on-deck calibration. During Cruise B, this hypothesis would be tested. Several drops were so programmed that the package would remain for the entire duration of the immersion in the relatively shallow waters where temperature remains moderate. Others would be lowered into the cold waters near the bottom and resulting performance of the two cases compared. Data from this cruise then would provide valid spectral attenuation profiles in the shallow and intermediate waters and also perhaps verify the nature of the electronics problem.

Stations B-1 and B-2 were located in the same proximity about 450 miles east of the Virginia shore and slightly southeast of the waters of the Gulf Stream. A shallow lowering to only 300 meters was planned for drop B-1 in order to determine whether the "hysteresis effect" would be induced by the small temperature variation within the surface waters. The five day ordeal in the rough seas preceding the drop apparently produced in both men and equipment a "mal de mer" because performance of the instruments and the resulting data were of extremely low quality. Equipment problems were really quite minor and were rather easily corrected for the next drop, but nevertheless drop B-1 data were so poor that rigorous analysis was not deemed feasible. However, enough information was available for us to conclude that no "thermal hysteresis" was present between signals recorded during lowering and retrieving. This established that the system response had remained stable for a three hour period in waters which varied from 24° to 17°C in temperature.

On 21 October sunny skies and moderating seas seemed to reverse the misfortune which had plagued the proceeding operations. Remedial instrument repair and adjustment were easily accomplished, drop B-2 operations went smoothly, and recorded data were of good quality. Since α signal levels from drop B-1 had remained stable, drop B-2 was lowered somewhat deeper to 1000 meters where water temperature decreased to around 6°C. System response again remained linear. However, for most of the 150 minute immersion, the package was within relatively warm water which at 600 meters had dropped to only about 15°. Estimated time that the package was exposed to temperatures below 15°C was about 20 minutes so a cool down of sufficient magnitude to produce significant distortion apparently did not occur.

Drops B-3 and B-4 of the next two successive nights were at stations about 50 miles further north and within the warmer water of the Gulf Stream. Since no distortion of signal response was evident in the first two drops, the package was lowered in drop B-3 into quite frigid waters below 1000 meters and held there for a significant interval of time. The package was subjected for over an hour to temperature between 5 and 2.5°C which was reached at depths of 900 and 3000 meters respectively. This time a sizeable signal hysteresis was present which confirmed that the problem was indeed a thermal effect.

At station B-4 the bathythermograph cast prior to the drop revealed an interesting thermal profile which included a significant thermal inversion at a depth of around 240 meters. Consequently the package was lowered and retrieved slowly in order to carefully record sudden variation in attenuation within the thermal layers of the water column. A maximum depth of 565 meters was reached. Water temperature dropped to 6°C and "up" α values fell below the "down" curves.

Drop B-5 on the evening of 24 October was located another 60 miles north, well outside the waters of the Gulf Stream. Test objectives of this drop were to obtain absolute reproducibility of the "up" and "down" attenuation profiles and to map in detail the attenuation layer which was presumed to exist at the primary thermocline. Objectives were successfully achieved in a lowering to 200 meters.

Drop B-6 was just slightly further north and this time it was decided to set the package on the bottom. Silt was kicked up from the bottom at a depth of 2880 meters and temporarily blotted out the optical signal. Needless to say, signal hysteresis was present.

III CRUISE B DATA PRESENTATION

Attenuation data will be presented in two forms: (1) as an attenuation profile where the spectral attenuation coefficient, $\alpha(\lambda)$, at a specific wavelength is presented as a function of depth and (2) as attenuation spectra where $\alpha(\lambda)$ is plotted as a function of wavelength at selected depths. Attenuation profiles of drops B-2 through B-6 are presented in Figures 2 through 7. The three wavelengths which are plotted in the profiles are 483 nm which is near the nominal center of the transmission window and 408 and 577 nm at the two extremes of the spectral measurement interval. Also included on the profiles is a plot of temperature. Attenuation spectra from drops B-2 through B-6 are presented in Table II. Shape of the spectral signature is illustrated in Figure 8 where spectra from drop B-5 are plotted.

When viewing data from Cruise B keep in mind that DOOM equipment was still undergoing sea trials and that signal processing electronics were far from optimum. There is obvious distortion to the attenuation profiles in the mid and latter stages of drops B-3, B-4, and B-6 due to the thermal instability of the electronics. Some additional problems associated with data recording that were experienced during the cruise are signal level drift and random noise. A drift correction, derived from the reference signal which is recorded internally within the optical housing each minute, was satisfactorily applied to correct signal amplitude. Intermittent noise was not a serious problem but perhaps did lead to some spread in data points. Although these equipment deficiencies do limit the quantitative and qualitative accuracy of the Cruise B data, it is

felt that these data should be published since surface measurements are generally valid and some interesting optical attenuation phenomena are illustrated. Distortions which are inherent in the data are included in the illustrations but will be explained in the discussion of individual drops.

There are reasons other than equipment malfunction which also may lead to seeming discrepancies and point spread within the data. Since the two parameters, depth and wavelength, against which the attenuation coefficient is plotted, are not scanning instantaneously, local inhomogenities and vertical structure within the water column may give rise to apparent inconsistency within the data. A spectrum is scanned each minute so the measurement interval at each of the 18 wavelengths is for one period of three seconds. During the lowering operation, motion of the package through an irregularly structured water column may produce sizeable changes in optical attenuation in a matter of seconds which is but a fraction of the scan interval. Since the various attenuation profiles are measured at different times within the spectral scan, their shapes may differ somewhat from one another in these layers of rapid turbidity change. Spectral signatures will be similarly distorted when attenuation changes take place within the spectral scan interval. However, an effort is made to select spectra when optical signatures remain nearly constant, that is, when the package is stationary in the water column or at depths where water properties are essentially uniform.

Attenuation profiles of drop B-2 are presented for the three wavelengths 408, 483, and 577 nm, in Figure 2. No electronic distortion occurred during the drop so profiles are accurate in both shape and amplitude. Attenuation is nearly constant in the isothermal surface waters of the first 50 meters, but then peaks rapidly in the steep gradient of the primary thermocline at around 75 meters. Peaks of the three curves do not necessarily fall at the same depth since the package was in motion and each wavelength was sampled at a slightly different time and hence a different depth. Below the thermocline, α decreases and stabilizes at a minimum value between depths of 200 and 600 meters. The value of α in the transmission window at 483 nm drops from a surface value of 0.11 m^{-1} to 0.06 m^{-1} in the minimum. Within the substantially weaker gradients of a secondary thermocline between 500 and 1000 meters, a broad peak develops which is much smaller than that associated with the initial thermocline. The shape of the B-2 profiles is characteristic of the waters in this ocean area and will recur in the data from succeeding drops.

Profiles of drop B-3 shown in Figure 3 include data during both lowering and retrieving which clearly illustrates by the continuous divergence of the "up" trace below that of the "down" trace the effect of the non-linear signal response. Profiles behave in a normal manner to a depth of around 1200 meters, i.e., there is the characteristic minimum below the primary thermocline, then the slight

peak associated with the secondary thermocline. The traces then should normally level off somewhere between 1200 and 2000 meters; but these traces continue to drop so distortion probably begins in this interval and persists throughout the remainder of the drop. A feature to note between the two profiles is the difference in relative amplitude of the attenuation spikes situated at the top of the thermocline. It is assumed that dense nepheloid layers produce selectively stronger scattering at the shorter wavelengths and hence a relatively larger variation in α.

Some signal non-linearity is present in the drop B-4 profiles of Figure 4 but it is confined mainly to the latter stages of the "up" measurements. Of extreme interest in this drop are the varied fluctuations of the attenuation profiles within the layered thermal structure of the Gulf Stream and the change in both thermal and optical profiles during the time interval of the cast. Attenuation maxima of the profiles correspond to negative thermal gradients; the wide peak just below 200 meters is, in addition, associated with the thermal inversion. The nature of the change in thermal structure during the two hour immersion was an upward shift of the negative gradients and the inversion to slightly shallower depths. The associated attenuation peaks similarly shifted to shallower water. A comparison of α in the surface layer, which changes from 0.11 m^{-1} at the beginning of the drop to 0.10 m^{-1} just prior to package recovery, perhaps indicates the degree of signal distortion during the drop. Profiles at three different wavelengths for the down direction only are shown in Figure 5. Of interest here are the very large amplitude variations of the 408 nm curve relative to the much smaller excursions of the longer wavelength curves at 482 and 577 nm. Large peaks are present in the 408 nm profile at depths of 80, 150, and 220 meters which again must be attributed to high selective scattering and absorption at the shorter wavelength interval within the concentrated nepheloid layers.

Station B-5 was located north of the Gulf Stream in less structured water where surface temperature of 23°C, down from the 27°C of the Stream, remained isothermal to about 50 meters and then decreased smoothly with depth as shown in Figure 6. The drop was programmed to remain in the warm surface waters above 200 meters and thus stay within the linear region of the system response. The profiles clearly illustrate the attenuation spike associated with the nepheloid layer which is present near the top of the primary thermocline. Surface water attenuation of 0.14 m^{-1} at 483 nm is somewhat higher than measured in the warmer waters to the south.

In drop B-6, again north of the Gulf Stream, the test objective was to look for major changes in attenuation in waters near the bottom at a depth of 2880 meters. Signal distortion in the deep cold water was anticipated and is evident from the profile of Figure 7. Typical features of the profile in the surface waters are the peak at the primary thermocline, a minimum between 200 and 500 meters, and the minor peak associated with the bottom of the secondary thermocline. Somewhere below 1000 meters the non-linear signal response

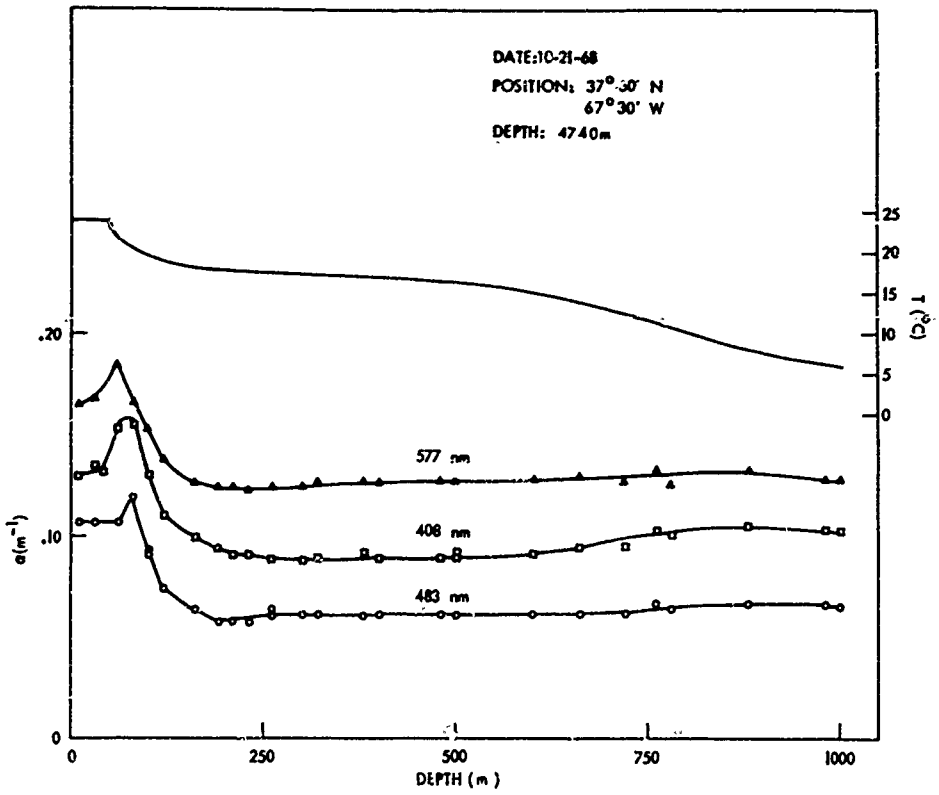

FIG. 2 OPTICAL ATTENUATION AND TEMPERATURE PROFILES FROM DROP B-2.

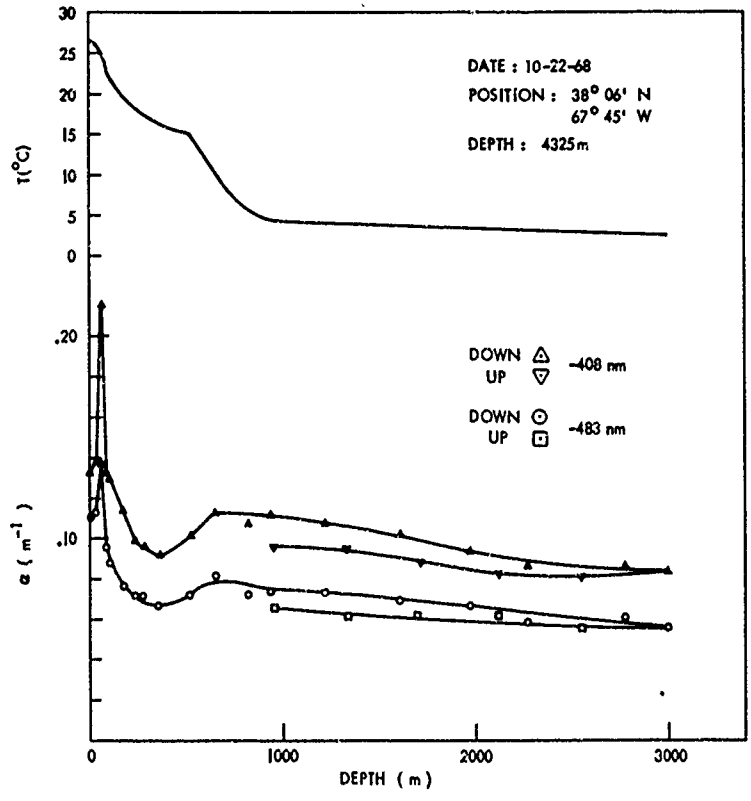

FIG. 3 OPTICAL ATTENUATION AND TEMPERATURE PROFILES OF DROP B-3.

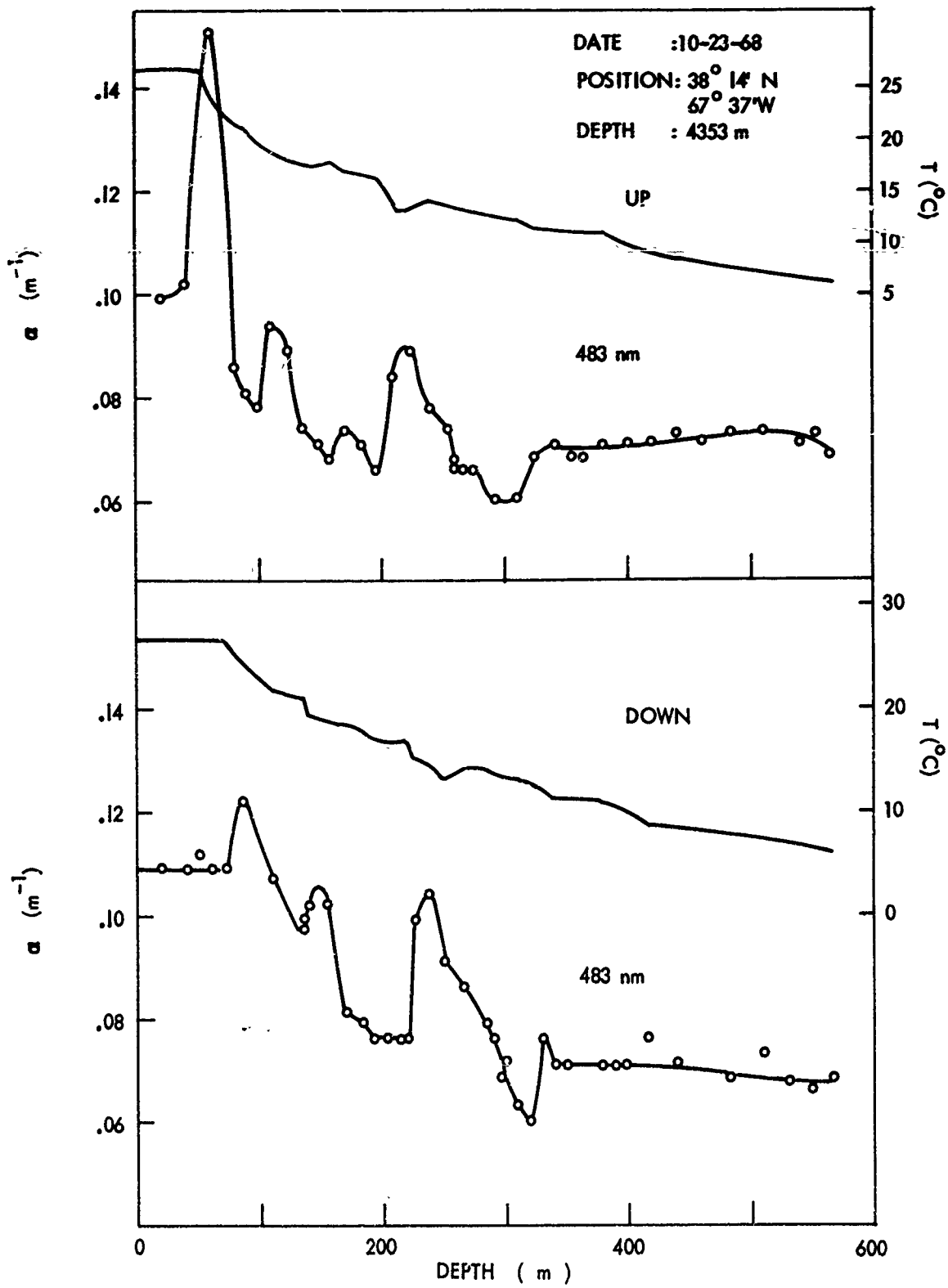

FIG. 4 OPTICAL ATTENUATION AND TEMPERATURE PROFILES DURING LOWERING AND RETRIEVING FROM DROP B-4.

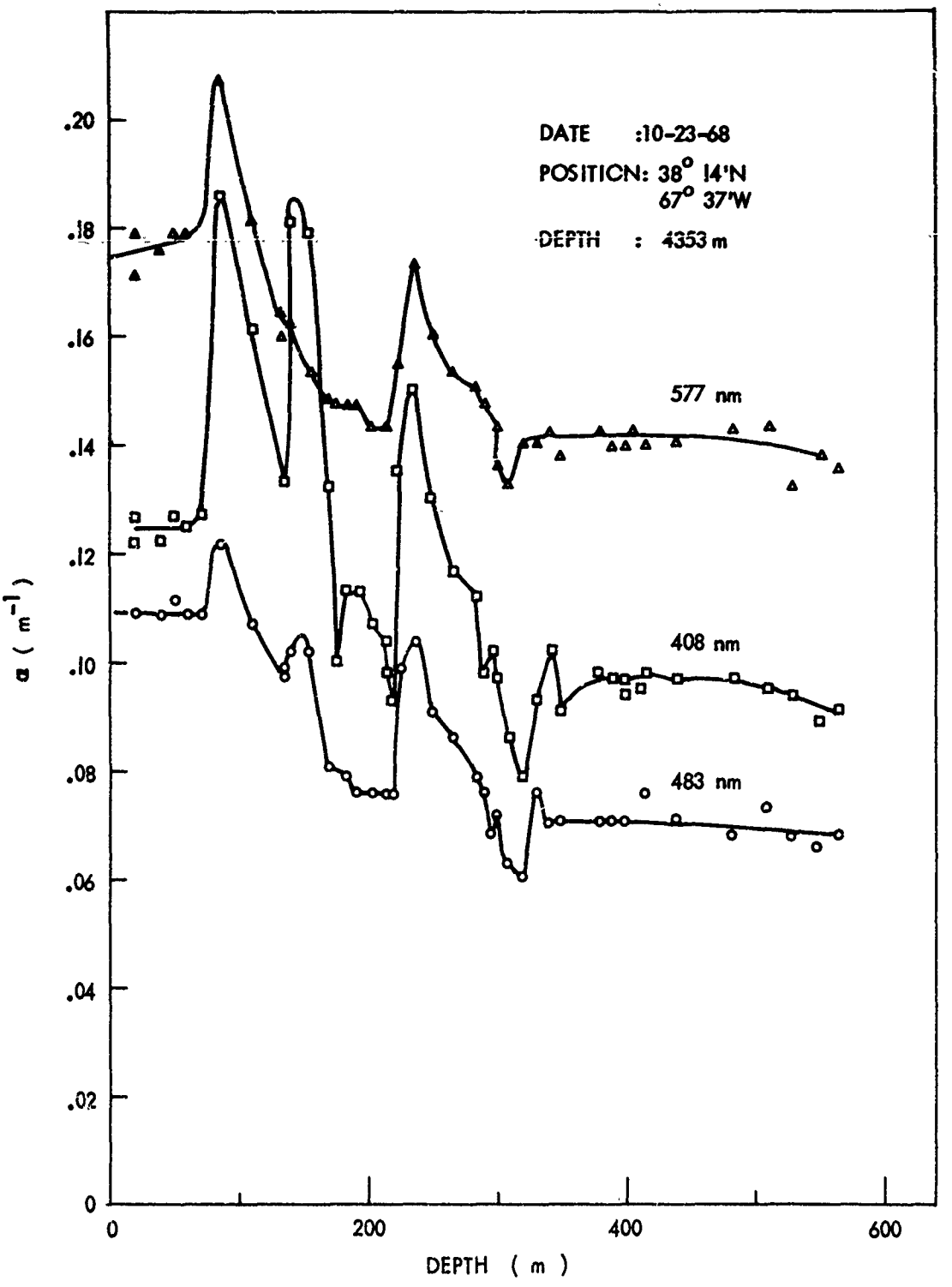

FIG. 5 SPECTRAL ATTENUATION PROFILES DURING LOWERING FROM DROP B-4.

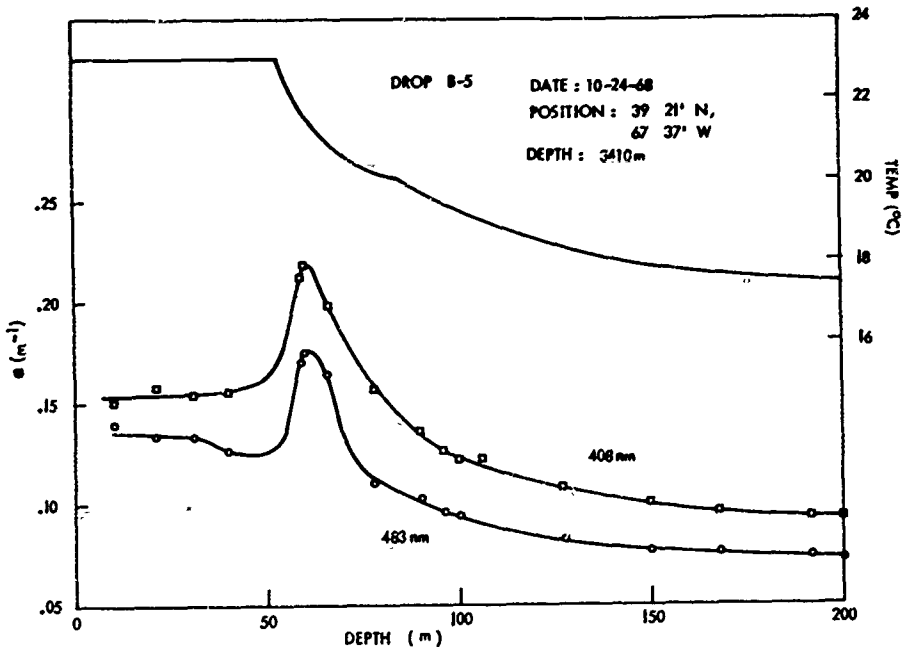

FIG. 6 OPTICAL ATTENUATION AND TEMPERATURE PROFILES FROM DROP B-5.

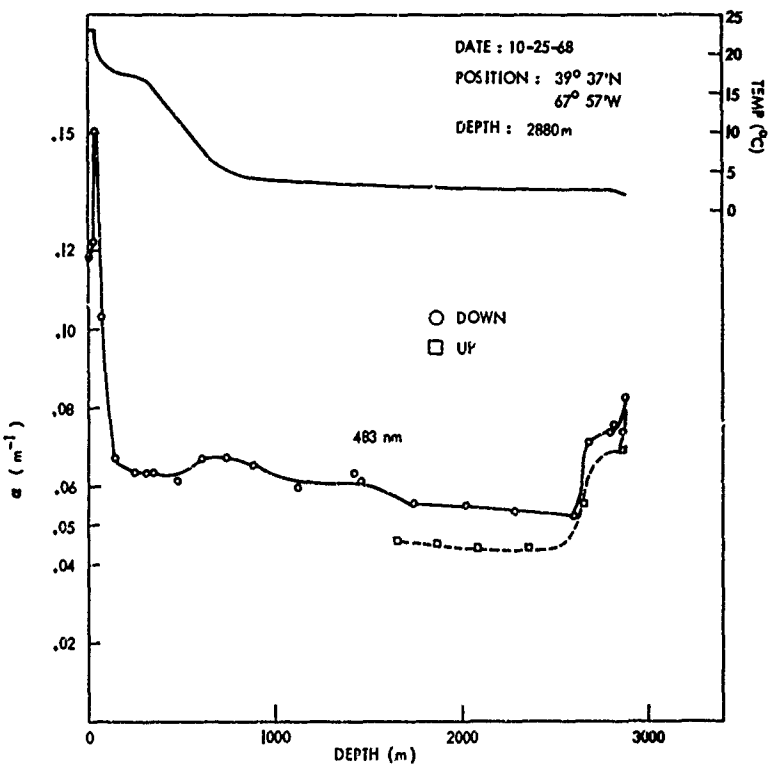

FIG. 7 OPTICAL ATTENUATION AND TEMPERATURE PROFILES FROM DROP B-6.

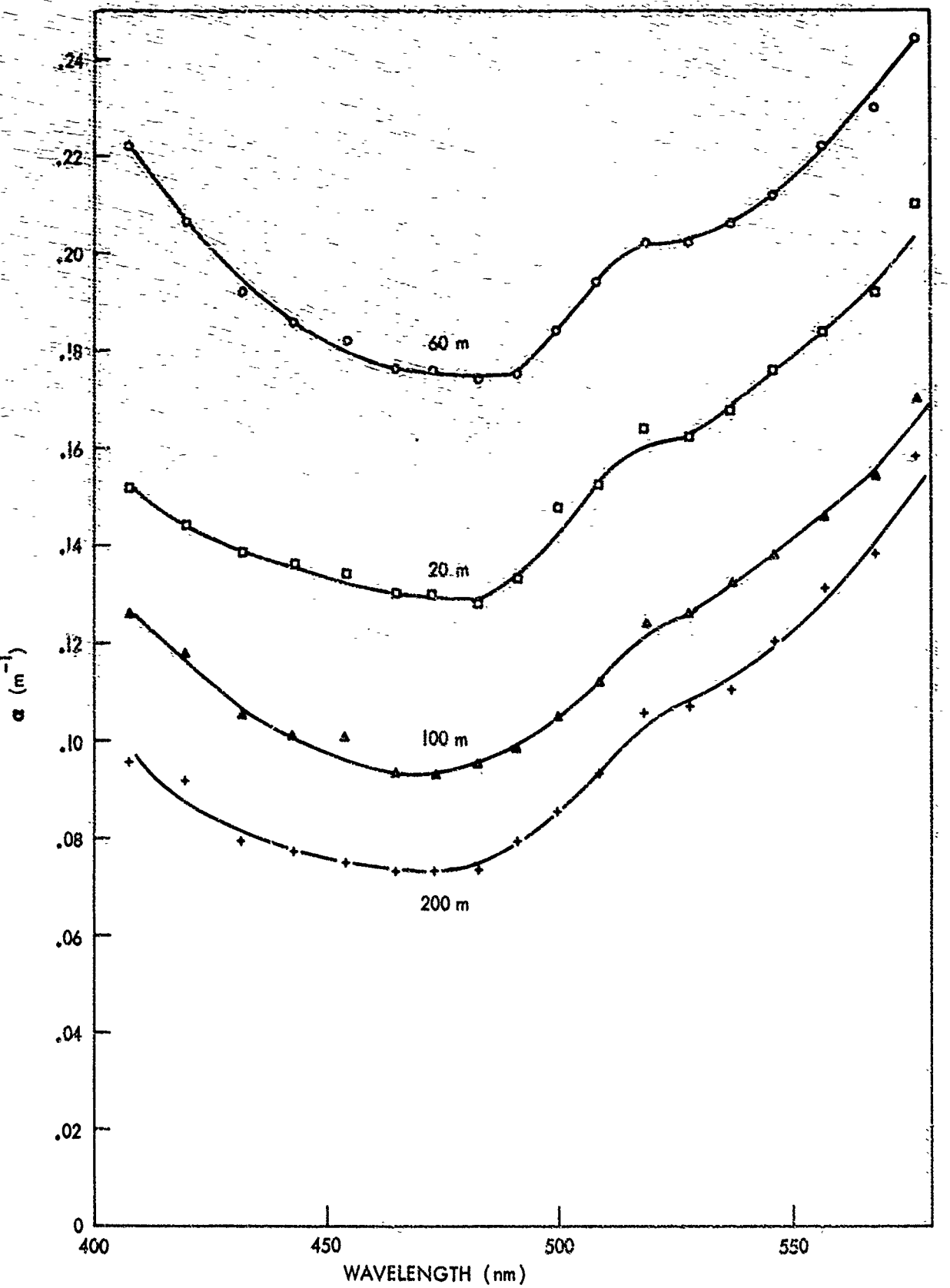

FIG. 8 OPTICAL ATTENUATION SPECTRA FROM DROP B-5 AT SELECTED DEPTHS.

TABLE II - ATTENUATION SPECTRA FROM CRUISE B

Drop B-2

Depth (m)	10 m	100	200	300	500	660	880	1000
λ (nm)	$\alpha (m^{-1})$							
408	.130	.130	.091	.091	.091	.094	.107	.102
419	.127	.120	.083	.081	.083	.098	.099	.096
432	.117	.107	.071	.071	.076	.071	.084	.081
443	.110	.102	.066	.068	.068	.068	.078	.076
454	.107	.096	.061	.061	.068	.066	.071	.068
465	.107	.094	.061	.061	.064	.064	.068	.064
473	.107	.091	.058	.061	.063	.064	.066	.064
483	.107	.091	.058	.063	.063	.064	.066	.063
491	.107	.093	.061	.064	.063	.066	.068	.061
500	.107	.096	.064	.066	.066	.068	.071	.066
508	.120	.107	.074	.068	.076	.076	.078	.074
519	.127	.112	.081	.083	.086	.086	.091	.084
528	.130	.112	.084	.086	.088	.088	.094	.086
537	.138	.122	.088	.094	.096	.096	.102	.094
546	.145	.125	.093	.098	.105	.102	.107	.102
557	.146	.132	.096	.104	.107	.107	.115	.110
568	.155	.138	.110	.112	.117	.117	.117	.115
577	.165	.150	.122	.127	.130	.130	.138	.127

TABLE II (Continued)

Drop B-3

Depth (m)	10 m	35	100	240	500	850	1900	2980
λ (nm)	α (m^{-1})							
408	.129	.127	.127	.096	.096	.102	.089	.081
419	.124	.122	.117	.091	.091	.096	.083	.078
432	.122	.120	.107	.081	.083	.086	.076	.068
443	.114	.112	.096	.068	.074	.076	.066	.061
454	.112	.114	.094	.068	.073	.073	.066	.058
465	.110	.112	.091	.066	.068	.069	.061	.061
473	.110	.110	.089	.066	.066	.068	.061	.059
483	.110	.110	.091	.066	.068	.068	.063	.058
491	.112	.112	.091	.071	.069	.068	.064	.059
500	.117	.115	.096	.076	.076	.076	.068	.063
508	.127	.127	.104	.081	.086	.083	.076	.071
519	.132	.135	.114	.091	.093	.091	.083	.076
528	.138	.138	.112	.091	.096	.096	.086	.081
537	.138	.140	.117	.096	.099	.096	.088	.083
546	.143	.145	.120	.099	.102	.102	.093	.091
557	.153	.155	.132	.114	.114	.114	.104	.102
568	.160	.163	.140	.124	.124	.124	.117	.110
577	.174	.174	.150	.135	.132	.134	.127	.122

TABLE II (Continued)

Drop B-4

Depth (m)	20	135	215	225	300	400	565	365	260	170
λ (nm)	$\alpha(m^{-1})$									
408	.127	.148	.104	.130	.097	.095	.091	.091	.086	.127
419	.130	.130	.099	.127	.095	.095	.091	.088	.086	.120
432	.117	.120	.091	.112	.081	.084	.081	.084	.081	.104
443	.117	.112	.084	.105	.076	.079	.076	.081	.074	.096
454	.114	.104	.076	.102	.079	.076	.072	.076	.071	.096
465	.112	.099	.074	.097	.076	.074	.066	.071	.066	.086
473	.109	.099	.074	.094	.072	.071	.066	.068	.066	.086
483	.112	.099	.074	.097	.072	.073	.068	.068	.066	.088
491	.114	.100	.076	.099	.073	.076	.068	.071	.070	.091
500	.122	.108	.083	.104	.081	.081	.074	.076	.073	.093
508	.127	.113	.089	.117	.090	.085	.081	.081	.081	.105
519	.140	.125	.104	.127	.099	.097	.094	.096	.091	.114
528	.138	.125	.102	.127	.099	.099	.094	.094	.091	.114
537	.145	.130	.109	.132	.107	.104	.099	.102	.099	.117
546	.145	.135	.112	.140	.109	.109	.107	.117	.105	.120
557	.155	.140	.112	.148	.120	.120	.112	.115	.112	.127
568	.163	.148	.130	.155	.127	.125	.120	.122	.120	.135
577	.179	.153	.143	.171	.143	.140	.135	.135	.134	.148

TABLE II - (Continued)

Drop B-4		Drop B-5			
Depth (m)	80	20	60	100	200
λ (nm)	$\alpha(m^{-1})$	$\alpha(m^{-1})$			
408	.122	.152	.222	.126	.095
419	.117	.144	.206	.118	.091
432	.102	.138	.192	.105	.079
443	.094	.136	.186	.101	.077
454	.094	.134	.182	.101	.075
465	.084	.130	.176	.093	.073
473	.084	.130	.176	.093	.073
483	.086	.128	.174	.095	.073
491	.089	.133	.175	.098	.079
500	.092	.148	.184	.105	.085
508	.102	.152	.194	.112	.093
519	.112	.164	.202	.124	.105
528	.112	.162	.202	.126	.107
537	.115	.168	.206	.132	.110
546	.120	.176	.212	.138	.120
557	.130	.184	.222	.146	.131
568	.132	.192	.230	.154	.138
577	.145	.210	.244	.170	.158

TABLE II - (Continued)

Drop B-6

Depth (m)	30	300	1500	2600	2880
λ (nm)	$\alpha(m^{-1})$				
408	.166	.095	.097	.081	.122
419	.150	.083	.083	.071	.109
432	.142	.075	.077	.063	.097
443	.134	.067	.065	.057	.089
454	.128	.063	.059	.051	.083
465	.128	.063	.064	.053	.083
473	.126	.061	.061	.049	.081
483	.126	.055	.063	.053	.085
491	.132	.069	.069	.057	.092
500	.140	.075	.073	.063	.092
508	.150	.087	.081	.074	.101
519	.158	.095	.093	.081	.093
528	.162	.100	.093	.085	.112
537	.166	.107	.101	.087	.118
546	.172	.112	.109	.095	.121
557	.184	.124	.119	.105	.132
568	.190	.128	.124	.110	.140
577	.203	.143	.137	.125	.157

begins to influence the decreasing value of α. The significant increase in turbidity which starts at 2600 meters and continues to the bottom at 2880 meters is real and is probably close to the indicated increase of 0.03 m^{-1}. High bottom turbidity is attributed to suspended sediments transported by deep lateral ocean currents.

Spectral data from drop B-5 are presented in Figure 8 to illustrate the general character of attenuation spectra of ocean water in the visible spectral interval. The transmission window is situated between 460 and 480 nm and a weak absorption band appears at around 520 nm. Relative change in α between spectra is somewhat larger at the shorter wavelengths in the violet and becomes progressively smaller towards the longer wavelengths in the green-yellow spectral interval. Spread of points is attributed to local impurity. Spectra from the remaining Cruise B drops are presented in Table II.

IV CRUISE F NARRATIVE

The sixth DOOM measurement expedition, Cruise F, departed Port Everglades, Florida, on 7 January, 1970, aboard the USNS LYNCH, T-AGOR-7 for two weeks of operations north of the Greater Antilles which would culminate in the deep trench north of Puerto Rico. Debarkation was scheduled on 20 January in San Juan, Puerto Rico. From Port Everglades, the Lynch steamed east through the Bahama Islands into the open Atlantic Ocean but was forced to backtrack on 8 January to the port of Nassau to disembark a technician who had suddenly become ill. Upon return to the open ocean, rough seas were encountered so shelter was sought for the first station on 9 January in a protected sound south of Long Island in the southern Bahamas. Initial problems with the DOOM instrument package delayed operations until the night of 10 January when the first measurement, drop F-1, was attempted. On successive nights from 11 to 19 January nine additional lowerings were completed, the first two while en route along the passage north of Hispaniola and the remaining seven in the trench area northwest of Puerto Rico. The cruise track denoting the ten stations is shown on the chart of Figure 9. Technical problems with the DOOM equipment resulted in loss of data from drops F-7, F-8, and F-9. Relevant data on the remaining drops are presented in Table III.

Just two months prior to Cruise F, the DOOM program had been at sea in the Atlantic on Cruise E during which the DOOM package had been subjected to some rather harsh treatment by the elements. In fact Cruise E was aborted when required access to the instrument sphere was barred because of mechanical damage to the lifting mechanism which could not be repaired at sea. Equipment had been off-loaded at the NOL Facility at Port Everglades for repair and preparation for Cruise F. The attenuation and scattering measurement sections, which had performed satisfactorily during Cruise E prior to the damage sustained on the last drop, fortunately still operated normally after minor adjustment during pre-cruise F checkout and calibration. A problem which had developed with the scattering

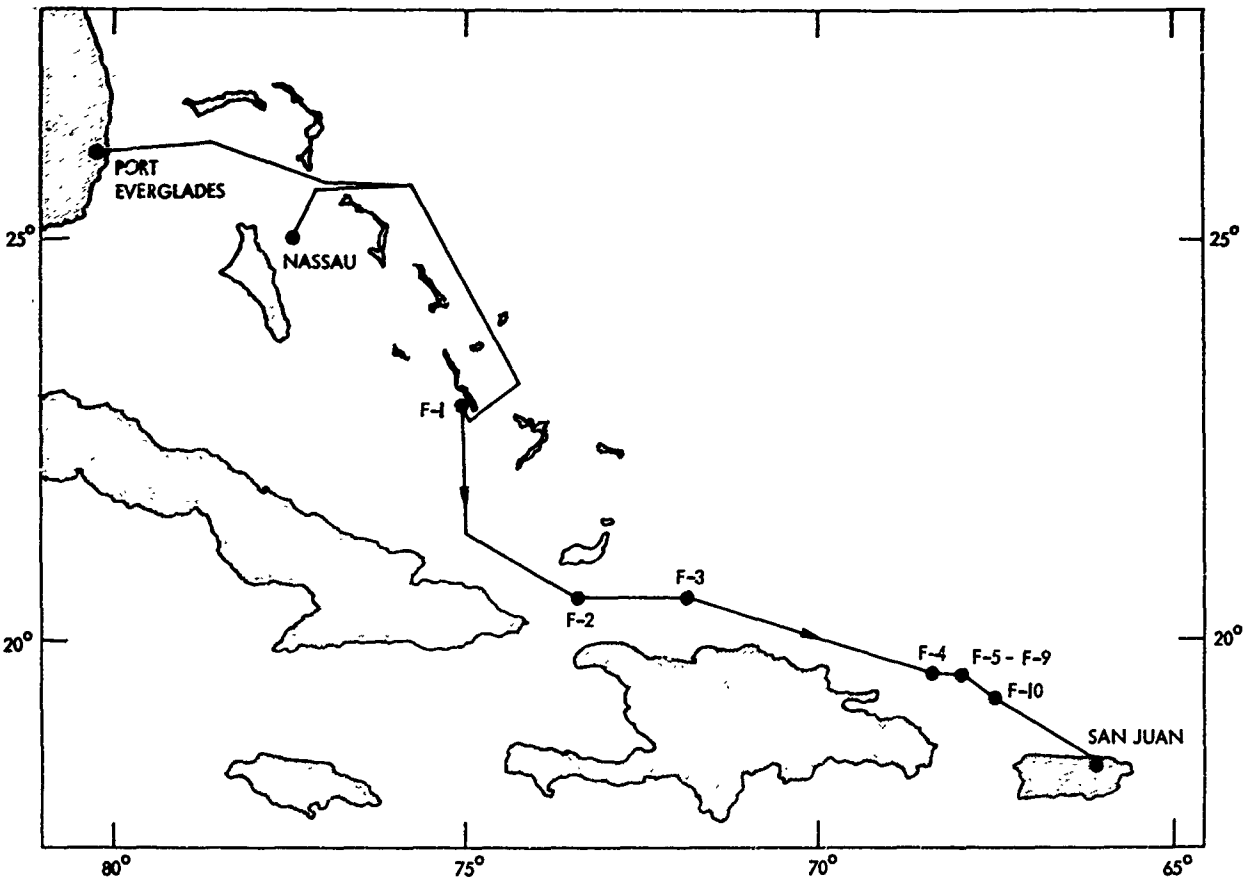

FIG. 9 TRACK CHART OF DOOM CRUISE F

TABLE III. PERTINENT DATA OF CRUISE F STATIONS

Drop #	Date	Time	Latitude North	Longitude West	Depth (m)	Measurement Depth (m)
F-1	1-10-70	1843	22° 57'	75° 00'	1756	1755
F-2	1-11-70	1947	20° 29'	73° 25'	3365	3350
F-3	1-12-70	1922	20° 27'	71° 51'	4060	4045
F-4	1-13-70	2151	19° 33'	68° 21'	7681	7307
F-5	1-14-70	1935	19° 40'	67° 55'	7955	7955
F-6	1-15-70	1848	19° 38'	67° 55'	7955	7943
F-10	1-19-70	1943	19° 15'	67° 30'	6680	300

measurement during Cruise E was the unreliable performance of the external stepping motor at depths below a thousand meters. Driving torque for the motor is provided by a capacitance discharge through the windings. In an attempt to solve this problem, the energy supplied the motor, and hence the driving torque was increased by doubling the capacitance and raising the charging voltage. Hopefully then stepping reliability would be improved at the larger hydrostatic pressures. The background measurement suffered from high noise levels and low sensitivity during the past cruise. This deficiency was remedied by the installation of a new photomultiplier tube and minor modification of signal processing circuitry. Thus, the DOOM system was 100 percent ready for sea.

A seemingly catastrophic failure occurred the evening of 9 January when the DOOM package was initially operated aboard ship. During final assembly at Port Everglades two power cables within the optics cylinder were inadvertently crushed while securing the end caps which resulted in direct shorting to ground of both the primary AC and DC power. The system at this time was operating on external, current-limiting power supplies which combined with fusing within the DOOM package was able to minimize the resulting damage. Although most damage was repairable, system performance was somewhat degraded. Casualties included the background measurement which was lost for the duration of the cruise and the control circuitry for the stepping motor which performed erratically and at times drew excessive current. Because of this difficulty the stepper motor was not energized during the first half of the cruise and thus the scattering measurement was at a fixed angle.

The initial drop F-1 on 10 September was made in the lee of Long Island some nine nautical miles offshore in 1756 meters of water. Due to problems with the stepper motor drive circuitry, the scattering instrument was operated a fixed angle of about 15 degrees. Motor windings were energized at a constant voltage in order to magnetically lock the scattering mirror at the intended angle. During launch of the package a combination of circumstances produced a shift in the scattering angle to about 11.5 degrees.

As the cruise track proceeded south from the Bahamas and then east through the passage north of Haiti, instrument drops F-2 and F-3 were made in progressively deeper water at depths of 3,350 and 4,045 meters respectively. The stepper motor mirror was repositioned to deflect the source light beam at 16 degrees from the scattering receiver. During drop F-2, the scattering signal began to vary irregularly below a depth of 1200 meters because of angular disorientation of the scattering mirror. Since mirror position is held electro-magnetically, it was speculated that voltage transients were producing anomalous stepping and hence mirror disorientation. A satisfactory solution to this problem could not be found during the cruise, so subsequent scattering data was generally restricted to depths above 1200 meters. An exception was drop F-3 where the mirror angle remained locked throughout the drop.

Station F-4 was located north of the eastern tip of Hispaniola at the western end of the Puerto Rico Trench in 7,680 meters of water. Lowering was stopped an estimated 370 meters from the bottom because of pinger failure due to flooding in the early stages of the drop.

On 14 January drop F-5 was lowered into the Brownson Deep which was sounded by a precision fathometer at a depth of 7,955 meters. The package was stopped an estimated distance of 5 meters from the bottom but slowly continued to settle until it rested on the floor of the trench. Bottom contact was confirmed by deposits of mud on the DOOM framework when the package was recovered.

An objective of this cruise was to measure the optical characteristics of the deepest water in the Atlantic Ocean which was denoted on hydrographic charts as a depression within the Brownson Deep with a depth of 8,740 meters. A concentrated effort over the next several days was made to locate this maximum depth which is called the Milwaukee Depth. A search pattern, consisting of many traversals of the trench, failed to find this deep hole but did reveal the true nature of the trench topography. Walls drop sharply to the trench floor which is rather flat and ranges in width from about 2 to 8 nautical miles. The uncorrected depth as recorded on the precision fathometer was consistently within plus or minus 40 meters of the mean depth of about 7,925 meters. Subsequent examination of recent bottom contour hydrographic charts show that this indeed is an accurate portrayal of this area of the Puerto Rico trough. Drops F-5 through F-9 were all made in this vicinity.

In the early drops, F-1 through F-5, it was hoped that variations in the profile of total attenuation could be correlated at all depths with those from the fixed angle scattering measurement. Correlation below 1200 meters proved futile due to inability to acquire accurate scattering data at these depths. It was therefore decided to activate the stepping motor in order to gather additional information on the volume scattering function in the surface waters. The stepping motor circuitry was energized for drop F-6 and performed reliably to a depth of 1500 meters.

As previously mentioned no data was acquired from drops F-7, F-8, and F-9.

In drop F-10, the contour of the bottom was immaterial since the cast was to be shallow, so station position was chosen for convenience a bit closer to Puerto Rico. In this drop as in drop F-7 an experiment was attempted in which the optical properties in the surface waters would be correlated with plankton concentrations. Ten plankton nets were deployed at 20 meter intervals from 20 to 200 meter depths for a period of 90 minutes. Simultaneously the DOOM package was slowly lowered and stopped at the depth of each of the deployed nets for a period of at least five minutes. The tests were performed well after dark to insure that the vertical migration of plankton would have stabilized. Unfortunately the nets did not

deploy satisfactorily in drop F-10 and optical data was lost in drop F-7 due to connector flooding so that test objective was not accomplished.

V CRUISE F DATA PRESENTATION

Operations during this cruise were technically intriguing due to the locale of operation and the nature of the experiment; that is, the unique experience of lowering a quantitative optical measuring device into the deepest trench in the Atlantic Ocean. It is also exciting to realize that the DOOM instrument actually recorded data while resting on the bottom of the Atlantic a distance of nearly 8000 meters below the level of the sea. Some characteristics of the optical data obtained within the trench are quite unique and merit special treatment in this presentation. First, however, the more conventional data from routine operation in the shallow and intermediate waters will be discussed.

Profiles of attenuation and temperature as a function of ocean depth are presented in Figures 10 through 16 for each of the seven successful drops. Spectral attenuation coefficients are plotted at three wavelengths, 386 and 555 nm which correspond to the limits of the spectral scan and 478 nm which is the nominal center of the transmission window. Attenuation spectra are presented at selected depths in Figures 17, 18, and 19. Figures 17 and 18 are illustrative of the shallow and intermediate waters while Figure 19 consists of the deep trench data. Spectra from all drops are tabulated in Table IV.

Scattering data from drops F-1 through F-5 are presented as profiles versus depth of the volume scattering function $\sigma(\theta)$ at the fixed angle of measurement. Also included is a profile of the attenuation coefficient σ at 432 nanometers which is near the wavelength of the $\sigma(\theta)$ at 436 nanometers. General shape of the profiles are graphically illustrated in Figure 20; a complete tabulation is included in Table V. In drops F-6 and F-10, σ was recorded at five angles, 6°, 13°, 20°, 28°, and 35°, which permits an estimate of the total volume scattering coefficient, s. This data for drops F-6 and F-10 is presented in Tables VI and VII at selected depths within the water column and includes α at 432 nm, the estimated s, and the volume scattering functions for the five angles. Scattering profiles at two angles, 6° and 13°, are plotted from drop F-10 data in Figure 21.

Cruise F attenuation profiles for shallow and intermediate waters are typical of tropical oceanic waters and are very similar to data recorded on previous courses D and E in the Bahama area. Attenuation is highest and somewhat variable in the mixed, isothermal layer at the surface. A frequent small peak at the top of the thermocline is followed by a rapid drop in attenuation to a minimum at around 200 to 300 meters depth which corresponds roughly to the bottom of the primary thermocline. Attenuation then rises to a

slight maximum between 800 and 1200 meters which generally corresponds to the base of the second or permanent thermocline before leveling off and remaining reasonably constant to the bottom. Drop F-3, Figure 12, exhibits these features but does also show a slight rise in turbidity near the bottom at 4000 meters probably due to suspended sediments. In some cases there are weak turbidity layers within the thermocline which give rise to minor structure in the profile as in drop F-2, Figure 11, where small maxima occur at 200 and 360 meters. Attenuation in the window at 478 nm varies from 0.10 to 0.14 m^{-1} at the surface, drops to a minimum of from 0.04 to 0.05 m^{-1}, and then levels off between 0.05 and 0.06 m^{-1}.

Contours of the α profiles at the three wavelengths in general track one another but at different levels of attenuation; the 386 nm and the 555 nm curves are displaced above the window values at 478 nm by about 0.02 and 0.05 m^{-1} respectively. However, the extent of variation within a profile between maxima and minima is a function of wavelength; the larger excursions are towards the shorter wavelengths. For instance in drop F-3, Figure 12, the change is α between the minima at 260 meters and the maxima at 800 m decreases progressively with increasing wavelength from 0.02 m^{-1} at 386 nm to 0.01 m^{-1} at 478 nm to 0.005 m^{-1} at 555 nm. This difference in the relative rates of change of spectral attenuation profiles can also be observed in the shape of attenuation spectra. Spectra for the surface and intermediate waters of drop F-3 are presented in Figure 17. Please observe the two sets of spectra at depths of 260 and 460 meters and at 750 and 1450 meters. In each of the two sets there is an appreciable divergence of the curves at the shorter wavelengths to the left of the figure while at the longer wavelengths above 500 nm the spectra are virtually coincident. Similarly if the level of the highest spectrum of this group, the 750 meter curve, is compared with the lowest spectrum at 260 meters, a proportionally larger difference in α of over 0.015 m^{-1} is present at the shorter wavelengths while above 500 nm the difference is only about 0.005 m^{-1}.

The previous example of spectral difference in attenuation profiles was confined to discussion of intermediate waters of drop F-3. That similar spectral variation occurs in the surface layers is evident from the profiles of drop F-10, Figure 16, where again trace excursions are most pronounced at the shorter, 386 nm wavelength. In Figure 18, spectra are presented at various levels within the profile. In the surface waters above the primary thermocline at about 110 meters, a relatively small change of about 0.005 m^{-1} occurs in attenuation at wavelengths longer than 500 nm. Below 500 nm to the left of the figure, profiles diverge with decreasing wavelength until a difference in α of 0.025 m^{-1} is reached at 386 nm. In the clearer water region below the thermocline, the profiles at 478 and 555 nm level off and remain reasonably constant below a depth of 160 meters. However, the 386 nm curve continues to drop with increasing depth. The consequence of this difference in slopes of the spectral profiles is a crossover of the two spectra at 160 and 300 meters at a wavelength of around 440 nm. The 300 meter

spectra, which has slightly lower values of α below 440 nm, climbs above the 160 nm spectrum at the longer wavelengths and remains just slightly higher.

There are two extraordinary features in attenuation data from the deep trench area of drops F-4, F-5, and F-6 as shown in the profiles of Figures 13, 14, and 15. First, there is an attenuation peak at 5000 meters in the usually clear mid-depths of the deep water column and secondly, there is a gradual convergence of the 478 nm and the 386 nm traces below 5000 meters which is within the trench canyon. Attenuation features of the upper 2000 meters of the water column are consistent with the previously discussed data, that is, high surface attenuation which drops to a minimum between 200 and 400 meters, then rises to a slight maximum at around 1000 meters before a general leveling off at a low level of α. Departure from previous data begins below 2000 meters where profiles begin a gradual rise which climbs rapidly below 4200 meters to the peak. In drops F-5 and F-6 this peak is at a depth of 5100 meters and in drop F-4 at 4900 meters. Drop F-4 was located about 30 miles distant from the station of drops F-5 and F-6. Below the peak, α drops rapidly to a plateau and remains reasonably constant all the way to the bottom. In the transmission window at 478 nm attenuation at the peaks is about 0.02 m^{-1} higher than the adjacent plateau which is at a level of 0.06 m^{-1}. The relative change in α from peak to plateau is of about the same magnitude at the longer wavelength, 555 nm, but becomes more pronounced at the ultraviolet wavelength, 386 nm, where the drop is perhaps 0.03 m^{-1}. Below the peak, the 386 nm profile continuously drops until it nearly equals the attenuation at 478 nm on the bottom of the trench. An explanation for the mid-column peak can be deduced from the nature of the bottom topography of the region. The sill of the North Atlantic Basin just north of the trench is at a depth of about 5000 meters. Water is laterally transported from the North Atlantic basin over the trench and the peak consists of bottom layers from the basin which are laden with suspended sediments.

To more fully determine the nature of the relative decrease in short wavelength attenuation within the trench, let us examine changes over the entire spectral interval. Spectra from drop F-5 are presented in Figure 19 at depths selected to illustrate major differences in spectral characteristics. The amplitude of spectra drops rapidly from a maximum near the surface at 10 meters to a minimum at 480 meters a depth corresponding to the bottom of the primary thermocline. Spectra then generally increase uniformity as depth increases until the peak in the middle of the water column is reached at 5080 meters. Although these four spectra, all within the basin water above the trench, differ substantially in amplitude, the relative shapes of the curves are essentially the same. Below the 5080 meter peak, there is sudden general decrease in overall spectral attenuation which is progressively stronger at the shorter wavelengths especially below 450 nm. As depth increases this effect becomes more pronounced and eventually the level of the two shortest wavelengths below 400 nm actually drops below the values of the longer wavelength

410 nm. A comparison of the 5590 and 7955 spectra shows that the curves track each other rather closely at the longer wavelengths and deviate only below 410 nm. This effect where the near ultraviolet attenuation falls below that of the blue-violet at extreme depths was observed in all three of the deep trench drops. No explanation has been postulated to explain this phenomenon. The physical parameter which is unique in this measurement is the extremely large hydrostatic pressure which at the bottom exceeds 13,000 psi.

Scattering measurements were restricted to shallow and intermediate waters due to the instrumental difficulties which were previously mentioned. Data for the most part, drops F-1 through F-5, were also restricted to a single angle. In Figure 20 profiles of the scattering function at 16°, $\sigma(16^\circ)$, and the attenuation coefficient at 432 nm, α(432 nm) are presented from drop F-3 as illustrative examples of the variation of these parameters with depth. Although the total percentage change in $\sigma(16^\circ)$ is much greater than that in α(432 nm), the two curves do exhibit the same general features. An area of disagreement perhaps is at the top of the thermocline at 65 meters where $\sigma(16^\circ)$ begins to fall just prior to the peak in α. Another difference appears between 2500 and 3000 meters where the $\sigma(16^\circ)$ trace drops slightly while the α trace begins a gentle climb. This difference may be real but perhaps it may be due to instrument errors which troubled the scattering measurement at these depths during the other drops.

In Figure 21 scattering profiles from drop F-10 are presented at two angles, 6° and 13°, along with α(432 nm). The α curve as compared to the $\sigma(6^\circ)$ trace has a more prominent peak at 100 meters just above the thermocline, which is at a slightly greater depth than the $\sigma(6^\circ)$ peak at 80 meters. This feature was observed in a number of the drops and indicates a strong absorbing layer near the top of the primary thermocline. The $\sigma(13^\circ)$ trace, although about a factor of five less than the $\sigma(6^\circ)$ trace, varies in much the same manner but with perhaps less small scale deviation. The total drop in the level of the two scattering functions from surface to 300 meters is about a factor of five for both angles.

The total volume scattering coefficient, s, is estimated from the measured scattering function data between 6° and 35° by a method explained in reference 2 where it is assumed in clear oceanic waters that 0.23 of the total scattering integral falls within the DOOM angular measurement range. The values of s in Tables VI and VII indicate that scattering contributes strongly to the total attenuation near the surface but its importance diminishes rapidly with depth. The large relative contribution of estimated s to the total α for surface waters, which in drop F-6 is over 80 percent of the total α of 0.117 m^{-1}, indicates that our technique for determining s in this type of water at the surface is not very accurate. Estimates in the deeper clear water, which yield absorption coefficients of from 0.04 to 0.06 m^{-1} appear more reasonable.

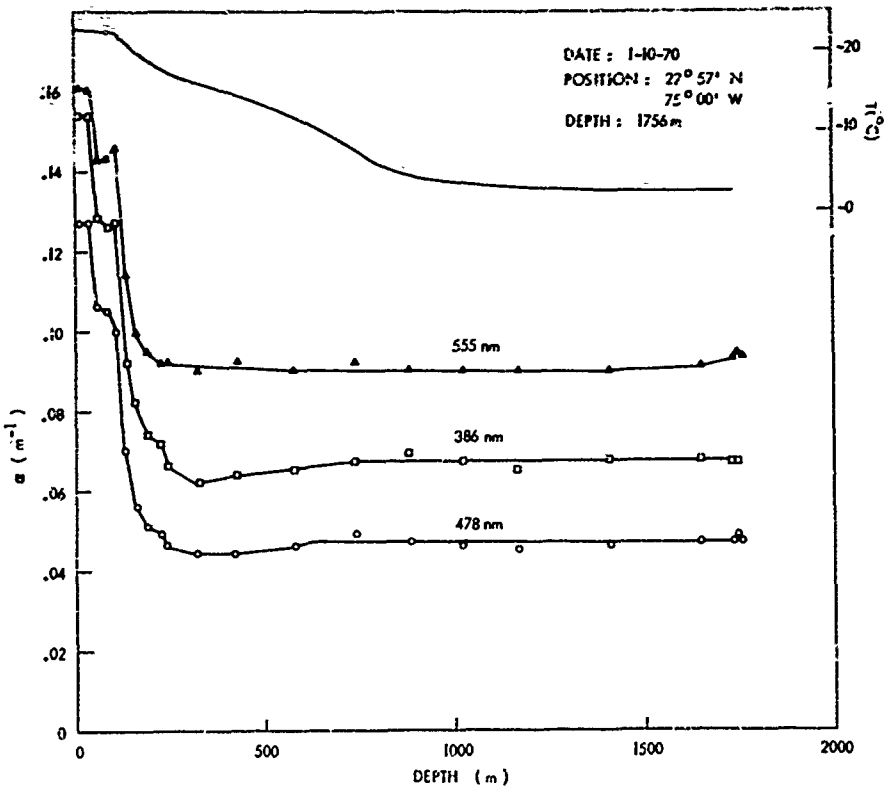

FIG. 10 OPTICAL ATTENUATION AND TEMPERATURE PROFILES OF DROP F-1.

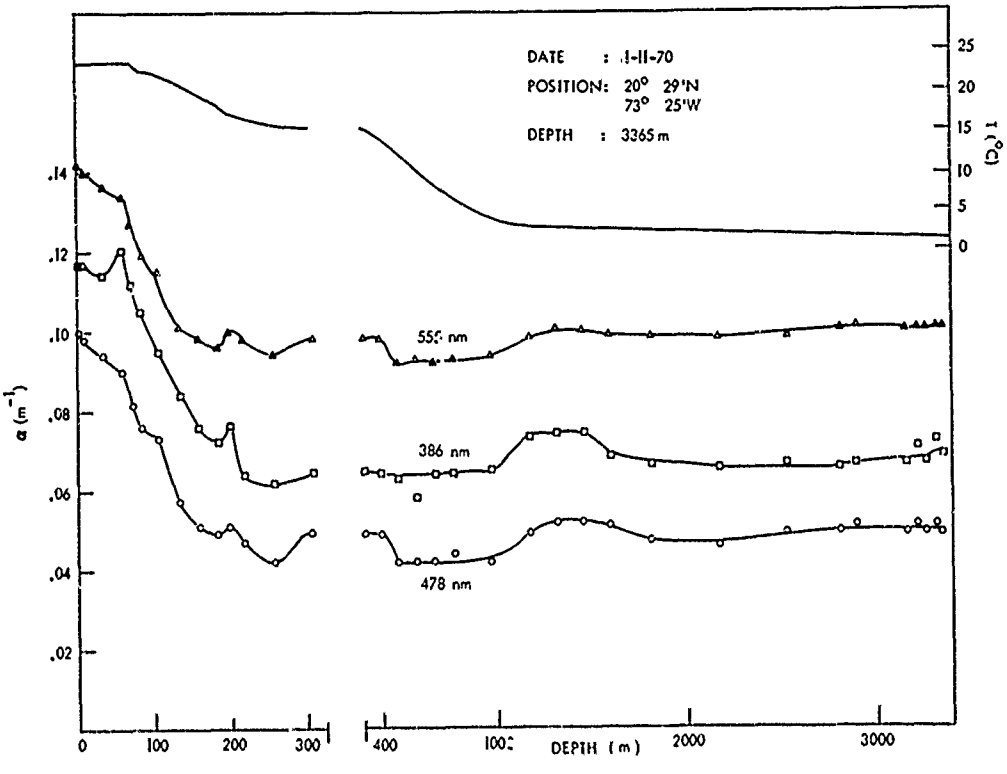

FIG. 11 OPTICAL ATTENUATION AND TEMPERATURE PROFILES OF DROP F-2

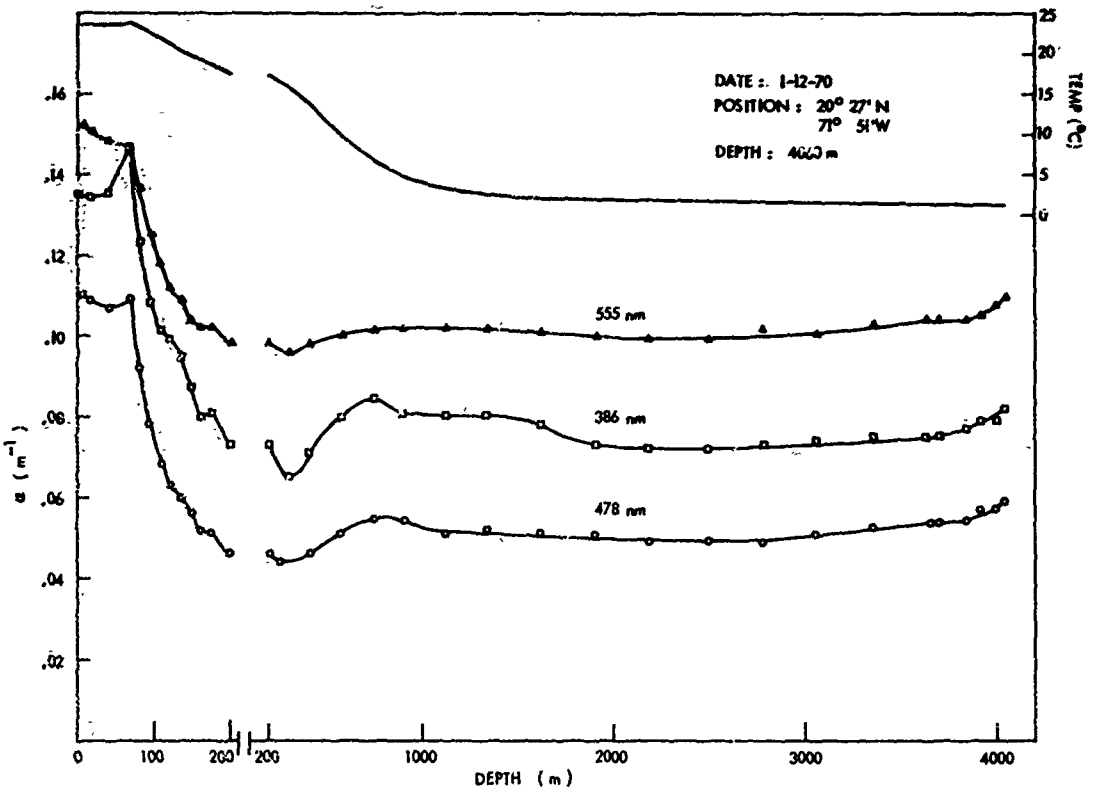

FIG. 12 OPTICAL ATTENUATION AND TEMPERATURE PROFILES OF DROP F-3.

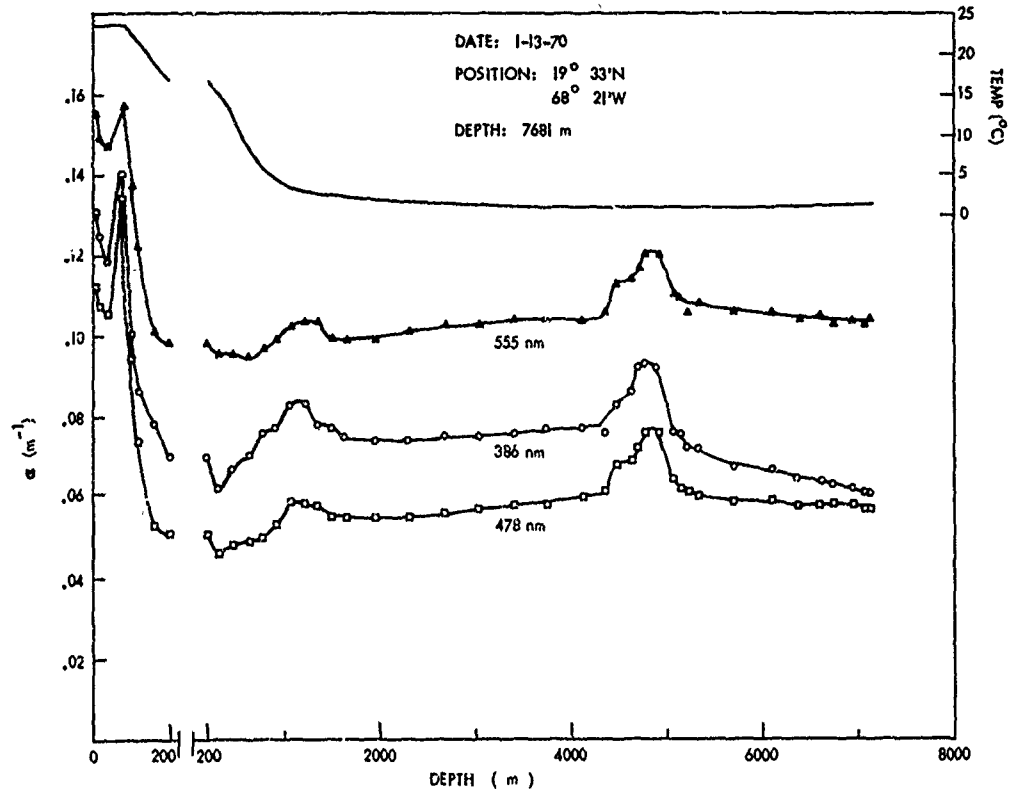

FIG. 13 OPTICAL ATTENUATION AND TEMPERATURE PROFILES OF DROP F-4.

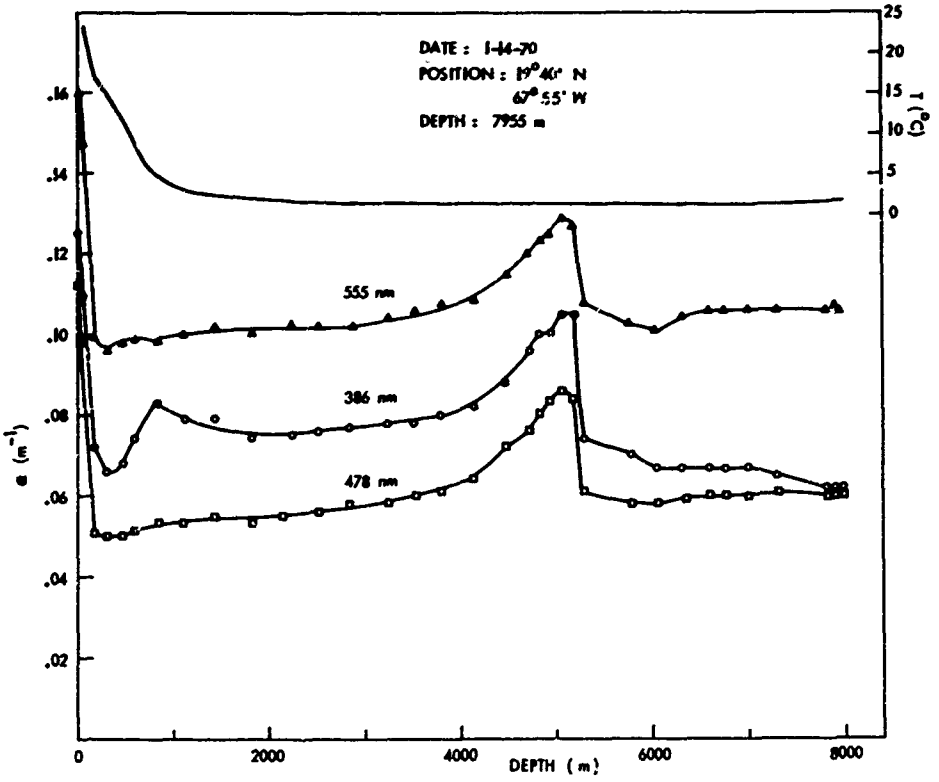

FIG. 14 OPTICAL ATTENUATION AND TEMPERATURE PROFILES OF DROP F-5.

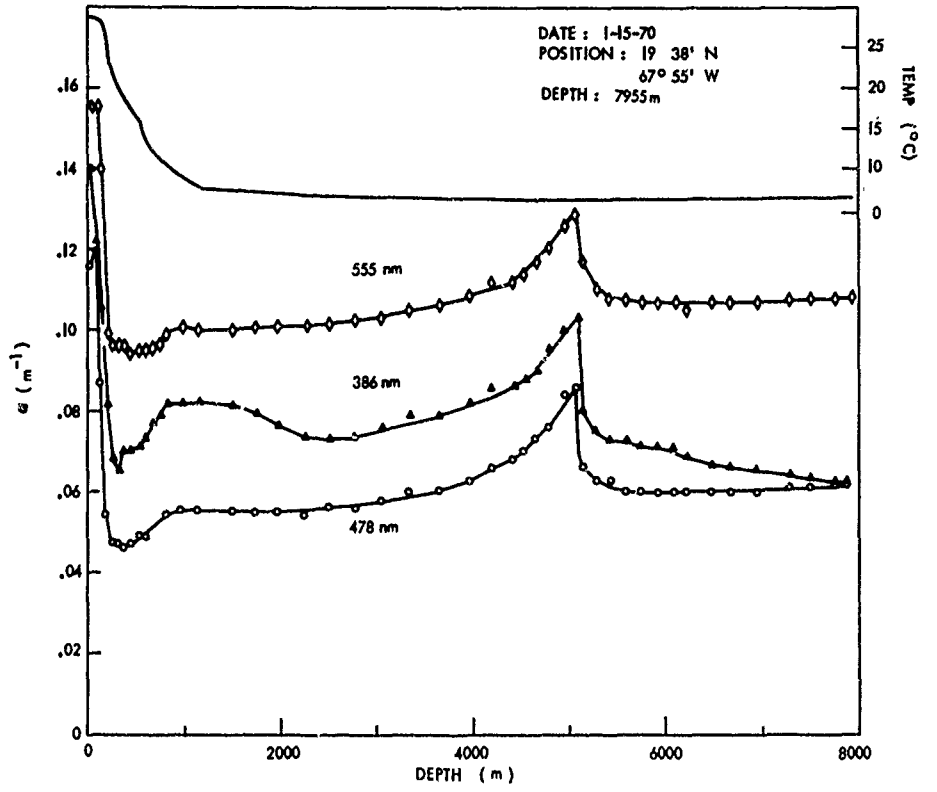

FIG. 15 OPTICAL ATTENUATION AND TEMPERATURE PROFILES OF DROP F-6

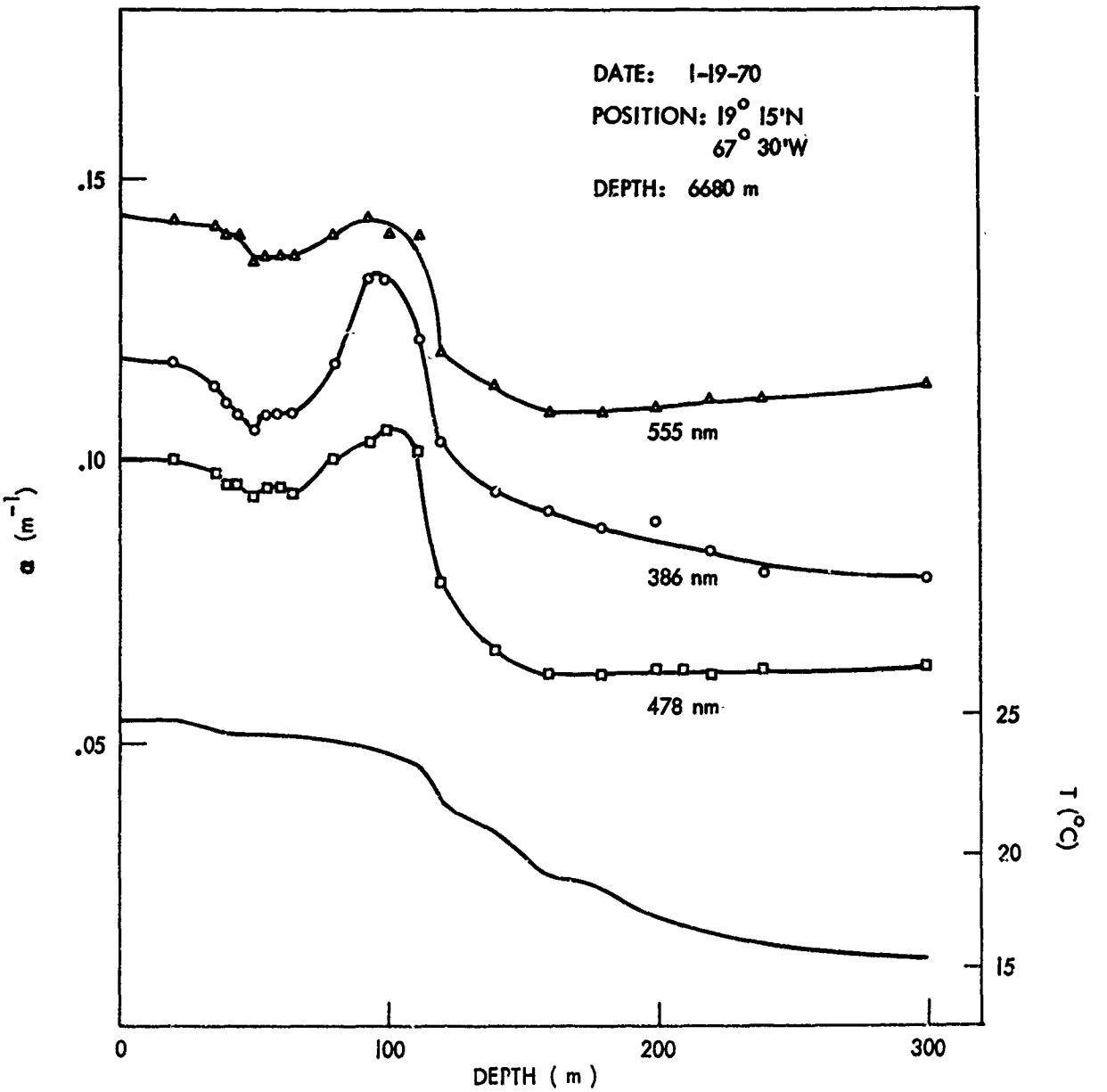

FIG. 16 OPTICAL ATTENUATION AND TEMPERATURE PROFILES OF DROP F-10.

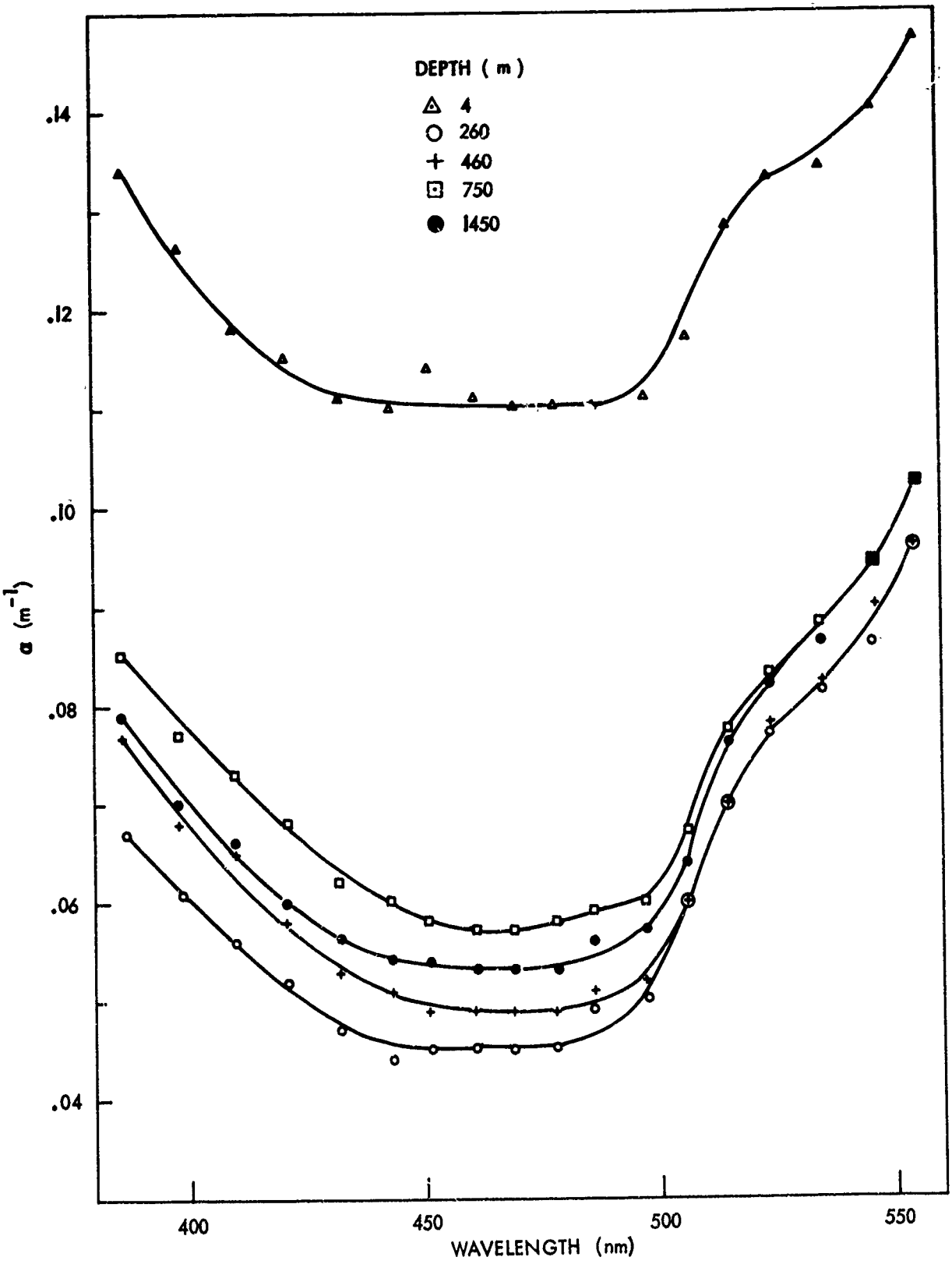

FIG. 17 OPTICAL ATTENUATION SPECTRA FROM DROP F-3.

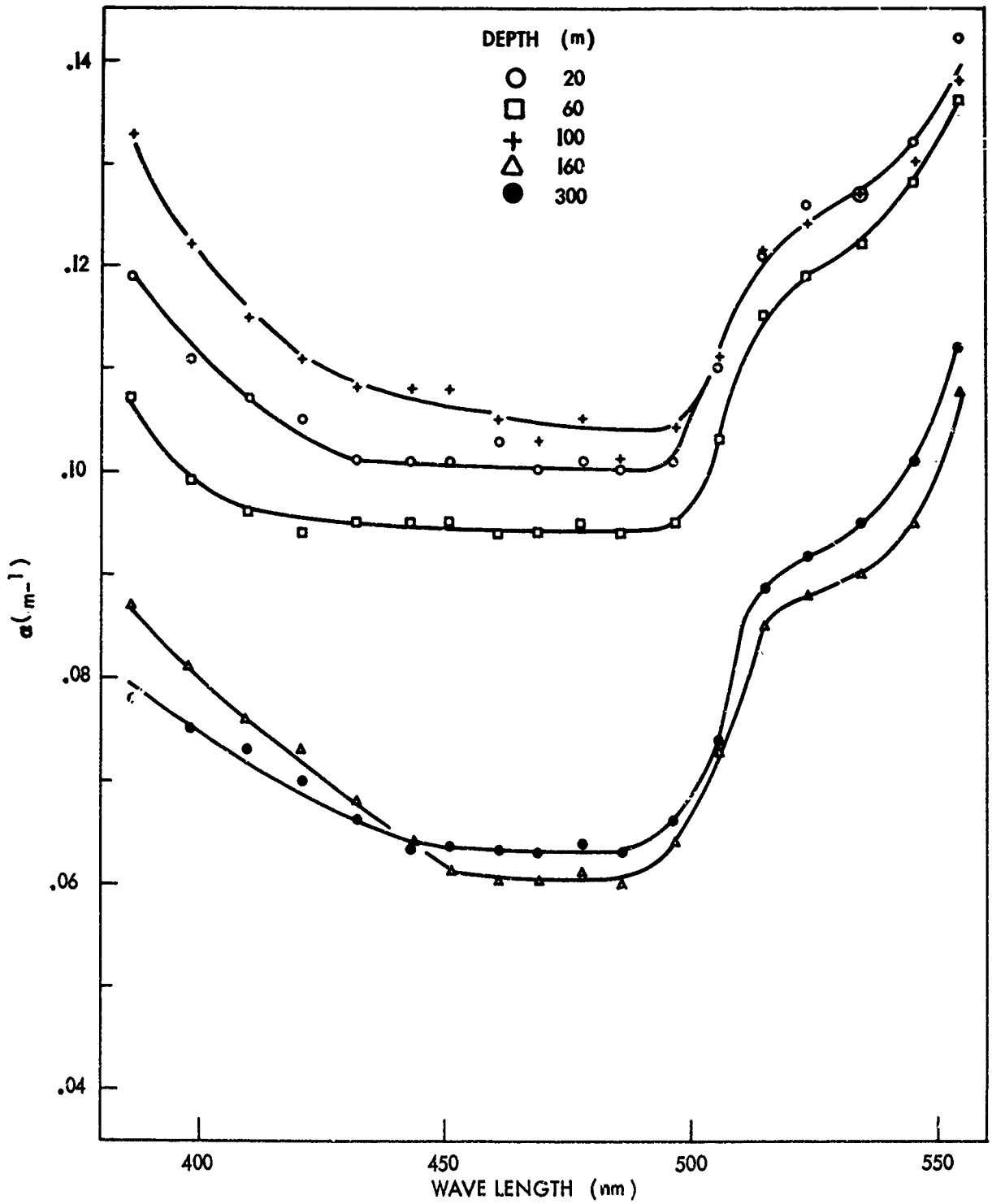

FIG. 18 OPTICAL ATTENUATION SPECTRA FROM DROP F-10.

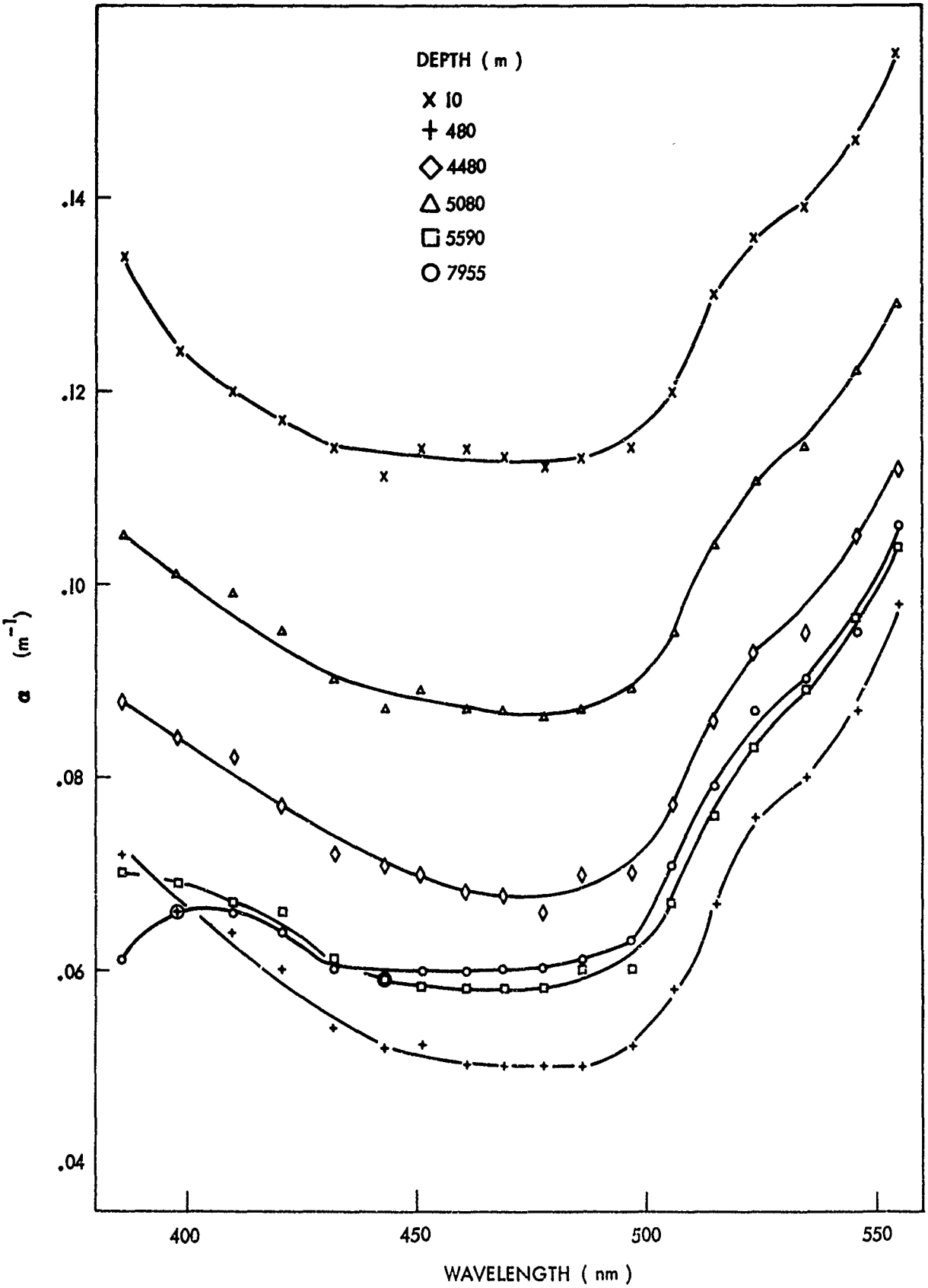

FIG. 19 OPTICAL ATTENUATION SPECTRA FROM DROP F-5.

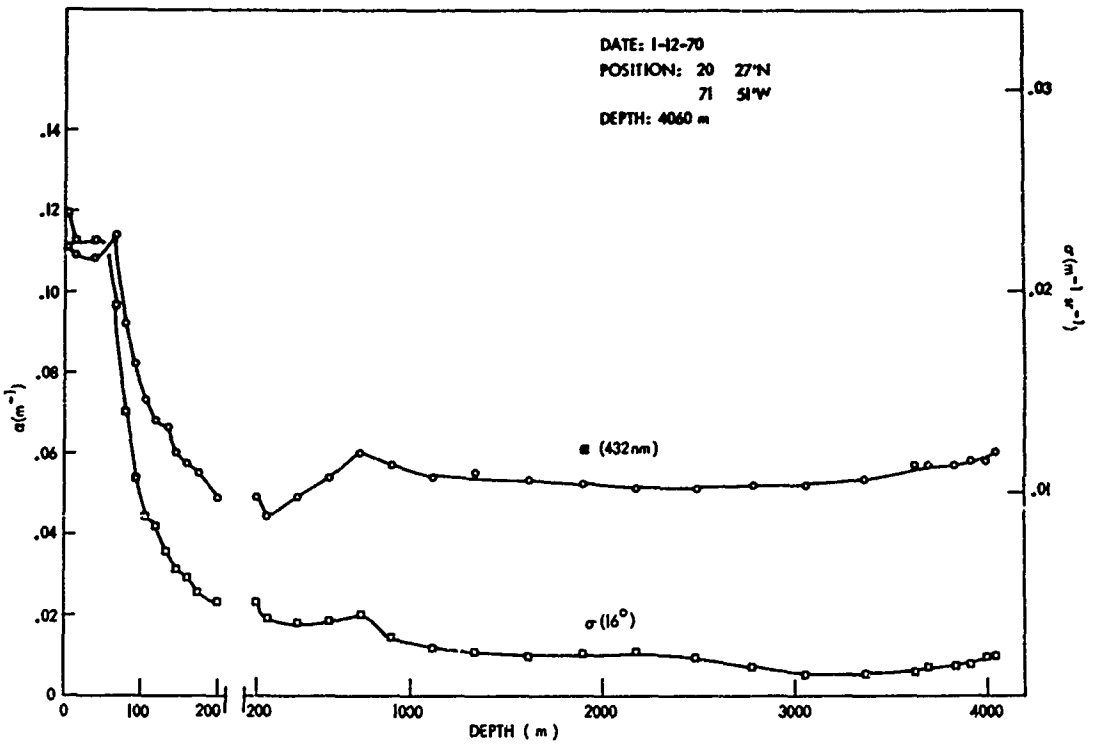

FIG. 20 OPTICAL ATTENUATION AND SCATTERING PROFILES FROM DROP F-3.

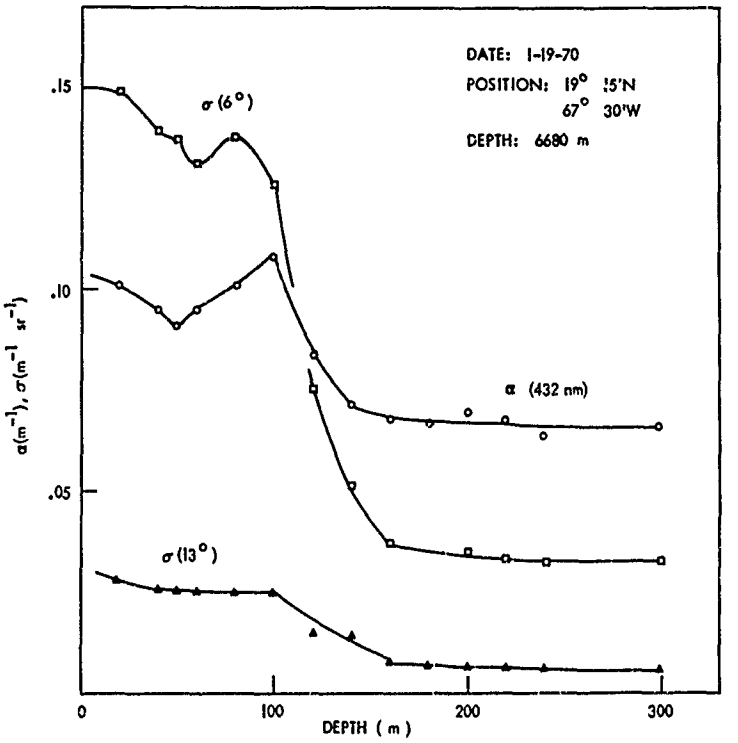

FIG. 21 OPTICAL ATTENUATION AND SCATTERING PROFILES FROM DROP F-10.

TABLE IV - ATTENUATION SPECTRA FROM CRUISE F

Drop F-1

Depth (m)	10	20	85	225	325	685	1020	1410	1755
λ (nm)	Attenuation Coefficient $\alpha(m^{-1})$								
386	.155	.155	.128	.073	.063	.068	.070	.070	.068
398	.146	.146	.119	.068	.058	.063	.064	.064	.065
410	.138	.138	.113	.063	.054	.057	.057	.059	.060
421	.134	.133	.111	.060	.052	.055	.054	.056	.056
432	.132	.131	.108	.054	.047	.051	.052	.052	.054
443	.130	.130	.109	.051	.047	.049	.049	.052	.052
451	.130	.130	.107	.047	.046	.047	.047	.047	.052
461	.128	.128	.105	.047	.044	.044	.046	.047	.049
469	.126	.127	.103	.046	.044	.044	.044	.047	.047
478	.126	.127	.105	.047	.045	.045	.045	.047	.047
486	.126	.126	.105	.046	.045	.047	.047	.049	.049
497	.130	.131	.107	.049	.051	.049	.049	.051	.052
506	.136	.138	.111	.055	.056	.058	.056	.057	.058
515	.142	.143	.123	.064	.063	.063	.063	.064	.066
524	.146	.146	.127	.073	.071	.071	.072	.071	.073
535	.149	.152	.128	.076	.076	.074	.076	.077	.079
546	.154	.156	.134	.082	.082	.080	.082	.082	.084
555	.162	.163	.144	.092	.092	.090	.090	.090	.093

TABLE IV (Continued)

Drop F-2

Depth (m)	3	96	200	260	355	490	850	1460	2180	2900	3350
λ (nm)	Attenuation Coefficient $\alpha(m^{-1})$										
386	.121	.108	.074	.068	.072	.070	.072	.080	.070	.073	.076
398	.108	.094	.070	.054	.060	.059	.063	.070	.062	.063	.064
410	.103	.090	.068	.051	.058	.057	.060	.068	.058	.061	.062
421	.101	.086	.063	.049	.057	.051	.053	.062	.054	.058	.060
432	.098	.080	.057	.046	.053	.047	.049	.057	.049	.055	.056
443	.098	.079	.054	.041	.051	.045	.044	.055	.049	.053	.054
451	.101	.078	.054	.044	.051	.044	.045	.054	.047	.052	.053
461	.101	.079	.053	.044	.052	.044	.045	.054	.047	.052	.054
469	.098	.078	.051	.043	.051	.044	.045	.054	.047	.052	.054
478	.098	.078	.053	.043	.051	.044	.045	.054	.047	.053	.053
486	.100	.078	.054	.044	.053	.044	.045	.054	.049	.054	.054
497	.105	.081	.057	.047	.056	.047	.049	.057	.053	.057	.057
506	.108	.087	.063	.054	.061	.053	.055	.063	.058	.063	.063
515	.122	.098	.076	.066	.074	.068	.068	.076	.070	.076	.076
524	.122	.101	.080	.073	.077	.073	.073	.080	.076	.080	.080
535	.128	.105	.087	.079	.084	.079	.080	.087	.082	.089	.089
546	.132	.112	.093	.087	.094	.087	.089	.092	.090	.097	.095
555	.142	.119	.101	.094	.101	.094	.095	.100	.097	.103	.103

TABLE IV (Continued)

Drop F-3

Depth (m)	4	52	147	260	460	750	1450	2490	3520	3920	4045
λ (nm)	Attenuation Coefficient $\alpha(m^{-1})$										
386	.134	.122	.087	.067	.077	.085	.079	.072	.075	.079	.083
398	.126	.117	.080	.061	.068	.077	.070	.065	.070	.076	.079
410	.118	.110	.075	.056	.065	.073	.066	.063	.066	.071	.074
421	.115	.109	.068	.052	.058	.068	.060	.058	.062	.064	.070
432	.111	.105	.060	.047	.053	.062	.056	.054	.056	.060	.062
443	.110	.103	.058	.044	.051	.060	.054	.051	.054	.059	.061
451	.114	.108	.058	.045	.049	.058	.054	.051	.054	.058	.060
461	.111	.106	.057	.045	.049	.057	.053	.051	.049	.057	.060
469	.110	.105	.057	.045	.049	.057	.053	.051	.052	.057	.060
478	.110	.105	.057	.045	.049	.058	.053	.051	.054	.058	.060
486	.110	.107	.060	.049	.051	.059	.056	.054	.057	.060	.064
497	.111	.108	.062	.050	.052	.060	.057	.055	.059	.063	.066
506	.117	.114	.069	.060	.060	.067	.064	.063	.066	.069	.073
515	.128	.125	.080	.070	.070	.077	.076	.074	.077	.080	.082
524	.133	.128	.085	.077	.078	.083	.082	.080	.082	.086	.090
535	.134	.130	.090	.081	.082	.088	.086	.085	.086	.090	.092
546	.140	.134	.098	.086	.090	.094	.094	.093	.094	.098	.099
555	.147	.144	.105	.096	.096	.102	.102	.099	.102	.105	.109

TABLE IV (Continued)

Drop F-4

Depth (m)	20	40	320	640	1150	2300	3740	4480	4850	5710	7110
λ (nm)	Attenuation Coefficient $\alpha(m^{-1})$										
386	.126	.121	.062	.072	.082	.073	.078	.082	.094	.070	.063
398	.119	.114	.059	.065	.076	.070	.073	.079	.089	.070	.064
410	.115	.111	.057	.063	.073	.066	.071	.079	.089	.070	.066
421	.112	.109	.055	.061	.071	.063	.066	.073	.086	.068	.064
432	.110	.107	.051	.054	.063	.059	.061	.068	.078	.062	.060
443	.110	.105	.047	.052	.062	.057	.060	.066	.078	.060	.057
451	.115	.108	.049	.052	.061	.057	.060	.063	.076	.060	.058
461	.112	.107	.049	.051	.060	.057	.059	.064	.074	.060	.058
469	.110	.107	.047	.049	.060	.057	.059	.064	.074	.059	.058
478	.111	.108	.049	.052	.061	.057	.059	.066	.076	.060	.060
486	.110	.108	.051	.051	.060	.057	.060	.064	.076	.063	.060
497	.110	.110	.051	.053	.060	.057	.060	.066	.079	.063	.062
506	.116	.116	.059	.058	.068	.064	.068	.076	.086	.071	.071
515	.124	.124	.068	.066	.076	.073	.077	.084	.095	.079	.079
524	.132	.130	.074	.074	.084	.080	.084	.090	.100	.087	.087
535	.134	.133	.079	.079	.087	.086	.088	.096	.105	.088	.089
546	.140	.138	.087	.087	.093	.092	.095	.103	.112	.095	.096
555	.148	.147	.095	.095	.103	.101	.103	.112	.121	.105	.106

TABLE IV (Continued)

Drop F-5

Depth (m)	10	480	850	1130	2140	3250	4480	5080	5590	6610	7955
λ (nm)	Attenuation Coefficient $\alpha(m^{-1})$										
386	.134	.072	.084	.077	.074	.077	.088	.105	.070	.066	.061
398	.124	.066	.073	.071	.068	.074	.084	.101	.069	.066	.066
410	.120	.064	.071	.069	.068	.073	.082	.099	.067	.068	.066
421	.117	.060	.066	.065	.063	.066	.077	.095	.066	.065	.064
432	.114	.054	.060	.059	.057	.061	.072	.090	.061	.062	.060
443	.111	.052	.058	.057	.056	.059	.071	.087	.059	.060	.059
451	.114	.052	.057	.057	.055	.060	.070	.089	.058	.060	.060
461	.114	.050	.057	.055	.054	.060	.068	.087	.058	.059	.060
469	.113	.050	.056	.055	.054	.059	.068	.087	.058	.058	.060
478	.112	.050	.056	.055	.055	.058	.066	.086	.058	.061	.060
486	.113	.050	.056	.055	.055	.058	.070	.087	.060	.062	.061
497	.114	.052	.056	.055	.054	.060	.070	.089	.060	.063	.063
506	.120	.058	.063	.063	.063	.067	.077	.095	.067	.071	.071
515	.130	.067	.065	.071	.072	.077	.086	.104	.076	.080	.079
524	.136	.076	.077	.079	.080	.083	.093	.111	.083	.086	.087
535	.139	.080	.082	.083	.082	.087	.095	.114	.089	.089	.090
546	.146	.087	.089	.092	.090	.095	.105	.122	.096	.096	.095
555	.155	.098	.099	.098	.099	.104	.112	.129	.104	.106	.106

TABLE IV (Continued)

Drop F-6

Depth (m)	20	320	440	600	820	1160	1680	2270	2800	3350	3980
λ (nm)	Attenuation Coefficient $\alpha(m^{-1})$										
386	.140	.066	.072	.073	.082	.080	.079	.073	.073	.079	.082
398	.127	.058	.063	.063	.074	.073	.072	.068	.068	.074	.078
410	.121	.056	.060	.063	.070	.070	.069	.066	.068	.071	.076
421	.119	.054	.057	.058	.066	.065	.064	.061	.063	.066	.073
432	.117	.049	.053	.053	.062	.060	.059	.057	.057	.063	.068
443	.117	.046	.051	.051	.059	.058	.057	.057	.057	.060	.066
451	.118	.047	.050	.049	.057	.057	.056	.057	.056	.060	.063
461	.116	.046	.051	.047	.054	.056	.055	.056	.054	.058	.062
469	.116	.046	.051	.047	.055	.056	.056	.054	.054	.057	.062
478	.117	.046	.049	.047	.054	.056	.055	.056	.055	.058	.063
486	.119	.047	.049	.049	.055	.056	.056	.056	.056	.060	.063
497	.122	.049	.051	.053	.057	.058	.058	.060	.060	.063	.066
506	.127	.055	.055	.057	.063	.063	.063	.065	.064	.068	.066
515	.138	.066	.066	.066	.073	.074	.073	.075	.074	.079	.082
524	.143	.073	.073	.073	.078	.079	.079	.080	.080	.084	.089
535	.148	.079	.079	.079	.082	.086	.086	.087	.086	.089	.094
546	.152	.086	.086	.084	.088	.092	.092	.093	.092	.096	.100
555	.160	.092	.092	.092	.098	.098	.099	.101	.101	.105	.108

TABLE IV (Continued)

Drop F-6 (Continued)

Depth (m)	4420	4660	4960	5280	5760	6100	6480	6960	7500	7945
λ (nm)	Attenuation Coefficient $\alpha(m^{-1})$									
386	.087	.089	.100	.074	.073	.071	.066	.063	.062	.062
398	.082	.086	.095	.073	.072	.071	.068	.066	.064	.064
410	.080	.084	.092	.071	.070	.070	.068	.068	.067	.066
421	.076	.081	.089	.070	.068	.068	.065	.065	.065	.064
432	.073	.076	.086	.065	.062	.065	.062	.062	.062	.062
443	.072	.074	.082	.063	.062	.062	.060	.060	.061	.061
451	.070	.074	.079	.062	.060	.062	.060	.060	.060	.060
461	.068	.072	.080	.060	.059	.060	.059	.059	.060	.060
469	.068	.072	.082	.060	.059	.060	.058	.059	.060	.060
478	.068	.073	.082	.063	.060	.061	.059	.060	.061	.061
486	.070	.074	.082	.063	.061	.062	.060	.060	.063	.063
497	.072	.077	.086	.068	.064	.064	.063	.065	.067	.068
506	.077	.080	.089	.073	.070	.070	.070	.070	.073	.073
515	.087	.090	.100	.082	.079	.080	.079	.078	.082	.082
524	.092	.096	.105	.089	.086	.086	.084	.086	.089	.088
535	.100	.101	.110	.092	.089	.093	.094	.092	.094	.095
546	.105	.106	.114	.098	.096	.098	.097	.097	.099	.100
555	.112	.117	.126	.108	.105	.105	.105	.105	.106	.106

TABLE IV (Continued)

Drop F-10

Depth (m)	20	40	50	60	80	100	120	140	160	200	240	300
λ (nm)	Attenuation Coefficient $\alpha(m^{-1})$											
386	.119	.108	.101	.107	.119	.133	.105	.094	.087	.086	.080	.078
398	.111	.100	.096	.099	.108	.122	.098	.084	.081	.079	.076	.075
410	.107	.099	.092	.096	.105	.115	.092	.080	.076	.077	.073	.073
421	.105	.098	.092	.094	.101	.111	.086	.076	.073	.073	.068	.070
432	.101	.095	.091	.095	.101	.108	.084	.071	.068	.070	.063	.066
443	.101	.095	.091	.095	.101	.108	.079	.066	.064	.065	.061	.063
451	.101	.096	.093	.095	.101	.108	.079	.068	.061	.064	.060	.064
461	.103	.096	.095	.094	.099	.105	.079	.066	.060	.064	.061	.063
469	.100	.095	.093	.094	.098	.103	.078	.065	.060	.063	.060	.063
478	.101	.096	.093	.095	.098	.105	.078	.066	.061	.063	.061	.064
486	.100	.096	.093	.094	.098	.101	.078	.066	.060	.064	.061	.063
497	.101	.098	.095	.095	.101	.104	.079	.068	.064	.066	.064	.066
506	.110	.105	.103	.103	.110	.111	.089	.076	.073	.074	.073	.074
515	.121	.117	.112	.115	.117	.122	.092	.089	.085	.086	.086	.089
524	.126	.127	.119	.119	.121	.124	.101	.092	.088	.089	.089	.092
535	.127	.129	.121	.122	.126	.127	.103	.096	.090	.095	.095	.095
546	.132	.133	.124	.128	.130	.130	.108	.101	.095	.100	.100	.101
555	.142	.144	.133	.136	.140	.138	.119	.111	.108	.110	.111	.112

TABLE V

Profiles of Optical Scattering and Attenuation for Drop F-1

Depth (m)	α(432 nm) (m^{-1})	σ(11.5°) (m^{-1} sr^{-1})
10	.131	.064
38	.133	.068
60	.111	.053
85	.110	.050
110	.108	.044
132	.076	.023
160	.063	.017
190	.056	.012
225	.056	.011
240	.052	.0098
325	.049	.0090
425	.049	.0085
580	.049	.0071
740	.041	.0065
880	.054	.0061
1020	.053	.0061
1170	.053	.0061
1410	.053	.0059
1650	.053	.0047
1740	.054	.0049
1755	.054	.0049

TABLE V (Continued)

Profiles of Optical Scattering and Attenuation for Drop F-2

Depth (m)	α(432 nm) (m^{-1})	$\sigma(16^{o})$ (m^{-1} sr^{-1})
3	.099	.0213
10	.098	.0213
35	.095	.0191
60	.088	.0178
72	.086	.0137
84	.079	.0116
108	.073	.0102
134	.063	.0076
160	.056	.0060
186	.054	.0051
200	.055	.0058
220	.047	.0047
260	.043	.0040
310	.051	.0055
400	.049	.0057
490	.046	.0035
580	.046	.0035
680	.047	.0031
780	.047	.0028
980	.047	.0022
1180	.054	.0021
1320	.057	-
1460	.055	-
1600	.054	-

TABLE V (Continued)

Profiles of Optical Scattering and Attenuation for Drop F-3

Depth (m)	α(432 nm) (m^{-1})	$\sigma(16^{o})$ (m^{-1} sr^{-1})
4	.110	.0239
14	.109	.0225
40	.108	.0225
67	.114	.0193
80	.092	.0140
93	.082	.0107
107	.073	.0089
120	.068	.0083
134	.066	.0071
147	.060	.0062
160	.057	.0058
174	.055	.0051
200	.049	.0046
260	.044	.0038
410	.049	.0035
580	.054	.0036
750	.060	.0039
900	.057	.0028
1120	.054	.0023
1340	.055	.0021
1620	.053	.0019
1900	.052	.0021
2180	.051	.0021
2490	.051	.0019
2780	.052	.0014
3060	.052	.0010
3360	.053	.0010
3630	.057	.0011
3840	.057	.0016
3920	.058	.0015
4000	.058	.0019
4045	.060	.0019

TABLE V (Continued)

Profiles of Optical Scattering and Attenuation for Drop F-4

Depth (m)	α(432 nm) (m^{-1})	$\sigma(16^{o})$ (m^{-1} sr^{-1}
10	.111	.0236
20	.110	.0236
40	.105	.0215
80	.119	.0207
100	.084	.0125
120	.068	.0088
160	.060	.0058
200	.054	.0047
320	.049	.0042
480	.052	.0045
640	.054	.0033
790	.057	.0030
920	.060	.0028
1070	.063	.0031

TABLE V (Continued)

Profiles of Optical Scattering and Attenuation for Drop F-5

Depth (m)	α(432 nm) (m^{-1})	$\sigma(16^{o})$ (m^{-1} sr^{-1})
10	.112	.0298
50	.098	.0200
180	.051	.0053
320	.050	.0044
480	.050	.0044
600	.051	.0035
850	.053	.0030
1130	.053	.0029

TABLE VI

Profiles of the Volume Scattering Function and the Attenuation and Scattering Coefficients of Drop F-6

Depth	α(432 nm)	s(436 nm)	$\sigma(6^\circ)$	$\sigma(13^\circ)$	$\sigma(20^\circ)$	$\sigma(28^\circ)$	$\sigma(35^\circ)$
(m)	(m^{-1})		(m^{-1} sr^{-1})				
20	.117	.096	.227	.038	.016	.0070	.0032
80	.106	.086	.218	.036	.013	.0060	.0026
140	.105	.046	.112	.018	.0074	.0030	.0015
200	.060	.020	.044	.0069	.0031	.0017	.0010
260	.051	.016	.038	.0060	.0027	.0015	.0009
320	.049	.015	.035	.0056	.0026	.0013	.0008
380	.052	.015	.033	.0055	.0026	.0013	.0008
440	.054	.015	.036	.0050	.0023	.0012	.0008
540	.053	.013	.028	.0049	.0022	.0013	.0009
600	.052	.013	.027	.0041	.0019	.0011	.0007
680	.055	.011	.022	.0041	.0019	.0011	.0007
760	.058	.012	.024	.0045	.0019	.0010	.0008
820	.061	.012	.024	.0041	.0018	.0010	.0008
980	.061	.008	.015	.0033	.0013	.0009	.0007
1160	.060	.007	.013	.0030	.0013	.0008	.0007
1500	.060	.006	.012	.0027	.0012	.0008	.0007

TABLE VII

Profiles of the Volume Scattering Function and the Attenuation and Scattering Coefficients of Drop F-10

Depth	α(432 nm)	s(436nm)	$\sigma(6^o)$	$\sigma(13^o)$	$\sigma(20^o)$	$\sigma(28^o)$	$\sigma(35^o)$
(m)	(m^{-1})		(m^{-1} sr^{-1})				
20	.101	.069	.153	.028	.0115	.0051	.0026
40	.095	.062	.139	.025	.0105	.0049	.0021
50	.091	.064	.141	.025	.0104	.0049	.0021
60	.095	.059	.130	.025	.0104	.0047	.0021
80	.101	.062	.139	.025	.0106	.0048	.0020
100	.108	.059	.129	.025	.0104	.0045	.0019
120	.084	.033	.073	.015	.0058	.0024	.0012
140	.071	.027	.052	.014	.0044	.0020	.0011
160	.068	.020	.040	.0074	.0035	.0017	.0010
180	.067	.018	.037	.0071	.0033	.0016	.0010
200	.070	.017	.034	.0067	.0029	.0015	.0010
220	.068	.017	.0032	.0065	.0029	.0014	.0010
240	.063	.016	.0031	.0060	.0027	.0014	.0009
300	.066	.016	.0031	.0060	.0026	.0014	.0009

VI CRUISE I NARRATIVE

Cruise I embarked from the Athenian port of Piraievs, Greece, on the evening of 28 March 1972 aboard the USNS LYNCH, T-AGOR-7, for a 17 day oceanographic voyage in the Mediterranean Sea and in the Altantic Ocean adjacent to Gibraltar. Accompanying the DOOM personnel was an international team of marine geologists directed by Dr. Daniel Stanley of the Division of Sedimentology of the Smithsonian Institution who independently conducted their own research as DOOM operations permitted. A general cruise schedule specified equally spaced stations about 120 nautical miles apart along a westwardly track across the Mediterranean, through the Straits of Gibraltar into the Atlantic for roughly 200 miles, and then a back track to port at Rota, Spain, on 13 April 1972. Sixteen stations, 14 in the Mediterranean and 2 in the Atlantic, were planned. A delayed departure from Piraievs forced cancellation of the first station and an unscheduled refueling stop at Cartagena, Spain, on 8 April with subsequent rough weather on 9 April resulted in the loss of two more stations. Thirteen drops, which included two in the Atlantic, were successfully completed as shown in the track chart, Figure 22. Pertinent data on each drop is presented in Table VIII.

Prior to the cruise two modifications were made to improve the performance of the spectral attenuation measurement section. Dielectric mirrors with enhanced reflectivity in the blue-violet spectral interval were incorporated in the White optical system which provides the folded 7.5 meter sample path in water. The previously used aluminum surfaces overcoated with silicon monoxide had degraded slowly with exposure to the marine environment which resulted in periodic replacement and the subsequent painstaking re-alignment of the White mirror system at sea. Laboratory tests under simulated ocean conditions indicated that dielectric coatings were highly resistant to both salt water immersion and salt spray exposure. And indeed this proved to be true in the real maritime environment as well. The one set of three mirrors used during the entire duration of the cruise showed no degradation in optical reflectivity.

The second problem addressed by the α section modification was the rather large variation in system response as a function of wavelength. This variation is produced by different spectral characteristics of the various optical components, namely the tungsten lamp source, the photomultiplier detector, and the several mirrors and beamsplitters. Commercially available stock filters had previously been used to flatten the system spectral response but still a signal level difference of about a factor of six was present. A dielectric optical filter specifically designed to produce a more nearly constant response for the DOOM spectral attenuation measurement was procured. This filter reduced spectral variation to less than a factor of 1.5.

The reason for modifying the shape of the spectral response was to increase the effective dynamic range of the recording instrument. Some of this gain in dynamic range was lost early in

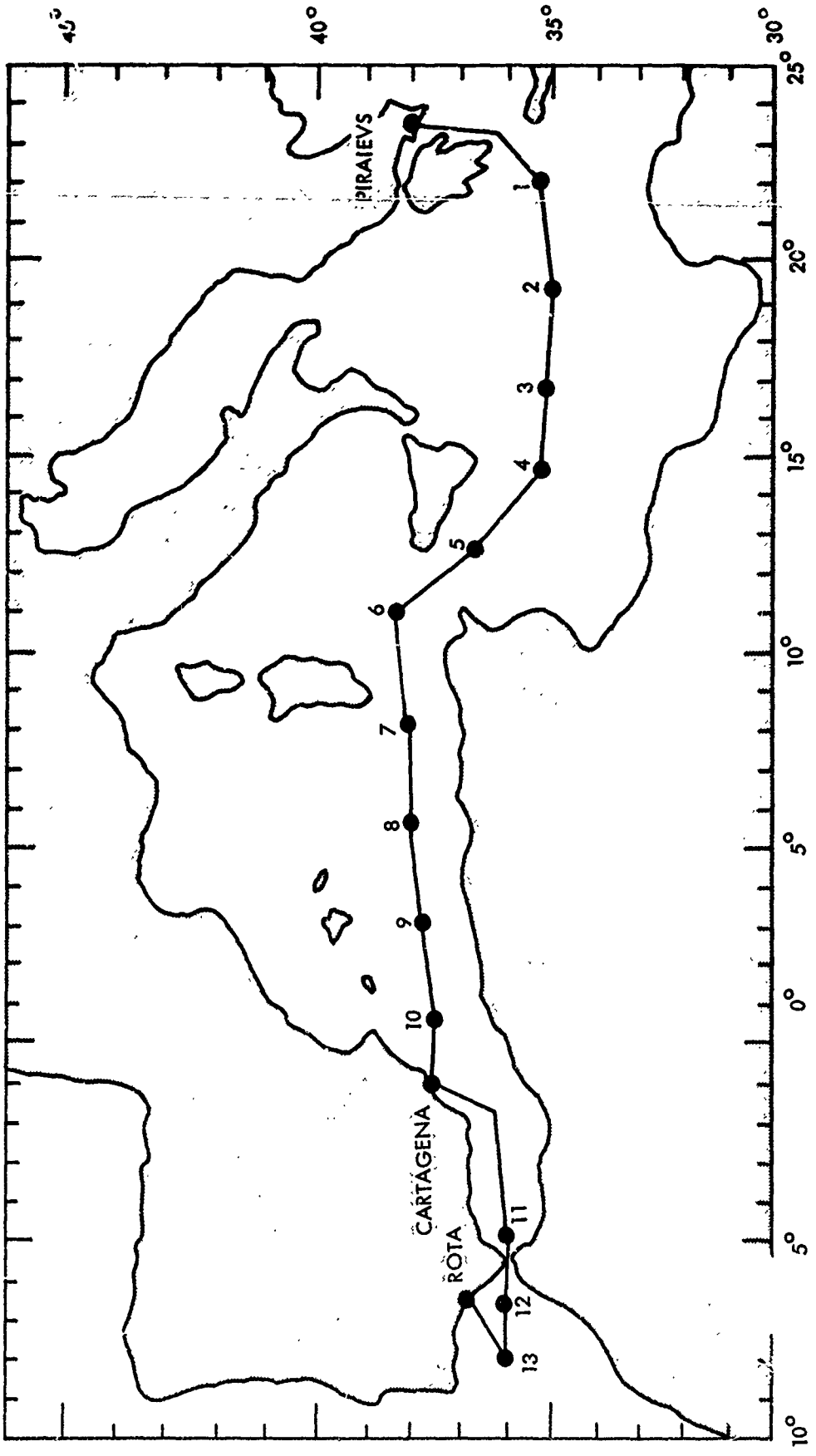

FIG. 22 TRACK CHART OF CRUISE I.

TABLE VIII

Pertinent Data on Cruise I Stations

Drop	Date	Time	Latitude	Longitude	Depth (m)	Maximum Measurement Depth (m)
I-1	3-29-72	1945	35° 09.5'N	21° 56.8'E	3115	3100
I-2	3-30-72	1957	34° 56.2'N	19° 13.6'E	3267	3267
I-3	3-31-72	1857	35° 03.9'N	16° 43.2'E	2667	2661
I-4	4-1-72	1906	35° 09'N	14° 36.6'E	549	549
I-5	4-2-72	1919	36° 39.5'N	12° 26.7'E	1258	1258
I-6	4-3-72	1926	38° 14.2'N	10° 56.4'E	666	628
I-7	4-4-72	1940	38° 01'N	07° 59'E	2640	2640
I-8	4-5-72	1940	37° 54.9'N	5° 30.9'E	2714	2714
I-9	4-6-72	2024	37° 46.2'N	2° 54.5'E	2676	2676
I-10	4-7-72	2015	37° 31.5'N	0° 20.3'E	2610	2602
I-11	4-10-72	2056	35° 56.3'N	4° 59.6'W	578	578
I-12	4-11-72	2049	36° 7.8'N	6° 51.7'W	673	673
I-13	4-12-72	2112	36° 1.7'N	8° 2.0'W	1570	1550

the cruise when a malfunction occurred in the regulation circuitry of the high voltage power supply for the photomultiplier tubes. This supply which steps up the 28VDC battery voltage continued to function but the regulation stage which maintains a constant 1200 VDC output ceased to operate. Then as the primary battery discharges, its voltage drop results in a proportional decrease in the high voltage and an effective decrease in photomultiplier gain. This change in gain is not crucial to the measurement since a reference signal level is continuously monitored and recorded so data can still be effectively processed. What is significant is that the voltage drop produces a continuous drift of signal to lower levels which decreases the dynamic range of the recording system. A characteristic of the silver zinc batteries used in the DOOM system is a relatively constant discharge voltage between 80 and 20 percent of full charge capacity. System voltage thus was held reasonable constant by initiating operation at 80 percent of nominal full charge. This 80 percent level is difficult to determine accurately so some drift and resultant loss or dynamic range was experienced throughout the cruise. This fact is not of critical importance to the data presentation but is mentioned in order to explain off scale signals which occurred from time-to-time in waters of high turbidity.

Since the scattering measurement section which varied as a function of angle had never performed entirely satisfactorily, it was decided that the scattering function would be measured at a fixed angle. A mechanical lock insured this angle would be maintained. An initial selection of a relatively small scattering angle of 15° from the incident beam would provide a high signal level and prevent the exit light beam from impinging on the supporting members of the DOOM package framework. Sensitivity of the scattering receiver had been improved by a slight enlargement of the field of view and installation of a more responsive photomultiplier tube. At the 15° angle, signal levels from the first several drops proved to be high even for the clear deeper waters. With this improved sensitivity, measurement of the scattering function at larger angles could be attempted without loss of accuracy in the resulting data. In order to correlate DOOM data with other investigators who nominally measure scattering at larger angles, 30° to 150°, the angle was increased after drop I-4 to an angle of around 30°.

The first three stations of cruise I were located over the deep basin of the Ionian Sea which lies between the islands of Greece to the east and Sicily and Malta to the west. The deep waters in this area of the eastern Mediterranean basin are separated from those of the western basin by the shallow sill at the Straits of Sicily. In this deepest of the Mediterranean basins, DOOM stations were at depths between 2600 and 3600 meters. Conditions were just right during this cruise for placement of the DOOM package on or very near the bottom in every drop. The sea state was generally calm, ship's personnel were competent and worked well with the scientific party, and pingers and PDR's functioned properly.

Drops I-4, I-5, and I-6 were in much shallower water in the vicinity of the sills between Africa and the islands of Malta and Sicily. Station I-4 was located south of Malta in 549 meters of water and was perhaps 30 miles west of the Malta ridge which is the western extremity of the Ionian basin. Station I-6 was situated north of the Silician sill on a plateau at 666 meters which is at the southern most edge of the Tyrrhenian basin. Drop I-5 was lowered to a 1258 meter depth in the depression between the two sills. The major exchange of water between the eastern and western basins takes place through this strait. Nominally the fresher, less saline waters of the western Mediterranean basin traverse the sill at the surface while the denser layers originating in the Northeast area of the eastern basin flow westward across the sill at intermediate depths.

During these early stages of the cruise the normal minor problems with the equipment had developed, as well as some potentially serious failures such as flooding of cables and shorting of underwater connectors which could have resulted in damage of a very serious nature. We were fortunate that these problems usually developed in the latter stages of the drops after the package was on the bottom so that the primary data recorded on the way down was not lost. The exception was drop I-6 where a cable flooded and shorted at a depth of 628 meters about 40 meters from the bottom. We were similarly fortunate that these failures produced no irrepairable damage and that the necessary replacement parts had been included in our inventory.

The next four stations, I-7 through I-10, are spaced across the western basin of the Balearic Sea between Cartagena, Spain, and a location to the southwest of Sardinia. All are over the deep plain at depths in excess of 2600 meters. Station I-7 is located at the eastern edge of the Balearia basin near the terminus of a trough leading to the Tyrrhenian basin. On the morning of 8 April following drop I-10 the LYNCH entered port at Cartagena for refueling. A late afternoon departure would permit a day of liberty in this ancient port city and still allow steaming time to the next station for the regularly scheduled evening drop. However, a brisk gale blowing in from the Atlantic had developed during the day which forced cancellation not only of that nights operations but also of the following night on 9 April.

By the evening of 10 April the seas had abated sufficiently for resumption of operations at a station located at the eastern end of the Strait of Gibraltar. On the subsequent nights of 11 and 12 April drops were made in progressively deeper water in the Atlantic west of the strait. The objective of these tests was to optically detect the dense, high salinity Mediterranean water as it flowed over the sill, sank, and spread into the Atlantic. Since this water was expected to form a layer at around 1200 meters, a criterion for the last station was that the depth exceed this figure by several hundred meters so the layer could be clearly delineated in the deeper Atlantic waters. On the morning of 13 April, after a thorough inspection by a Russian trawler, we entered port at Rota, Spain.

VII CRUISE I DATA PRESENTATION

Optical data for each of the 13 stations are presented as a function of depth in the attenuation profiles of Figures 23 through 35 and in Table IX and as a function of wavelength in the attenuation spectra of Figures 36 through 40 and in Table X.

Parameters selected for graphical illustration in the attenuation profiles are the attenuation coefficient α at a wavelength of 478 nm in the center of the transmission window and the volume scattering function σ at a fixed angle which was 15^{o} for drops I-1 to I-4 and 33^{o} thereafter. The σ is measured at the 436 nm mercury line, so the two parameters are plotted for slightly different wavelengths. Profiles of α at 432 nm, the spectrometer wavelength nearest the Hg line, closely paralleled the 478 nm traces at nearly the same amplitude which tended to clutter the illustration. For the sake of clarity and since a second trace added little additional relevant information, it was decided to plot a profile at but one wavelength. The 478 nm wavelength was selected because it was centered in the transmission window and minimum values of α would be illustrated. For direct comparison of attenuation and scattering at the same wavelength refer to Table IX where α(432 nm) and σ(436 nm) are presented. Also plotted in the profiles is the physical parameter of temperature which in the Mediterranean is considerably different than previously observed in the Atlantic. Temperature minima of from 12 to 13^{o}C were recorded in intermediate waters at depths around 1000 meters. Since surface water temperatures were measured between 14.5 and 16.5^{o}C, the total change in temperature within the water column was of the order of only several degrees centigrade. The amplitude of the small variations found in the temperature structure correspond closely to the resolution of the sensor which is about 0.1^{o}C. Small temperature fluctuations which are shown in the profiles have been correlated to a depth of 750 meters with XBT data taken just prior to the DOOM drop.

Depths at which spectra are selected for processing correspond to regions of characteristic attenuation properties as ascertained from the shape of the attenuation profiles. Spectra from all 13 drops are presented at the selected depths in Table X. One of the 18 wavelengths sampled during a scan may be missing from the spectra due to an instrumental problem which developed during the cruise. Synchronization of the reference signal with the grating drive mechanism would sometimes shift between drops; that is, when the system was stopped and started again, the reference signal would shift by one wavelength. This phase shift resulted in the reference signal replacing a wavelength within the spectrum; a wavelength which might vary from drop to drop due to the irregular performance. Illustrative spectra from the various Mediterranean basins and the Atlantic are presented in Figures 36 through 40.

Profiles of drops I-1, I-2, and I-3 to depths of around 3000 meters in the Ionian of the eastern Mediterranean are presented in Figures 23, 24, and 25. The depth ordinate of each is expanded in the upper 400 meters in order to more clearly illustrate the structure of the surface layers. In drop I-2 the protective cover over the scattering receiver window failed to detach until a 400 meter depth was reached. Although the general trend in the three profiles is for α to drop from high values of from 0.12 to 0.16 m^{-1} at the surface to about 0.06 m^{-1} at 400 meters, there are substantial differences in the character of both the attenuation and temperature traces in these surface waters. In drop I-1, α decreases rapidly at around 100 meters from a surface value of 0.16 m^{-1} to a secondary plateau at about 0.09 m^{-1}. This plateau lies between 100 and 300 meters and corresponds to a region of nearly constant temperature. In drop I-2, α climbs to a small peak of 0.13 m^{-1} at 50 meters which lies in an isothermal layer between 25 and 75 meters. It then decreases to the 0.06 m^{-1} value by around 150 meters. In drop I-3 the temperature profile becomes quite complicated with two narrow peaks near the surface and an inversion around 175 meters. The α profile reflects the layered thermal structure with an off-scale peak at 40 meters, a broad minimum centered at 125 meters, and a secondary peak corresponding to the temperature minimum at 175 meters. Below 400 meters, α for all three profiles falls gradually to a value of around 0.04 m^{-1} near the bottom. Temperature reaches a minimum around 13.2°C at 1000 meters and then gradually increases to about 13.8°C at the bottom. Scattering profiles generally reflect the same characteristics as the α curves. Values of σ drop from 0.12 to 0.14 m^{-1} $ster^{-1}$ at the surface to about 0.03 m^{-1} ster at 400 meters and then drop continuously to around 0.01 m^{-1} $ster^{-1}$ at the bottom. Attenuation profiles in the Ionian basin then appear quite uniform in the intermediate and deep water below 400 meters but vary considerably with physical parameters in the surface and transition layers of the upper 400 meters.

Stations I-4, I-5, and I-6 were located in the shallow waters south and west of Sicily in the sill area between Africa and Italy. Exchange of water between the eastern and western Mediterranean basins takes place across this sill area, so the water column is highly structural as evidenced by the thermal profiles of drops I-4 and I-5. The attenuation profile at station I-4, which was located just west of the Malta sill is similar to those of the earlier drops in the Ionian Sea in that α drops from 0.15 m^{-1} at the surface to about 0.6 m^{-1} between 200 and 400 meters. Attenuation then increases slightly towards the bottom. Superimposed on this general shape are smaller fluctuations in α that are attributed to the layered nature of the water. Values of σ, 0.13 m^{-1} $ster^{-1}$ at the surface and 0.04 m^{-1} $ster^{-1}$ at 400 meters, are in agreement with the earlier Ionian measurements. At station I-5, roughly midway between the two sills, attenuation has substantially increased throughout the entire water column. From a surface value of 0.26 m^{-1}, α generally decreases to 0.09 m^{-1} at 400 meters and remains essentially constant until near the bottom where it increases to just over 0.10 m^{-1}. A

comparison of σ with previous drops is not possible because the scattering angle was increased from 15° to 33°. The σ curve is incomplete near the surface due to off-scale deflections in α at 432 nm which must be used in the calculation of σ. Station I-6 although still in shallow water is north of the Sicilian sill near the edge of the Tyrrhenian basin. The thermal discontinuities of the previous two drops have generally disappeared with the exception of a major inversion centered at around 40 meters. This inversion corresponds to very high attenuation which produced off scale deflections in α signals. With the exception of this peak, α values were similar to those of drop I-5, dropping from 0.24 m^{-1} at the surface to around 0.10 m^{-1} at 200 meters and then rising slightly near the bottom. Also consistent was the value of σ of about 0.015 m^{-1} $ster^{-1}$ in the deeper, less turbid waters. Surface σ's of over 0.15 m^{-1} $ster^{-1}$ are somewhat confused due to off-scale data. Flooding of an electrical cable ruined data taken below 628 meters.

Drops I-7, I-8, I-9, and I-10 were all made to depths of around 2600 meters in the Balearic basin between the southern tip of Sardinia and the southeast coast of Spain. The α profile of I-7, which has a value of 0.25 m^{-1} at the surface, goes off scale near the base of a thermocline at about 50 meters and then levels off at 0.12 m^{-1} between 100 and 200 meters. So far it closely resembles the profile of drop I-6. However, at 300 meters there is a drop in temperature and an accompanying drop in α to about 0.06 m^{-1}. Then the curve varies in an irregular fashion between 0.05 and 0.07 m^{-1} until the bottom is reached at 2600 meters. There is a significant increase in α between the minimum of 0.05 m^{-1} at 1700 meters and the small peak of 0.075 m^{-1} at 1900 meters. This positive slope on the α profile happens to correspond to the depth of a trench connecting the Tyrrhenian and Balearic basins and perhaps then is caused by lateral transport of sediments flowing along the bottom of the trench. Profiles of drops I-8, I-9, and I-10 are characterized by high surface attenuation and peaks located in the region of the thermocline. Drop I-9 has the highest peak which slams off scale at an α in excess of 0.36 m^{-1}. The curves drop rapidly and level off between 100 and 200 meters but at different values of α which vary from 0.09 m^{-1} to 0.05 m^{-1}. However, below 200 meters α soon drops to about 0.04 m^{-1} and then gradually decreases to about 0.03 m^{-1} until in proximity of the bottom where some small perturbations appear. Values of the scattering function which generally track the σ profile, range from a maximum in the surface waters of 0.06 m^{-1} $ster^{-1}$ to a minima of 0.005 m^{-1} $ster^{-1}$ in the deep waters. There are two temperature minima; the first at around 140 meters, the second at close to 1000 meters. Minimum temperature of around 12.4°C is about a degree below the lowest measured in the eastern basin.

Station I-11 was located in the Alboran Sea about 25 miles east of the Strait of Gibraltar. The high attenuation in the surface layer drops from 0.4 m^{-1} at the surface to 0.12 m^{-1} at 50 meters. This layer consists of the lower salinity Atlantic ocean water which flows on the surface through the strait into the Mediterranean.

After some minor α excursions in the next 100 meters which correspond to thermal fluctuations, the profile decreases gradually to a minimum of 0.06 m^{-1} at 420 meters. Here it increases rapidly to 0.16 m^{-1} and remains at a high level to the bottom. The σ curve increases just as drastically from a minimum of 0.016 to around 0.04 m^{-1} $ster^{-1}$. This turbid bottom layer is perhaps the Levantine current which flows westward through the Mediterranean into the Atlantic and which has accumulated bottom sediments while crossing over the 500 meter ridge at the western end of the Alboran basin some 100 miles to the east. The intermediate water between 200 and 400 meters is also more turbid than the waters to the east; minimum values of α and σ are respectively 0.06 m^{-1} and 0.016 m^{-1} $ster^{-1}$ as compared to 0.04 m^{-1} and 0.005 m^{-1} $ster^{-1}$ in the Balearic Sea.

Stations I-12 and I-13 were located in the Atlantic Ocean approximately 60 and 120 miles respectively due west of Gibraltar. The primary test objective was to investigate optically the outflow of denser, more saline Mediterranean water as it sank and spread into the Atlantic. Although surface attenuation was expected to be high, the difference between the Mediterranean layer and the intermediate Atlantic water might not be large, so system gain was set to detect the smaller change and risk sacrifice of data from the surface waters. Surface attenuation to a depth of 50 meters proved to have an α above 0.36 m^{-1} which indeed was off-scale. In drop I-12, α drops to about 0.06 m^{-1} at 100 meters and then declines gradually to a minimum of 0.05 m^{-1} at 500 meters with the exception of a slight peak at 300 meters which corresponds to a minor irregularity in the temperature profile. Temperature also reaches a minimum of 10.5°C at 500 meters. From this minimum, α increases sharply and continues to rise to a value of 0.11 m^{-1} on the bottom at 673 meters. Temperature also increases to 12.4°C at the bottom. This rise in both attenuation and temperature below 500 meters delineates the Mediterranean water which has flowed through the strait and has spilled down the western continental slope seeking a level where its density matches that of the Atlantic water. Some mixing with clearer intermediate Atlantic water has perhaps reduced the level of attenuation below that found in the turbid layer near the bottom east of Gibraltar. Bottom temperatures of 12.4°C are however identical in both cases. Further to the west in the profile of drop I-13, there are two turbidity layers at depths of 260 and 400 meters; but these are associated with the thermocline and are strictly a function of the physical parameters of the Atlantic water. The Mediterranean water is seen as the attenuation peak centered at about 1330 meters. Mixing with Atlantic water has reduced both the α and temperature of the layer. That it has sunk to a level matching its own density is evident from the much cooler and clearer Atlantic water which is present below the layer.

In the Mediterranean Sea evaporation greatly exceeds fresh water intake by precipitation and run off, so there is a net inflow of Atlantic water through the strait of Gibraltar. This less saline Atlantic water flows in on the surface, is rapidly mixed with the Mediterranean surface water, and then flows generally eastwardly

throughout the entire Mediterranean basin. High density saline water forms in the eastern basin and spreads westwardly at intermediate depths spilling through the strait of Gibraltar along the bottom. It was thought that perhaps these various water types could be distinguished by their spectral characteristics. Although amplitude of the attenuation spectra varied over a wide range, spectral differences were not sufficient to provide conclusive identification of water type. Perhaps vertical mixing rates are large enough to mask any distinct spectral features peculiar to a particular water mass. Nevertheless we will examine examples of attenuation spectra from the various basins in the next several illustrations, Figures 36 through 40.

Selected spectra from drop I-3 in the eastern Mediterranean basin are presented in Figure 36. The two highest spectra from the surface waters at 5 and 75 meters flank an even higher level of turbidity at around 45 meters which produced off-scale deflection. Attenuation then dropped rapidly in a clear water layer between 100 and 140 meters, almost doubled in a more turbid region from 150 to 250 meters, and then cleared steadily with depth. All spectra exhibit the characteristic minimum at 485 nm and a weak absorption between 510 and 520 nm which in this drop is somewhat obscured by the missing wavelength at 515 nm. The major variation in spectra shape takes place on the short wavelength side of the window. Spectra from the more turbid surface waters have a stronger relative attenuation at the shorter wavelengths than do those from the clearer deep waters.

Spectra from drop I-8 in the western Mediterranean basin are presented in Figure 37. Attenuation in the surface layers is generally slightly higher than found in the eastern basin while attenuation in the deep water may run a little less. The 54 meter spectrum corresponds to the peak of a turbidity layer. Shape of the spectra is essentially the same as found in the eastern basin with the window centered at a wavelength of 485 nm. The one spectrum which differs somewhat is within the turbidity layer at 54 meters and exhibits a relatively high attenuation at shorter wavelengths.

At station I-11 just east of Gibraltar in the Alboran Sea, the surface spectrum at 9 meters, Figure 38, although larger in magnitude, possessed a signature quite representative of the surface waters to the east. Below the surface layer attenuation dropped steadily, reaching a minimum at 381 meters. The 381 meter spectrum, although a little higher in amplitude, has the characteristic shape of the previous deep water spectra. Spectra at 497 and 578 meters are from the turbidity layer at the bottom. Their shape does not significantly differ from other spectra within the Mediterranean which are at the same general level of attenuation.

In drop I-13 in the Atlantic west of Gibraltar, surface spectra were off scale. Spectra at 150 meters and 280 meters lie below the high turbidity surface region and are in the intermediate waters

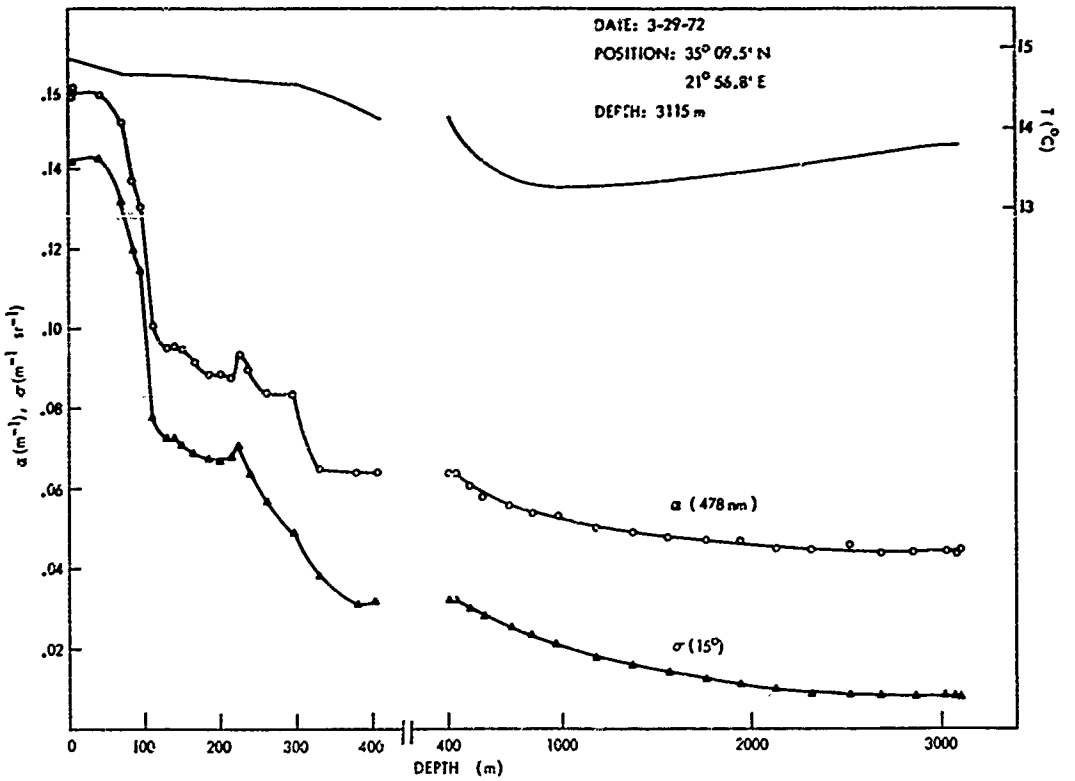

FIG. 23 OPTICAL ATTENUATION, OPTICAL SCATTERING, AND TEMPERATURE PROFILES OF DROP I-1.

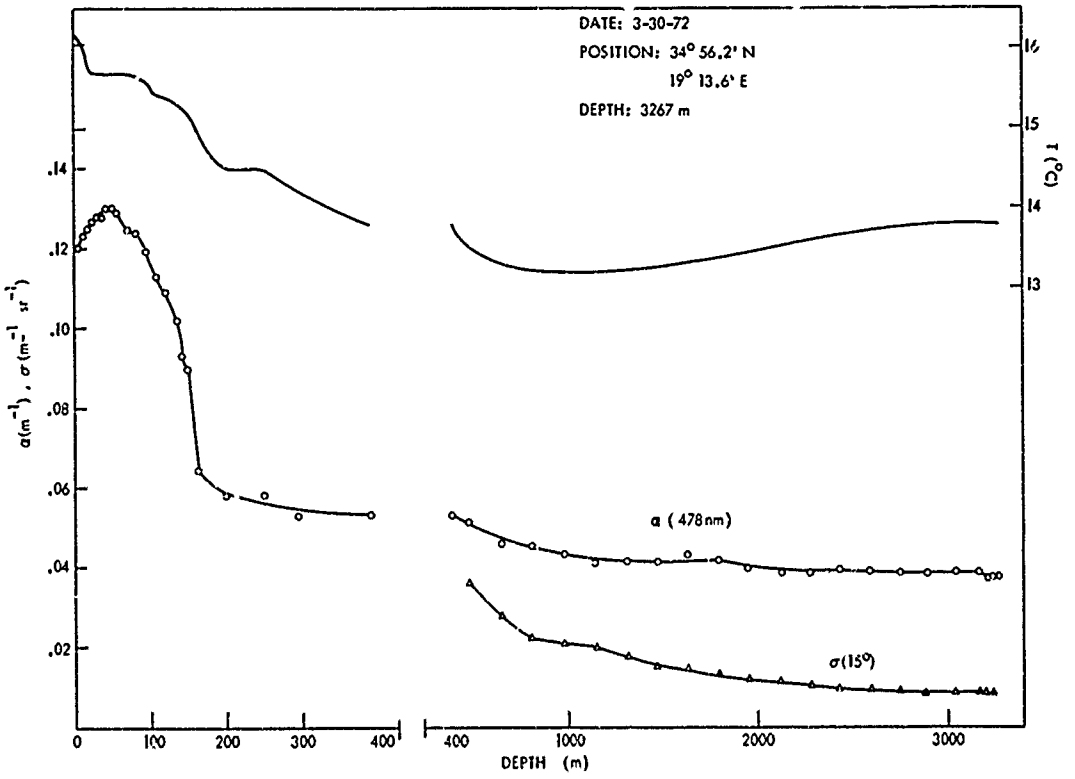

FIG. 24 OPTICAL ATTENUATION, OPTICAL SCATTERING, AND TEMPERATURE PROFILES OF DROP I-2.

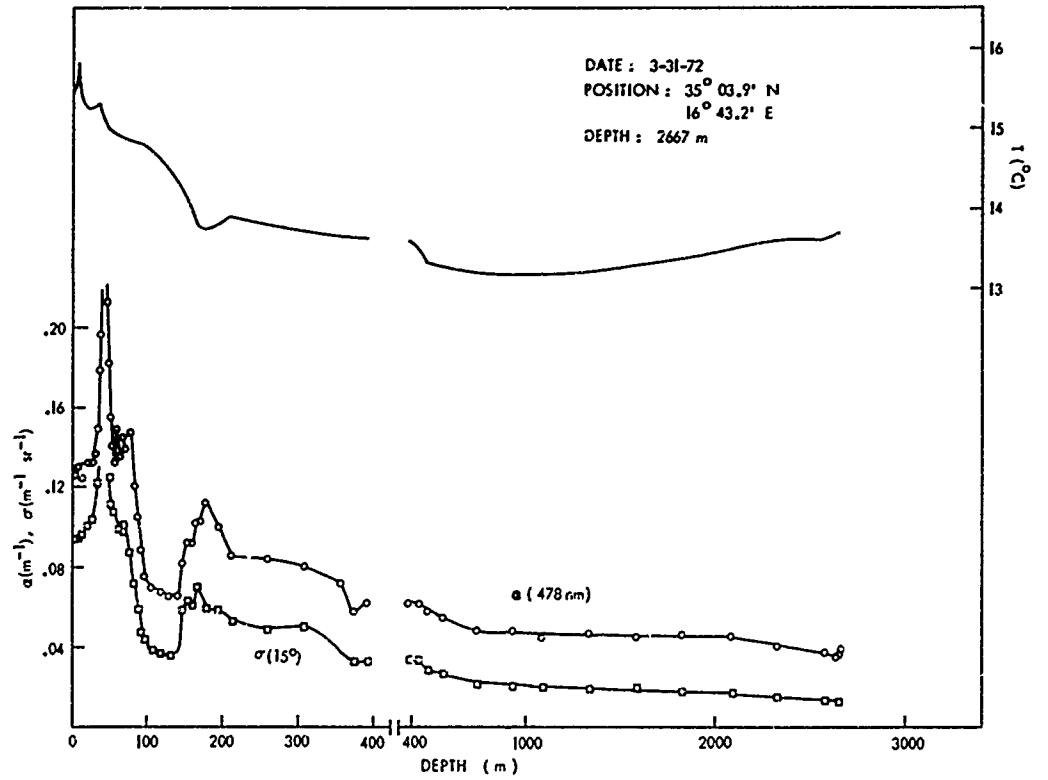

FIG. 25 OPTICAL ATTENUATION, OPTICAL SCATTERING, AND TEMPERATURE PROFILES OF DROP I-3.

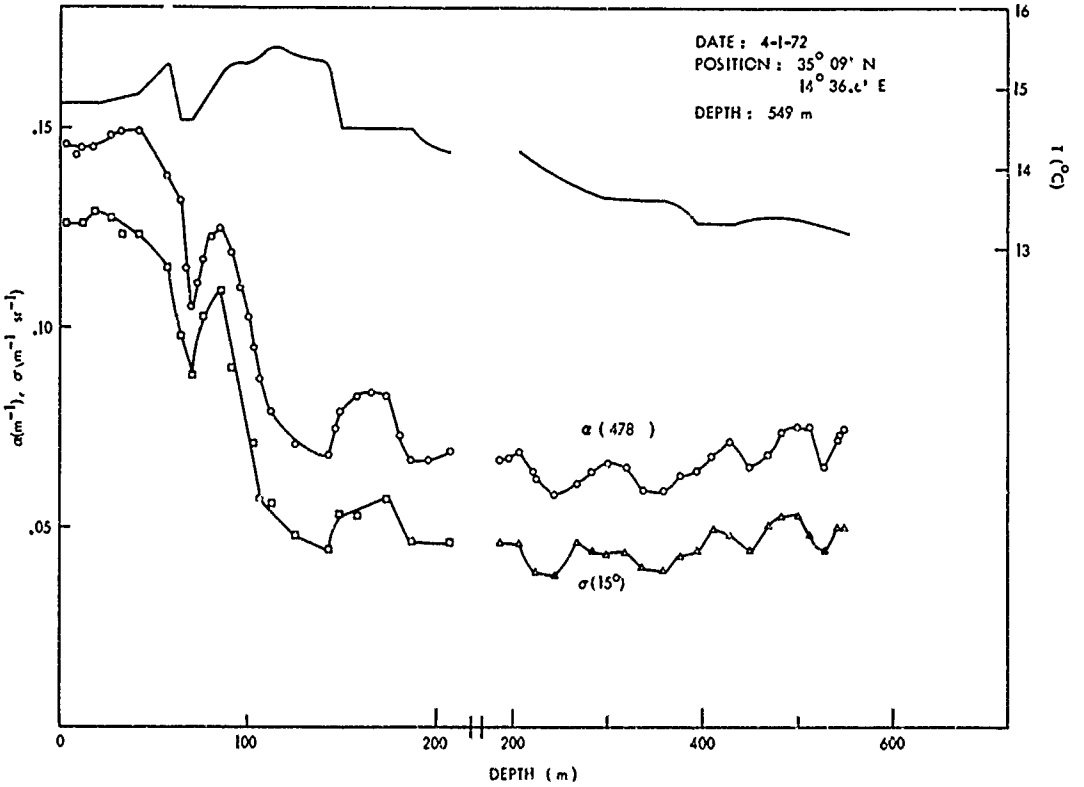

FIG. 26 OPTICAL ATTENUATION, OPTICAL SCATTERING, AND TEMPERATURE PROFILES OF DROP I-4.

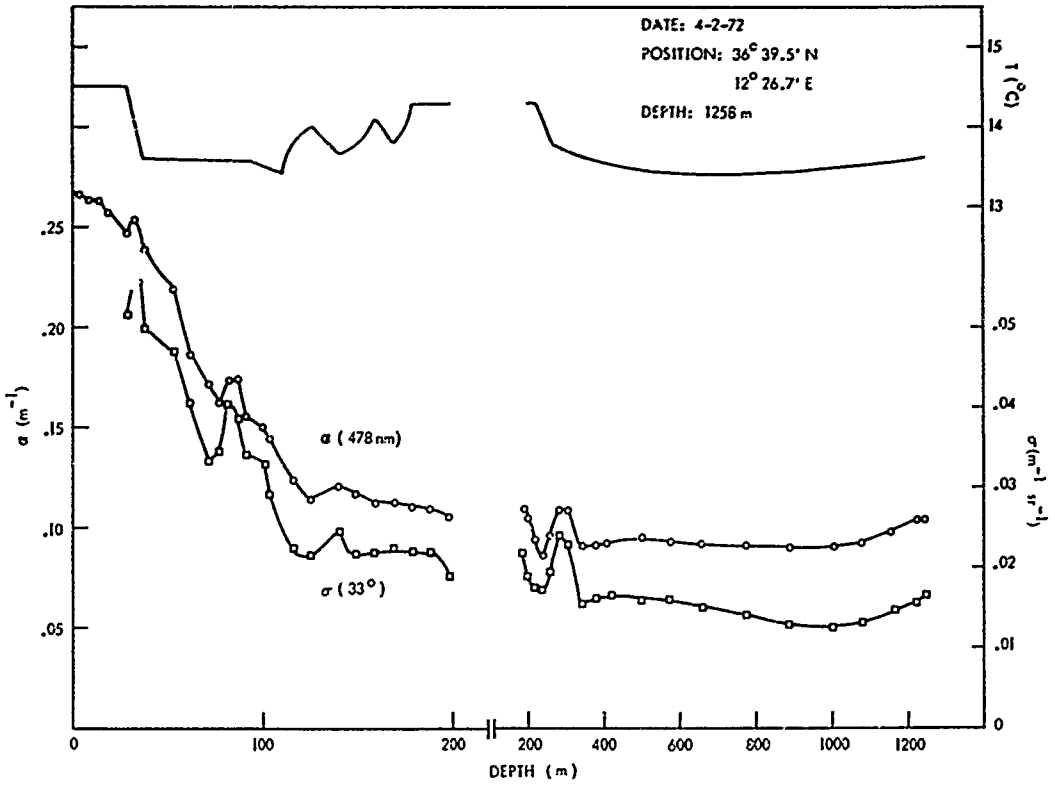

FIG. 27 OPTICAL ATTENUATION, OPTICAL SCATTERING, AND TEMPERATURE PROFILES OF DROP I-5.

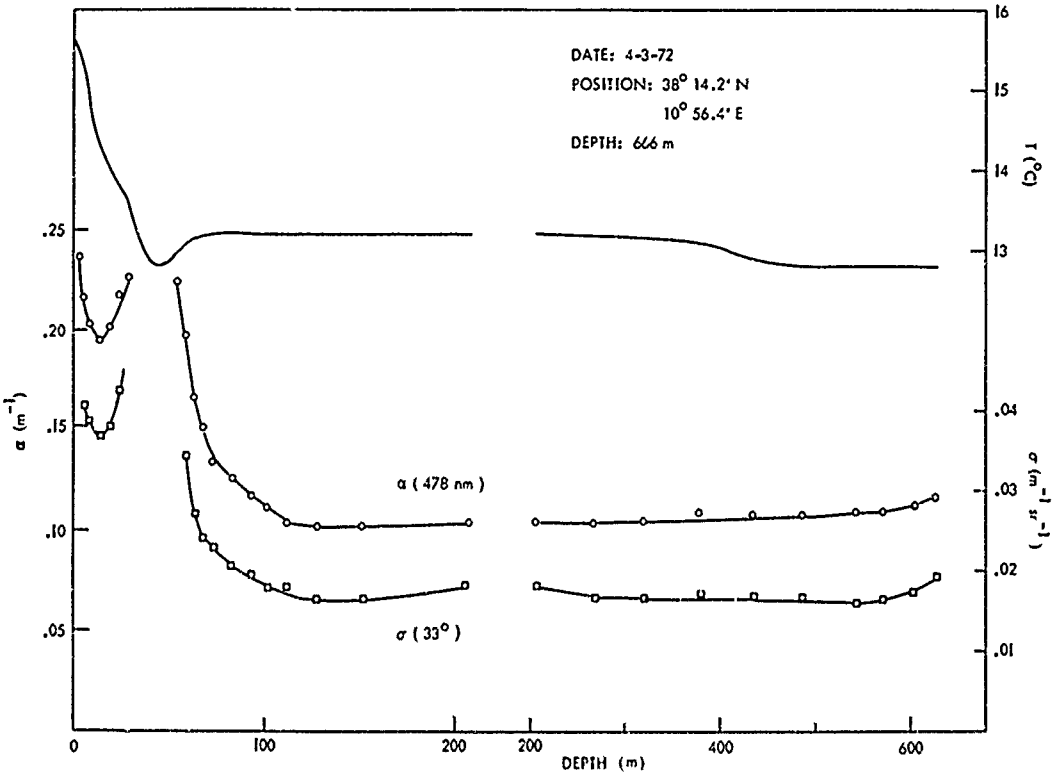

FIG. 28 OPTICAL ATTENUATION, OPTICAL SCATTERING, AND TEMPERATURE PROFILES OF DROP I-6.

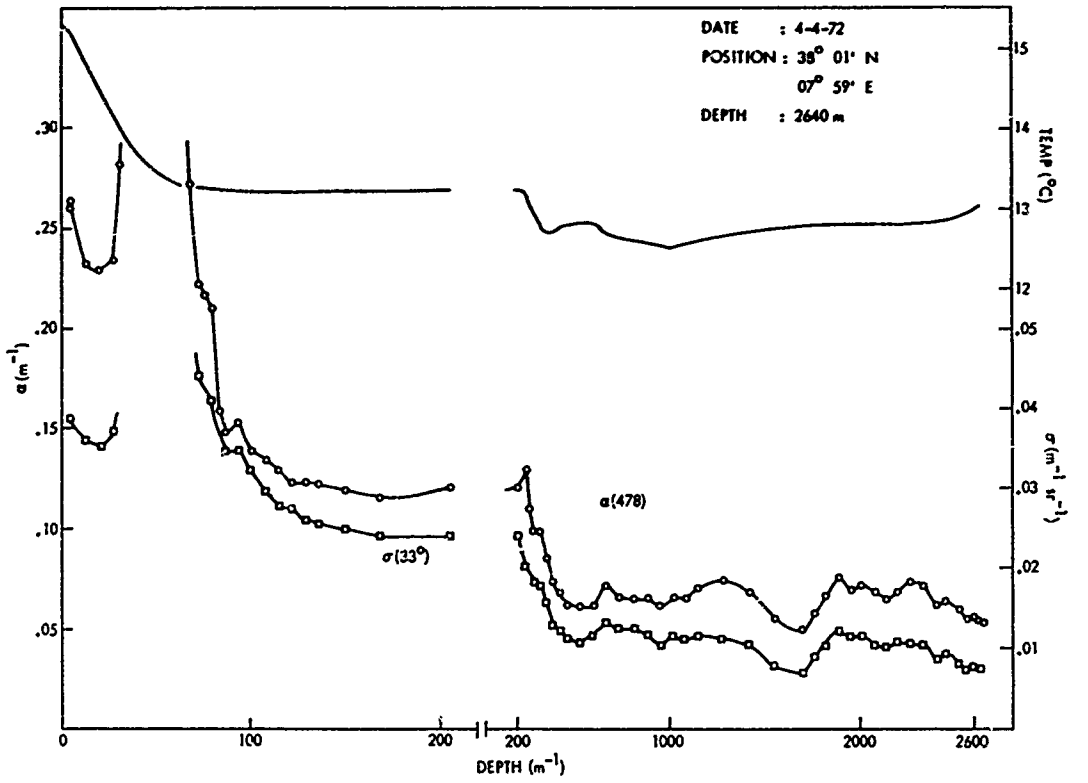

FIG. 29 OPTICAL ATTENUATION, OPTICAL SCATTERING, AND TEMPERATURE PROFILES OF DROP I-7.

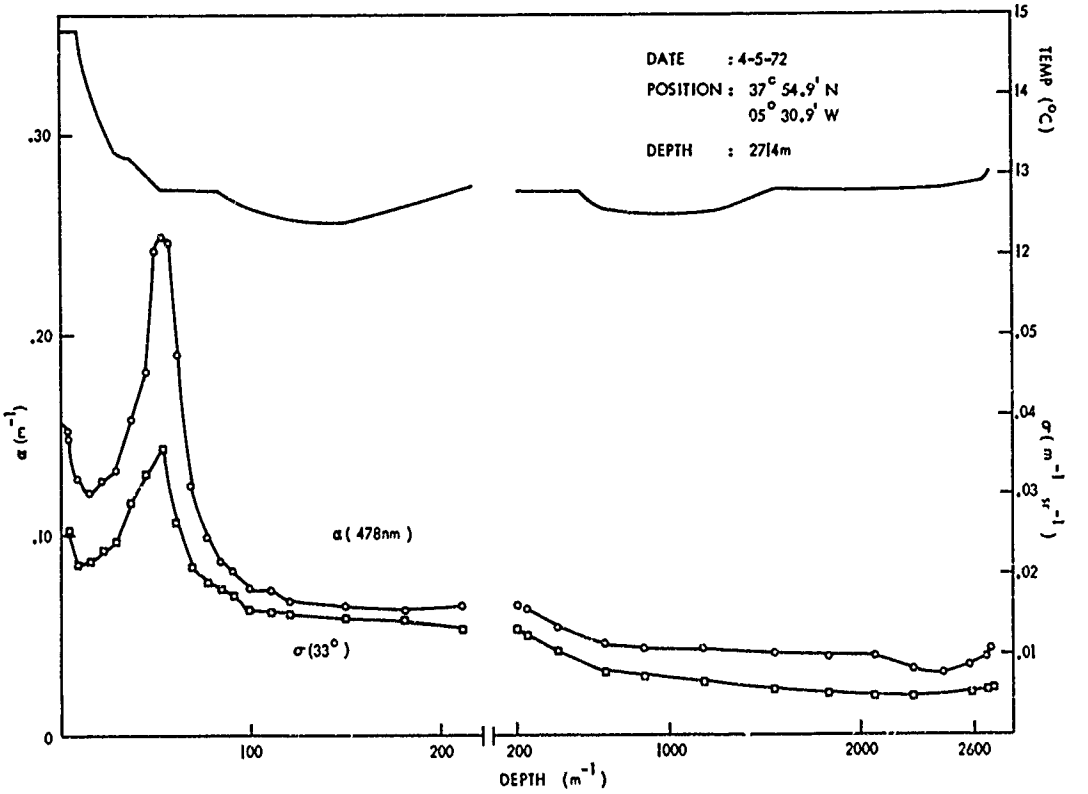

FIG. 30 OPTICAL ATTENUATION, OPTICAL SCATTERING, AND TEMPERATURE PROFILES OF DROP I-8.

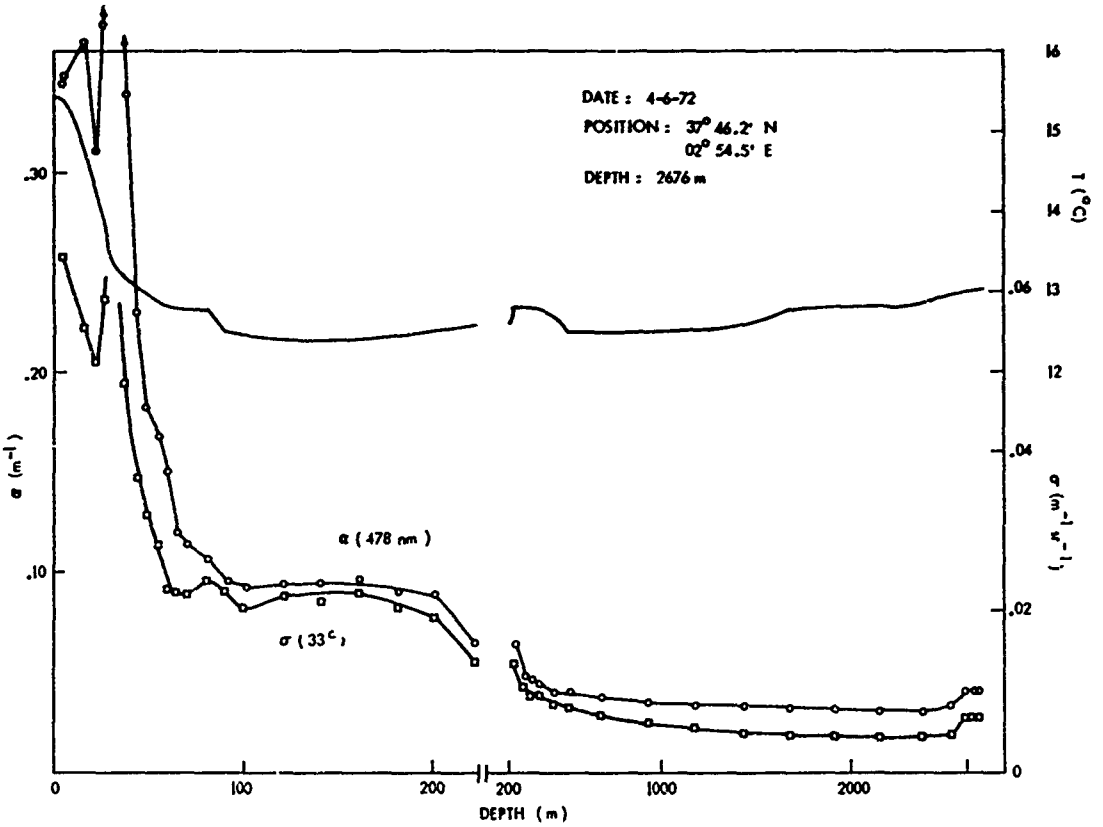

FIG. 31 OPTICAL ATTENUATION, OPTICAL SCATTERING, AND TEMPERATURE PROFILES OF DROP I-9.

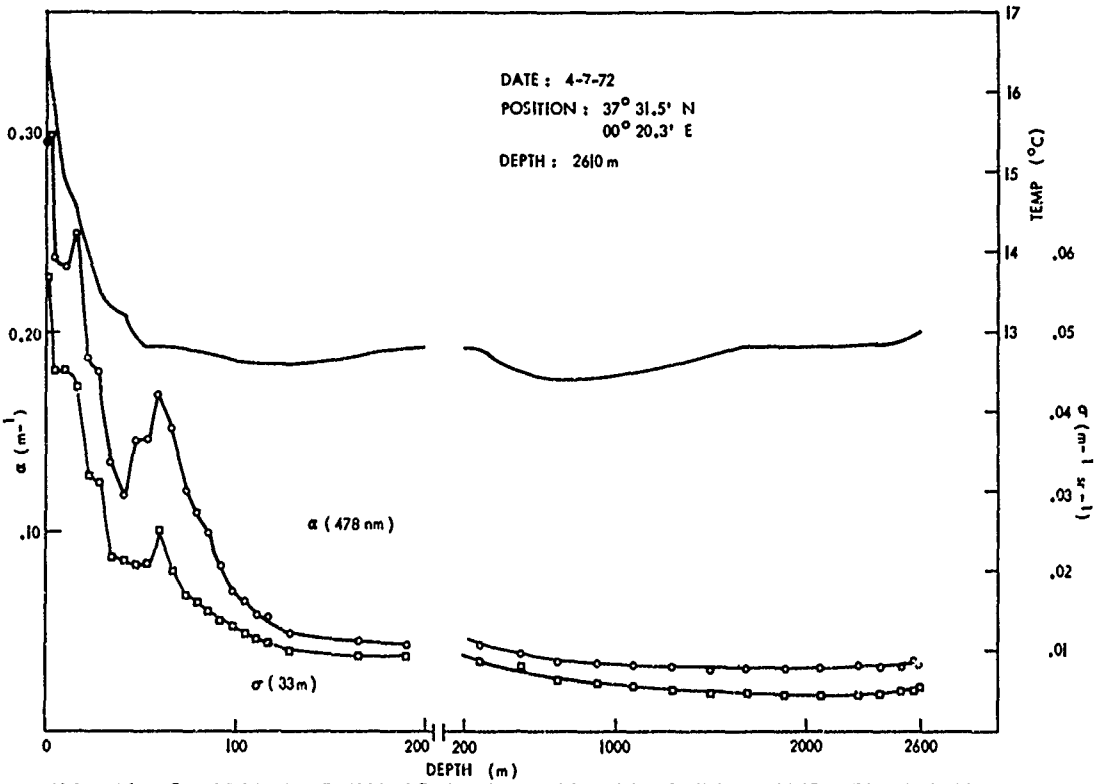

FIG. 32 OPTICAL ATTENUATION, OPTICAL SCATTERING, AND TEMPERATURE PROFILES OF DROP I-10.

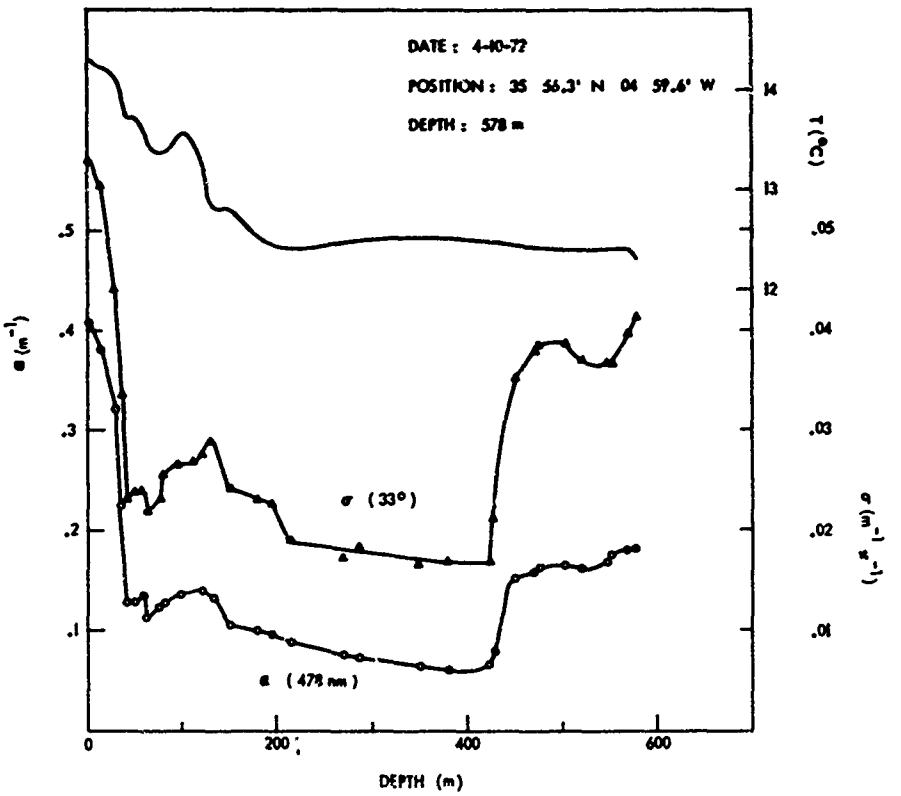

FIG. 33 OPTICAL ATTENUATION, OPTICAL SCATTERING, AND TEMPERATURE PROFILES OF DROP I-11.

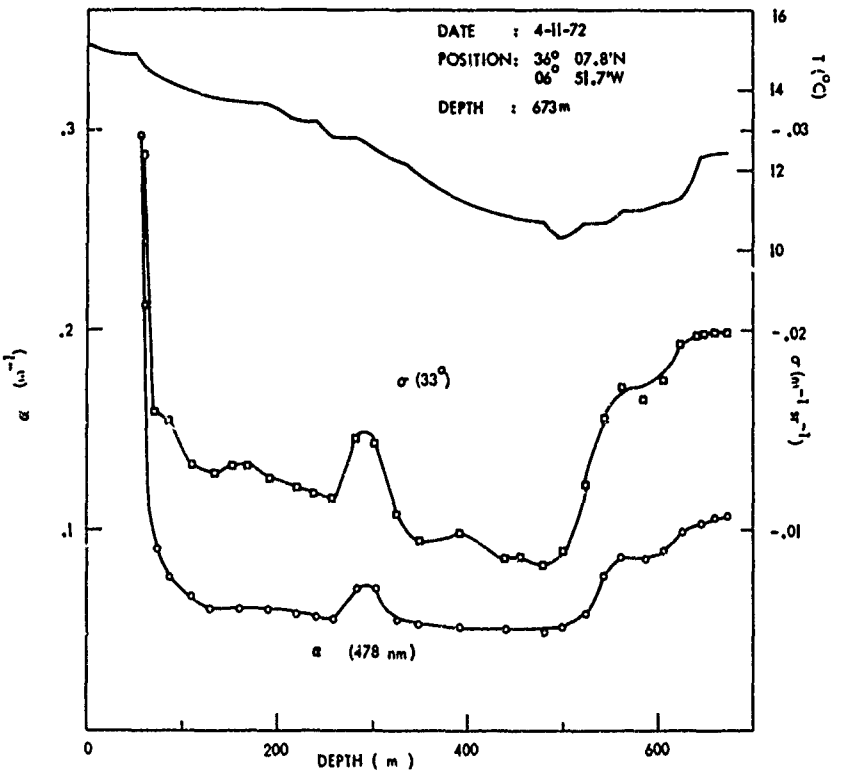

FIG. 34 OPTICAL ATTENUATION, OPTICAL SCATTERING, AND TEMPERATURE PROFILES OF DROP I-12.

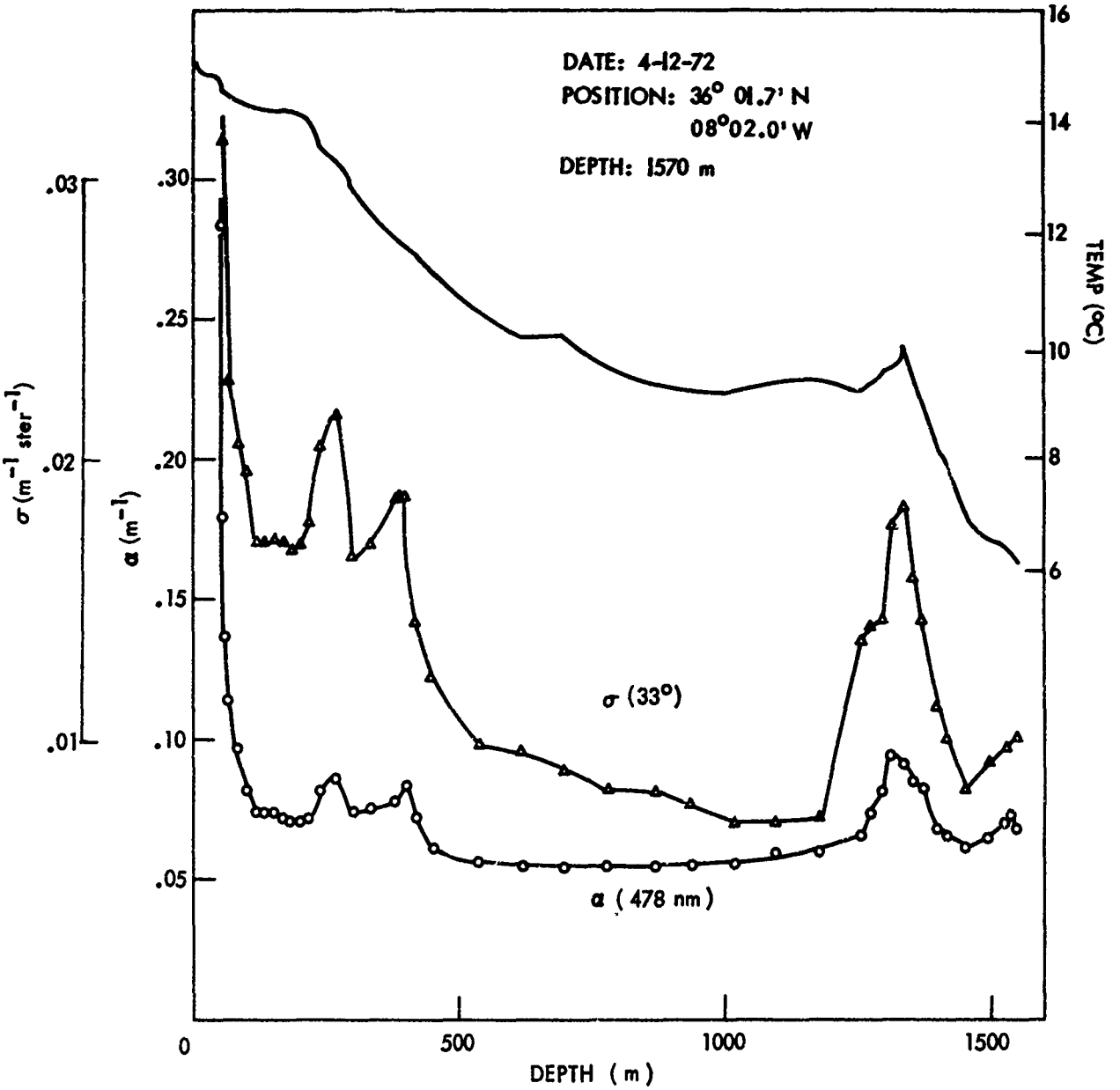

FIG. 35 OPTICAL ATTENUATION, OPTICAL SCATTERING, AND TEMPERATURE PROFILES OF DROP I-13.

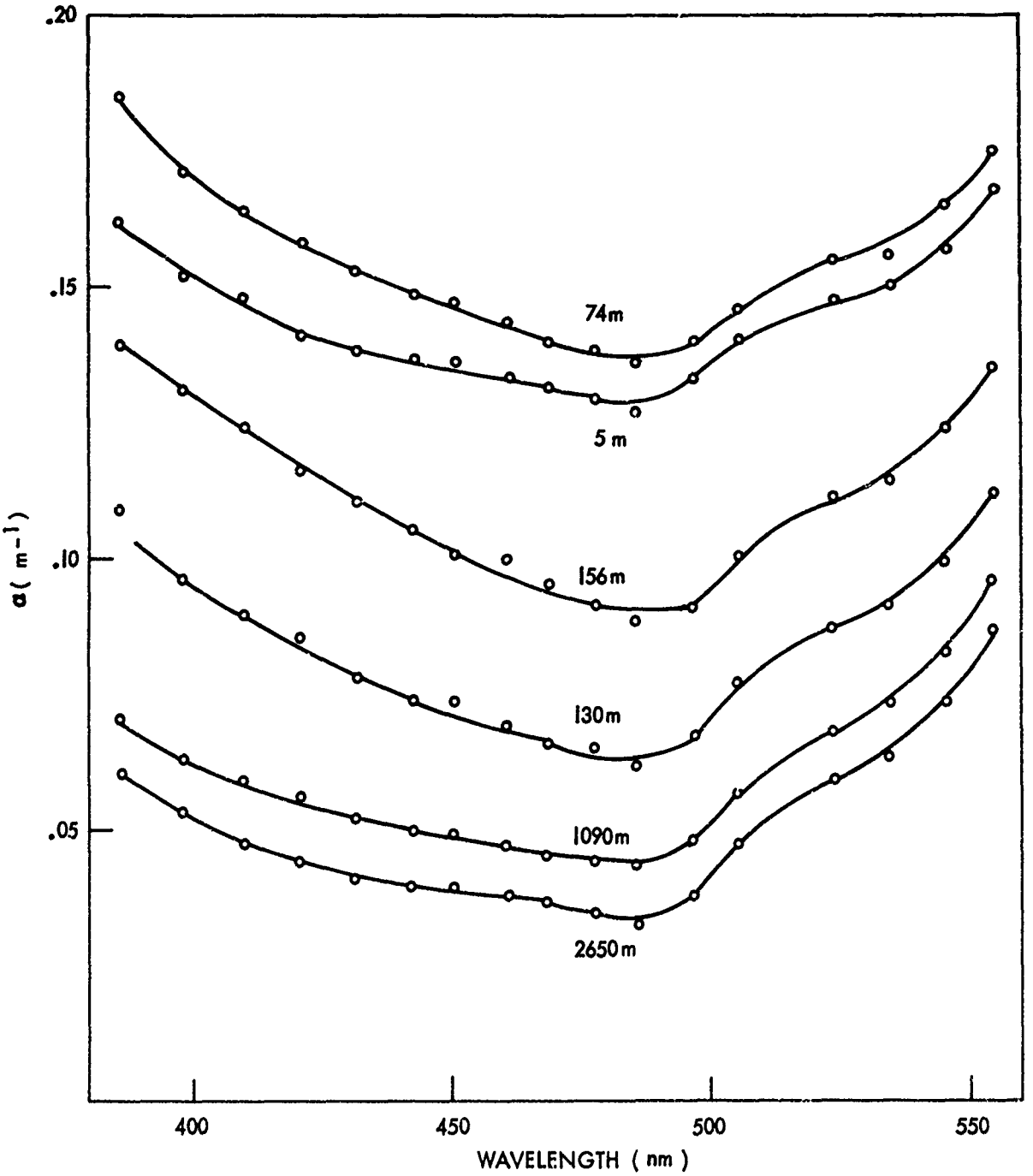

FIG. 36 OPTICAL ATTENUATION SPECTRA FROM DROP I-3 AT SELECTED DEPTHS.

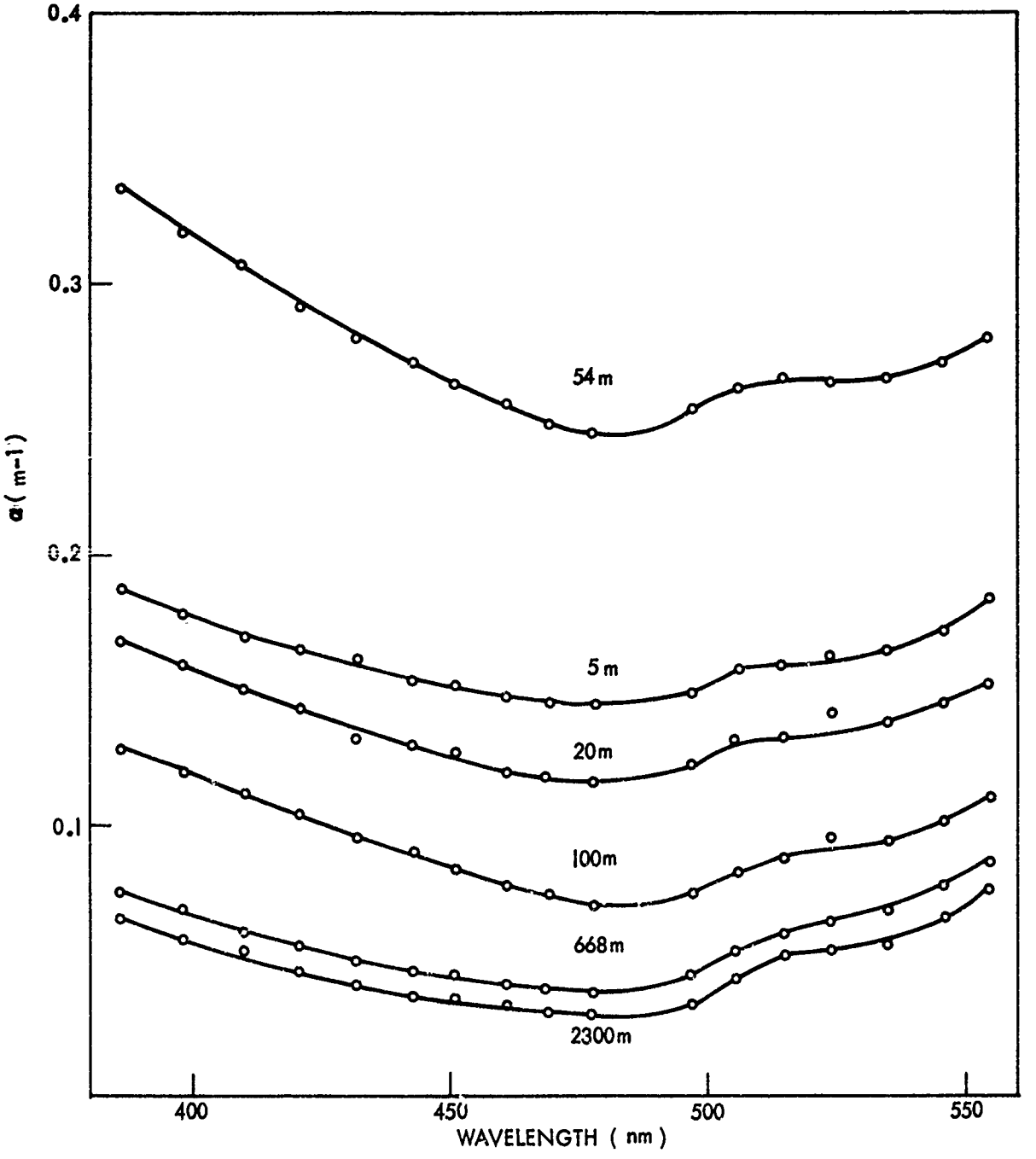

FIG. 37 OPTICAL ATTENUATION SPECTRA FROM DROP I-8 AT SELECTED DEPTHS.

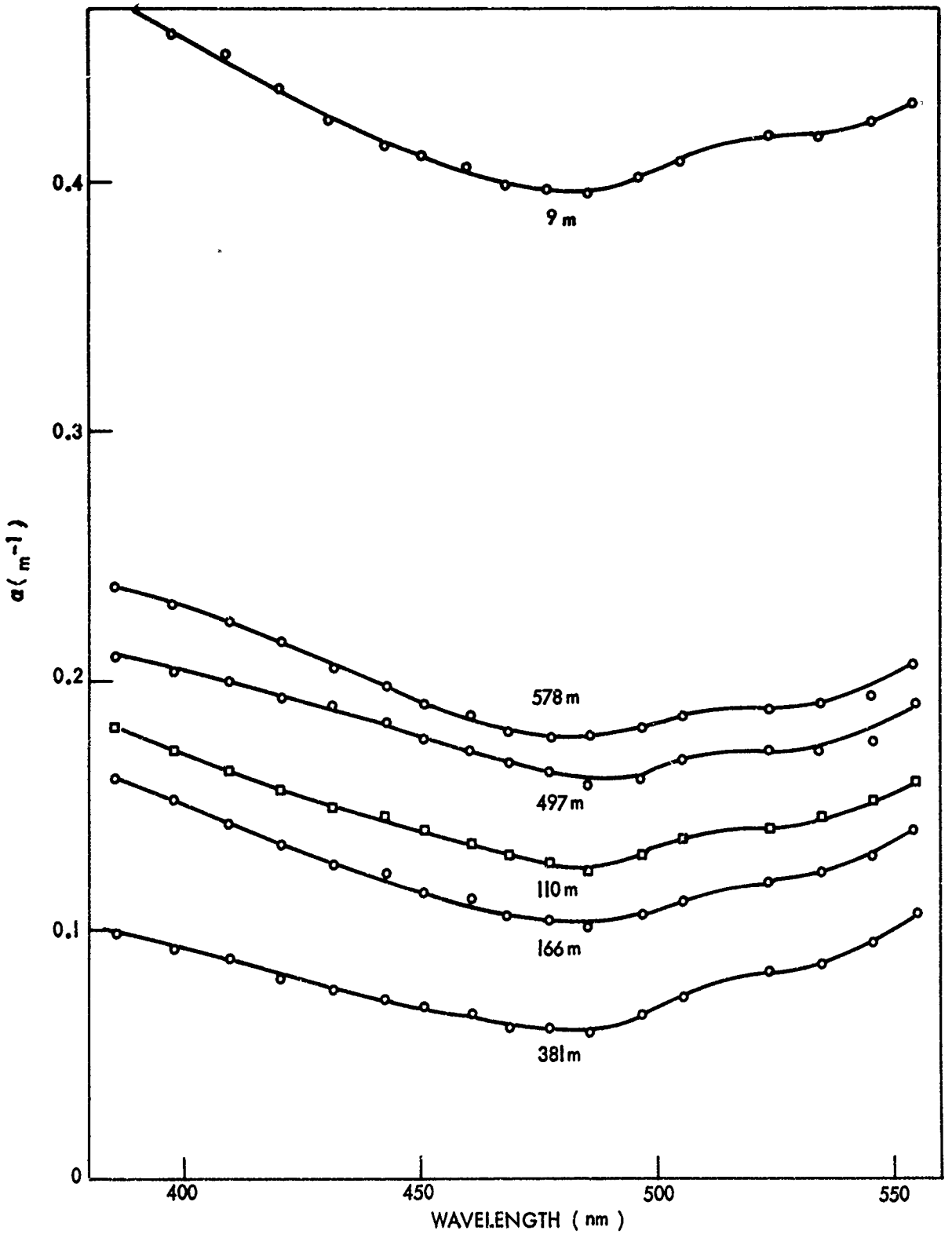

FIG. 38 OPTICAL ATTENUATION SPECTRA FROM DROP I-II AT SELECTED DEPTHS.

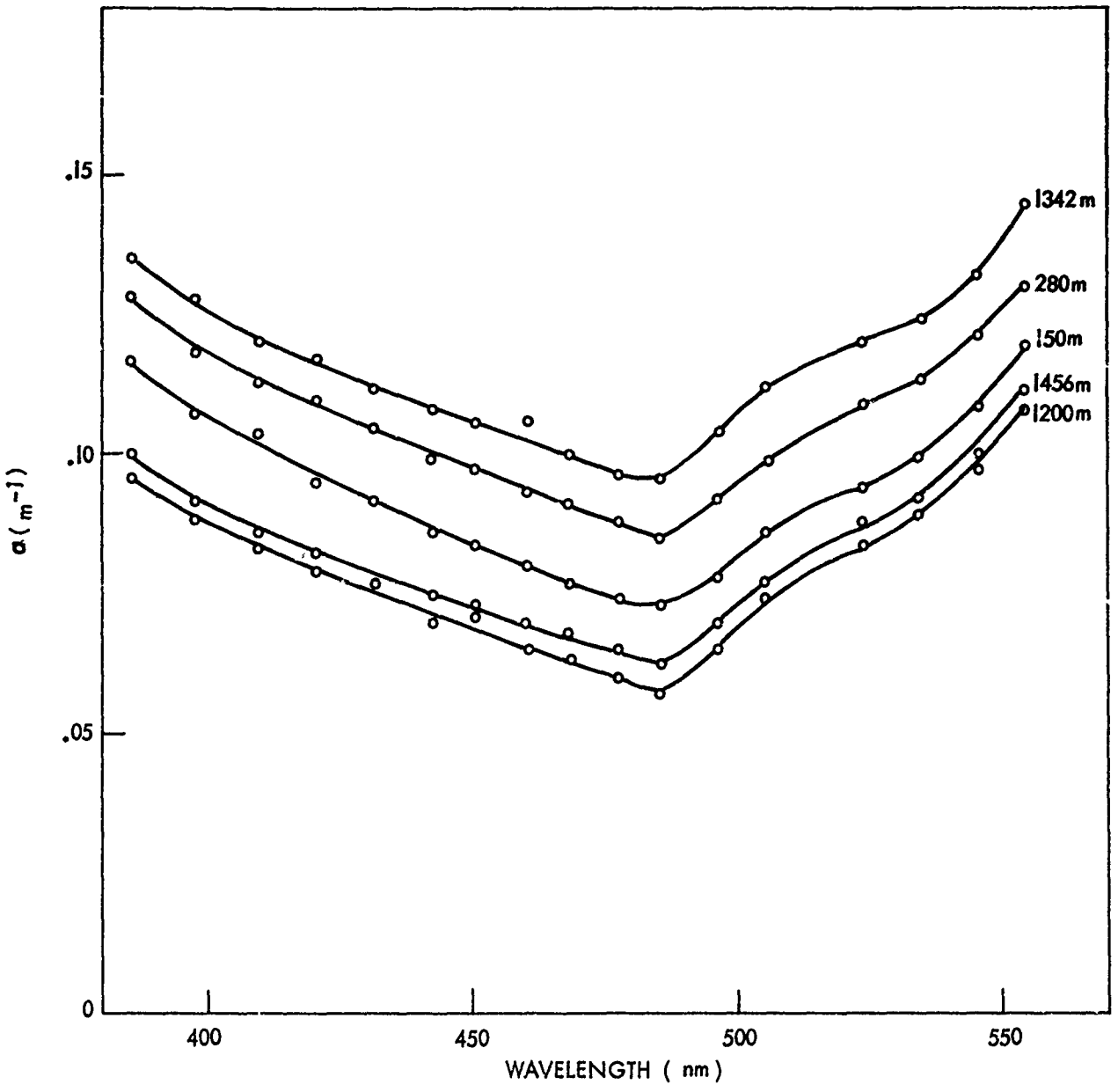

FIG. 39 OPTICAL ATTENUATION SPECTRA FROM DROP I-13 AT SELECTED DEPTHS.

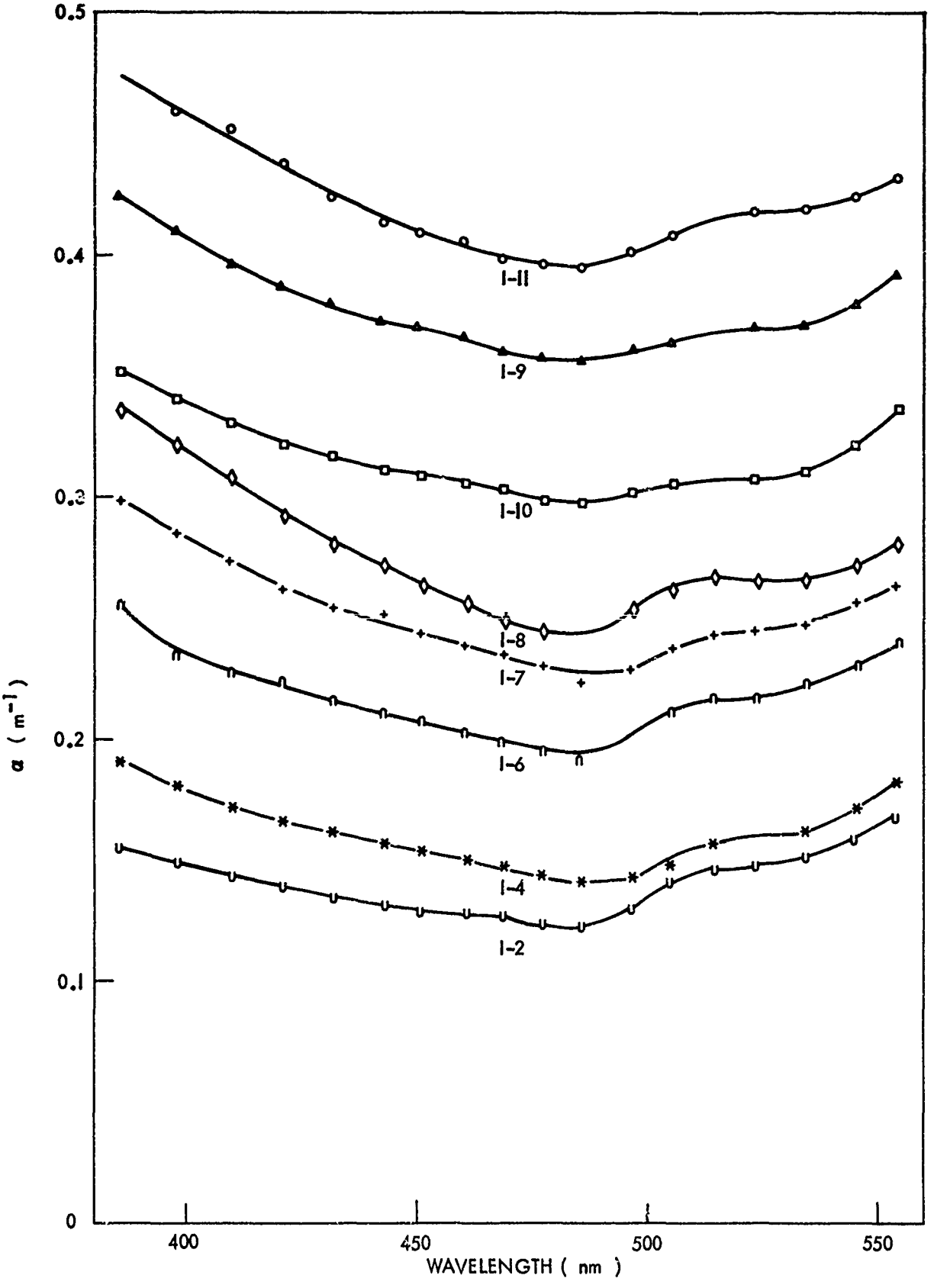

FIG. 40 OPTICAL ATTENUATION SPECTRA FROM SURFACE WATERS OF THE MEDITERRANEAN STATIONS.

TABLE IX

PROFILES OF ATTENUATION AND SCATTERING FOR CRUISE I

Drop I-1

Depth (m)	α(432 nm) (m^{-1})	$\sigma(15^{o})$ (m^{-1} sr^{-1})
5	.172	.139
40	.174	.143
71	.163	.132
83	.149	.120
96	.143	.115
110	.110	.078
128	.106	.073
138	.107	.073
148	.106	.071
166	.102	.069
186	.100	.068
201	.100	.067
213	.099	.068
225	.104	.071
237	.103	.064
261	.097	.057
297	.094	.049
332	.079	.038
380	.072	.031
403	.072	.032
439	.071	.032
510	.069	.030
582	.066	.028
712	.064	.025
843	.063	.024
974	.059	.021
1176	.056	.018
1366	.055	.016
1556	.053	.015
1758	.053	.013
1936	.054	.011
2126	.050	.0097
2316	.051	.0088
2518	.051	.0088
2684	.050	.0087
2863	.049	.0088
3029	.050	.0087
3088	.049	.0087
3100	.053	.0086

TABLE IX (Continued)

PROFILES OF ATTENUATION AND SCATTERING FOR CURISE I

Drop I-2

Depth (m)	α(432 nm) (m^{-1})	$\sigma(15^{o})$ (m^{-1} sr^{-1})
5	.129	-
11	.128	-
17	.135	-
23	.136	-
30	.137	-
42	.139	-
49	.140	-
56	.139	-
69	.138	-
82	.135	-
95	.131	-
108	.125	-
122	.120	-
136	.111	-
150	.102	-
165	.081	-
201	.071	-
297	.061	-
392	.061	-
475	.059	.036
653	.053	.027
819	.051	.022
986	.048	.021
1152	.047	.019
1318	.046	.017
1484	.044	.015
1639	.045	.014
1805	.046	.013
1960	.044	.011
2126	.042	.011
2292	.042	.010
2447	.042	.0091
2601	.041	.0090
2756	.043	.0088
2898	.044	.0080
3053	.043	.0083
3171	.042	.0080
3219	.041	.0080
3243	.041	.0080
3267	.047	.0081

TABLE IX (Continued)

PROFILES OF ATTENUATION AND SCATTERING FOR CRUISE I

Drop I-3

Depth (m)	α(432 nm) (m^{-1})	$\sigma(15^{o})$ (m^{-1} sr^{-1})
5	.138	.097
9	.138	.094
13	.136	.096
22	.144	.100
27	.145	.103
35	.174	.122
49	.183	.125
51	.165	.111
55	.151	.108
63	.151	.099
68	.160	.100
70	.154	.097
78	.158	.087
83	.142	.072
88	.115	.059
92	.096	.047
97	.088	.044
107	.084	.039
118	.080	.037
130	.078	.036
148	.102	.059
154	.110	.063
160	.109	.061
166	.120	.070
213	.101	.053
308	.092	.050
392	.071	.033
487	.064	.028
570	.062	.027
748	.053	.022
926	.054	.021
1092	.051	.020
1342	.051	.019
1591	.050	.020
1829	.050	.018
2090	.048	.017
2328	.044	.015
2577	.040	.013
2637	.040	.013
2649	.040	.013

TABLE IX (Continued)

PROFILES OF ATTENUATION AND SCATTERING FOR CRUISE I

Drop I-4

Depth (m)	α(432 nm) (m^{-1})	$\sigma(15^{o})$ (m^{-1} sr^{-1})
3	.163	.126
12	.162	.126
18	.163	.129
27	.165	.127
33	.166	.123
42	.167	.123
57	.156	.115
64	.147	.098
70	.124	.088
76	.138	.103
85	.141	.109
91	.133	.090
103	.104	.071
106	.099	.057
112	.091	.056
125	.087	.048
143	.082	.044
149	.097	.053
158	.099	.053
173	.104	.057
186	.087	.046
207	.080	.046
225	.073	.039
244	.072	.038
268	.072	.047
283	.077	.044
320	.077	.044
338	.072	.039
359	.072	.039
378	.075	.043
396	.077	.044
411	.081	.050
427	.084	.048
451	.078	.044
484	.084	.053
500	.088	.053
512	.088	.048
527	.078	.044
542	.087	.051
549	.086	.049

TABLE IX (Continued)

PROFILES OF ATTENUATION AND SCATTERING FOR CRUISE I

Drop I-5

Depth (m)	α(432 nm) (m^{-1})	$\sigma(33^{o})$ (m^{-1} sr^{-1})
29	.266	.052
38	.265	.050
53	.243	.047
62	.211	.040
72	.194	.033
77	.189	.035
82	.202	.040
87	.198	.039
91	.178	.034
101	.175	.033
111	.162	.029
116	.140	.022
125	.132	.021
140	.138	.025
149	.136	.022
159	.127	.022
169	.130	.022
179	.129	.022
188	.125	.022
222	.108	.017
261	.106	.019
304	.120	.023
343	.100	.016
382	.098	.016
420	.100	.017
503	.103	.016
575	.102	.016
658	.101	.015
774	.100	.014
890	.099	.013
1006	.097	.013
1078	.099	.013
1156	.107	.015
1224	.11	.016
1233	.115	.016
1248	.118	.017
1253	.118	.017

TABLE IX (Continued)

PROFILES OF ATTENUATION AND SCATTERING FOR CRUISE I

Drop I-6

Depth (m)	α(432 nm) (m^{-1})	σ(33°) (m^{-1} sr^{-1})
5	.229	.041
8	.219	.039
14	.215	.037
19	.221	.038
24	.241	.043
59	.205	.034
64	.185	.027
69	.169	.024
74	.158	.023
83	.143	.020
93	.133	.019
102	.122	.018
112	.121	.018
128	.120	.016
152	.116	.016
209	.119	.018
268	.114	.017
320	.115	.017
380	.120	.017
435	.119	.017
488	.119	.017
544	.120	.016
572	.120	.016
603	.123	.017
628	.128	.019

TABLE IX (Continued)

PROFILES OF ATTENUATION AND SCATTERING FOR CRUISE I

Drop I-7

Depth (m)	α(432 nm) (m^{-1})	σ(33°) (m^{-1} sr^{-1})
5	.278	.0386
13	.257	.0360
20	.250	.0353
28	.278	.0372
73	.249	.0439
80	.228	.0412
87	.176	.0347
94	.178	.0347
101	.165	.0325
108	.160	.0298
115	.154	.0278
122	.151	.0276
129	.149	.0260
136	.148	.0256
150	.146	.0249
168	.144	.0240
205	.145	.0240
243	.127	.0202
290	.119	.0182
327	.116	.0177
355	.100	.0159
393	.089	.0130
430	.083	.0123
468	.077	.0112
533	.076	.0109
608	.077	.0118
674	.084	.0132
739	.079	.0125

TABLE IX (Continued)

PROFILES OF ATTENUATION AND SCATTERING FOR CRUISE I

Drop I-7 (Continued)

Depth (m)	α(432 nm) (m^{-1})	σ(33°) (m^{-1} sr^{-1})
814	.080	.0125
889	.077	.0117
954	.073	.0105
1020	.077	.0115
1085	.078	.0112
1151	.081	.0116
1282	.080	.0113
1422	.081	.0106
1554	.064	.0080
1703	.060	.0069
1760	.074	.0089
1825	.077	.0102
1891	.087	.0122
1956	.080	.0113
2012	.083	.0114
2078	.081	.0103
2143	.077	.0102
2200	.085	.0107
2265	.085	.0107
2331	.085	.0104
2396	.073	.0086
2452	.076	.0093
2518	.071	.0080
2565	.067	.0073
2593	.068	.0077
2621	.067	.0075
2630	.066	.0073
2640	.066	.0073

TABLE IX (Continued)

PROFILES OF ATTENUATION AND SCATTERING FOR CRUISE I

Drop I-8

Depth (m)	α(432 nm) (m^{-1})	$\sigma(33^{o})$ (m^{-1} sr^{-1})
5	.164	.0254
10	.151	.0211
16	.135	.0216
23	.150	.0229
30	.158	.0240
38	.192	.0291
46	.231	.0325
54	.283	.0357
60	.208	.0265
70	.146	.0210
78	.123	.0190
85	.114	.0183
92	.106	.0174
100	.098	.0155
111	.096	.0154
121	.089	.0150
151	.083	.0145
182	.080	.0144
212	.080	.0131
263	.077	.0124
415	.069	.0104
668	.055	.0078
870	.050	.0071
1184	.052	.0065
1569	.048	.0055
1843	.049	.0049
2076	.046	.0047
2288	.044	.0046
2592	.046	.0051
2673	.051	.0055
2683	.051	.0053
2693	.058	.0055

TABLE IX (Continued)

PROFILES OF ATTENUATION AND SCATTERING FOR CRUISE I

Drop I-9

Depth (m)	α(432 nm) (m^{-1})	σ(33°) (m^{-1} sr^{-1})
5	.379	.0642
16	.391	.0556
27	.420	.0592
38	.350	.0487
44	.236	.0369
49	.206	.0319
60	.164	.0231
65	.144	.0222
70	.134	.0226
81	.132	.0241
101	.112	.0202
121	.114	.0217
141	.115	.0211
161	.115	.0227
202	.099	.0191
243	.068	.0113
283	.060	.0105
324	.056	.0095
364	.056	.0095
526	.050	.0080
688	.048	.0071
941	.043	.0063
1184	.042	.0055
1438	.042	.0049
1681	.040	.0044
1924	.039	.0043
2146	.039	.0043
2379	.039	.0042
2602	.052	.0066
2632	.052	.0066
2531	.046	.0045
2653	.050	.0066
2673	.050	.0066

TABLE IX (Continued)

PROFILES OF ATTENUATION AND SCATTERING FOR CRUISE I

Drop I-10

Depth (m)	σ(432 nm) (m^{-1})	$\alpha(33^{o})$ (m^{-1} sr^{-1})
2	.317	.0568
5	.256	.0453
11	.259	.0456
17	.266	.0429
23	.206	.0319
29	.206	.0311
35	.157	.0217
42	.144	.0212
48	.164	.0205
54	.174	.0210
60	.202	.0253
67	.168	.0201
74	.140	.0168
80	.129	.0159
86	.117	.0147
92	.102	.0137
99	.090	.0130
105	.086	.0120
111	.078	.0114
117	.077	.0109
129	.068	.0099
165	.064	.0091
190	.062	.0093
293	.056	.0087
496	.050	.0079
708	.046	.0061
911	.046	.0058
1103	.044	.0055
1306	.043	.0051
1498	.042	.0046
1691	.042	.0046
1893	.042	.0043
2086	.043	.0040
2278	.044	.0040
2389	.044	.0043
2511	.044	.0047
2582	.044	.0047
2592	.044	.0048
2602	.046	.0049

TABLE IX (Continued)

PROFILES OF ATTENUATION AND SCATTERING FOR CRUISE I

Drop I-11

Depth (m)	α(432 nm) (m^{-1})	σ(33°) (m^{-1} sr^{-1})
3	.441	.0571
15	.412	.0543
31	.318	.0440
35	.243	.0334
43	.150	.0227
51	.149	.0240
59	.146	.0240
62	.135	.0217
78	.148	.0233
82	.154	.0258
98	.166	.0265
122	.158	.0276
133	.157	.0290
153	.148	.0240
181	.128	.0232
216	.106	.0189
287	.095	.0183
381	.077	.0170
428	.100	.0213
452	.174	.0351
476	.194	.0387
519	.188	.0367
550	.185	.0364
570	.203	.0395
578	.209	.0414

TABLE IX (Continued)

PROFILES OF ATTENUATION AND SCATTERING FOR CRUISE I

Drop I-12

Depth (m)	α(432 nm) (m^{-1})	σ(33°) (m^{-1} sr^{-1})
55	.324	.0409
59	.226	.0288
74	.111	.0159
86	.099	.0155
110	.088	.0132
137	.083	.0128
169	.082	.0131
192	.081	.0125
220	.077	.0121
240	.078	.0118
259	.078	.0115
283	.090	.0146
303	.100	.0142
326	.076	.0108
350	.070	.0094
393	.071	.0098
440	.070	.0085
480	.068	.0082
499	.071	.0089
523	.082	.0122
543	.102	.0156
562	.108	.0171
586	.108	.0164
606	.112	.0175
625	.125	.0193
645	.127	.0197
661	.129	.0198
673	.129	.0198

TABLE IX (Continued)

PROFILES OF ATTENUATION AND SCATTERING FOR CRUISE I

Drop I-13

Depth (m)	α(432 nm) (m^{-1})	$\sigma(33^{o})$ (m^{-1} sr^{-1})
45	.386	.0576
55	.198	.0340
65	.129	.0228
82	.112	.0206
100	.104	.0196
120	.090	.0170
132	.088	.0170
150	.093	.0171
168	.092	.0170
184	.092	.0168
202	.089	.0170
220	.093	.0178
240	.099	.0205
270	.105	.0217
300	.090	.0165
334	.090	.0170
380	.094	.0186
400	.100	.0187
420	.086	.0143
452	.078	.0123
538	.072	.0099
620	.071	.0096
700	.070	.0089
780	.070	.0082
866	.074	.0082
940	.072	.0077
1020	.070	.0080
1100	.074	.0082
1180	.075	.0082
1260	.081	.0136
1276	.089	.0141
1300	.097	.0143
1316	.112	.0177
1342	.112	.0185
1356	.102	.0159
1376	.099	.0143
1400	.087	.0112
1421	.081	.0101
1456	.075	.0082
1503	.080	.0093
1530	.082	.0097
1543	.086	.0098
1550	.087	.0101

TABLE X - ATTENUATION SPECTRA FROM CRUISE I

Drop I-1

Depth (m)	5	22	135	207	410	1070	1760	2520	3030	3100
λ (nm)	Attenuation Coefficient $\alpha(m^{-1})$									
386	.196	.196	.141	.125	.094	.073	.070	.071	.073	.072
398	.188	.189	.133	.117	.087	.069	.063	.061	.062	.063
410	.180	.181	.128	.110	.082	.064	.058	.056	.056	.059
421	.177	.178	.122	.104	.079	.061	.055	.055	.053	.057
432	.171	.170	.116	.100	.074	.058	.054	.052	.050	.053
443	.167	.168	.110	.095	.071	.058	.053	.051	.049	.049
451	.162	.163	.109	.094	.068	.056	.051	.050	.048	.051
461	.162	.162	.109	.092	.067	.056	.051	.050	.048	.051
469	.159	.159	.105	.088	.062	.054	.048	.046	.047	.048
478	.156	.154	.101	.085	.063	.051	.046	.046	.044	.044
497	.157	.158	.104	.088	.064	.054	.049	.049	.048	.048
506	.163	.165	.111	.095	.074	.062	.059	.058	.057	.058
515	.175	.177	.126	.108	.084	.075	.070	.069	.068	.068
524	.178	.179	.128	.108	.087	.079	.071	.072	.069	.071
535	.178	.180	.129	.108	.090	.079	.075	.075	.074	.075
546	.187	.187	.138	.121	.100	.091	.087	.085	.084	.086
555	.196	.196	.147	.132	.110	.101	.096	.096	.096	.098

TABLE X (Continued)

Drop I-2

Depth (m)	5	42	76	143	300	480	990	1520	2410	3250
λ (nm)	Attenuation Coefficient $\alpha(m^{-1})$									
386	.155	.159	.159	.127	.081	.077	.063	.061	.060	.061
398	.148	.153	.153	.120	.077	.072	.058	.054	.053	.054
410	.143	.146	.146	.111	.071	.066	.054	.050	.047	.047
421	.139	.144	.142	.106	.067	.064	.052	.049	.045	.046
432	.134	.137	.137	.100	.061	.059	.048	.044	.041	.042
443	.132	.135	.135	.097	.059	.056	.046	.044	.040	.041
451	.129	.132	.134	.095	.057	.055	.045	.043	.040	.041
461	.129	.133	.132	.093	.056	.055	.046	.042	.040	.041
469	.127	.130	.128	.089	.054	.052	.044	.040	.038	.038
478	.124	.128	.126	.088	.053	.041	.043	.040	.037	.038
486	.122	.125	.125	.086	.052	.051	.041	.039	.035	.037
497	.130	.134	.134	.096	.061	.059	.049	.048	.043	.045
506	.142	.142	.142	.105	.071	.066	.059	.058	.053	.054
515	.147	-	-	-	-	-	-	-	-	-
524	.148	.150	.148	.112	.079	.078	.069	.067	.066	.065
535	.152	.154	.150	.113	.082	.081	.075	.071	.069	.068
546	.159	.161	.159	.124	.093	.092	.084	.082	.078	.080
555	.168	.172	.171	.134	.103	.101	.094	.093	.091	.092

TABLE X (Continued)

Drop I-3

Depth (m)	5	27	74	130	156	380	1090	2090	2650	2660
λ (nm)	Attenuation Coefficient $\alpha(m^{-1})$									
386	.162	.171	.185	.109	.139	.092	.070	.066	.060	.062
398	.152	.159	.171	.096	.131	.084	.063	.059	.053	.054
410	.148	.155	.164	.090	.124	.083	.059	.055	.047	.050
421	.141	.150	.158	.086	.116	.077	.056	.051	.044	.045
432	.138	.145	.153	.078	.110	.072	.052	.049	.040	.043
443	.136	.141	.148	.074	.105	.068	.050	.046	.039	.041
451	.136	.141	.147	.074	.100	.067	.049	.045	.039	.041
461	.133	.140	.143	.069	.099	.065	.047	.044	.038	.039
469	.131	.136	.140	.066	.095	.063	.045	.041	.036	.039
478	.129	.132	.138	.065	.091	.062	.044	.039	.034	.036
486	.127	.130	.136	.062	.088	.058	.043	.039	.032	.034
497	.133	.135	.140	.067	.091	.063	.048	.044	.038	.039
506	.140	.143	.146	.077	.100	.073	.057	.054	.047	.049
524	.148	.153	.155	.087	.111	.083	.068	.064	.059	.060
535	.150	.155	.156	.091	.114	.087	.073	.069	.063	.064
546	.157	.161	.165	.099	.124	.096	.083	.081	.073	.076
555	.168	.173	.175	.112	.135	.107	.096	.091	.087	.089

TABLE X (Continued)

Drop I-4

Depth (m)	6	30	50	120	225	310	370	440	527	548
λ (nm)	Attenuation Coefficient $\alpha(m^{-1})$									
386	.191	.195	.186	.113	.098	.094	.092	.100	.097	.103
398	.181	.187	.171	.104	.090	.089	.088	.094	.089	.099
410	.172	.178	.163	.097	.086	.082	.081	.089	.084	.092
421	.165	.173	.160	.091	.080	.080	.076	.084	.081	.089
432	.161	.169	.154	.087	.073	.076	.074	.081	.077	.085
443	.156	.164	.150	.083	.071	.071	.068	.078	.076	.081
451	.154	.161	.152	.082	.071	.069	.067	.077	.074	.081
461	.150	.158	.149	.081	.067	.069	.065	.077	.074	.079
469	.147	.154	.144	.077	.066	.066	.063	.074	.072	.076
478	.144	.150	.138	.076	.067	.063	.060	.072	.071	.073
486	.140	.146	.135	.073	.060	.060	.059	.068	.068	.069
497	.142	.149	.138	.077	.063	.064	.061	.073	.072	.073
506	.148	.155	.145	.086	.073	.074	.070	.081	.081	.081
515	.158	.162	.152	.093	.081	.083	.079	.087	.089	.090
535	.162	.167	.157	.099	.091	.090	.087	.095	.094	.098
546	.172	.178	.164	.108	.101	.100	.095	.104	.105	.106
555	.182	.188	.166	.119	.111	.110	.107	.116	.115	.119

TABLE X (Continued)

Drop I-5

Depth (m)	45	82	125	159	222	282	324	640	1025	1253
λ (nm)	Attenuation Coefficient $\alpha(m^{-1})$									
386	-	.240	.164	.157	.139	.143	.120	.119	.115	.142
398	.278	.229	.155	.144	.124	.136	.112	.109	.110	.133
410	.278	.218	.147	.138	.119	.133	.107	.105	.107	.129
421	.258	.207	.141	.134	.115	.126	.104	.101	.103	.125
432	.254	.201	.132	.127	.108	.121	.100	.096	.097	.119
443	.245	.193	.125	.123	.105	.118	.098	.096	.097	.116
451	.239	.184	.123	.119	.106	.117	.095	.094	.096	.118
461	.235	.181	.119	.116	.100	.114	.095	.095	.094	.114
469	.234	.176	.116	.115	.098	.112	.092	.092	.093	.111
478	.224	.171	.112	.112	.094	.110	.090	.090	.092	.112
486	.219	.165	.105	.108	.093	.105	.089	.086	.089	.108
497	.223	.173	.113	.114	.101	.111	.095	.095	.097	.114
515	.233	.191	.131	.129	.113	.131	.109	.109	.113	.131
524	.237	.192	.132	.132	.117	.131	.112	.114	.118	.134
535	.237	.193	.136	.137	.123	.134	.116	.116	.120	.142
546	.245	.203	.144	.145	.131	.146	.127	.127	.133	.150
555	.257	.212	.157	.157	.143	.160	.139	.139	.146	.159

TABLE X (Continued)

Drop I-6

Depth (m)	8	16	76	100	130	270	490	620
λ (nm)	Attenuation Coefficient $\alpha(m^{-1})$							
386	.260	.255	.194	.161	.151	.144	.147	.153
398	.240	.235	.182	.152	.142	.133	.136	.144
410	.232	.227	.172	.142	.134	.127	.129	.134
421	.224	.224	.164	.134	.127	.119	.124	.130
432	.220	.215	.155	.128	.122	.116	.118	.125
443	.214	.210	.152	.122	.114	.113	.115	.122
451	.212	.208	.147	.119	.111	.110	.113	.119
461	.211	.203	.144	.116	.108	.107	.112	.120
469	.207	.198	.140	.113	.102	.104	.109	.119
478	.203	.195	.139	.111	.100	.103	.107	.117
486	.201	.191	.135	.106	.098	.101	.106	.115
506	.222	.211	.153	.126	.118	.122	.125	.134
515	.226	.217	.157	.134	.127	.127	.133	.140
524	.229	.216	.160	.133	.127	.128	.135	.142
535	.235	.222	.164	.140	.133	.135	.141	.147
546	.244	.229	.176	.148	.142	.145	.149	.157
555	.255	.239	.185	.160	.153	.156	.160	.167

TABLE X (Continued)

Drop I-7

Depth (m)	17	90	155	530	730	950	1340	1700	1960	2270	2640
λ (nm)	Attenuation Coefficient $\alpha(m^{-1})$										
386	.298	.225	.186	.101	.104	.095	.105	.082	.105	.109	.093
398	.284	.213	.175	.094	.097	.089	.098	.075	.097	.102	.083
410	.274	.203	.165	.086	.090	.082	.090	.067	.091	.095	.076
421	.261	.195	.153	.082	.086	.078	.087	.063	.086	.090	.071
432	.254	.186	.146	.077	.081	.072	.082	.059	.081	.086	.065
443	.251	.181	.139	.072	.077	.071	.08	.057	.078	.081	.064
451	.243	.174	.134	.069	.075	.068	.078	.055	.075	.078	.061
461	.239	.169	.129	.067	.073	.065	.075	.052	.073	.076	.058
469	.235	.165	.124	.065	.068	.064	.073	.051	.072	.075	.056
478	.230	.159	.120	.062	.071	.062	.071	.051	.071	.074	.055
486	.224	.154	.114	.060	.065	.060	.067	.047	.068	.070	.051
497	.229	.160	.124	.068	.074	.066	.074	.055	.075	.078	.058
506	.237	.167	.131	.077	.084	.077	.085	.064	.085	.088	.069
515	.244	.173	.138	.085	.092	.085	.093	.073	.093	.097	.077
524	.245	.176	.140	.088	.092	.087	.095	.076	.093	.097	.079
535	.247	.177	.143	.092	.098	.091	.099	.080	.098	.101	.084
546	.256	.182	.148	.099	.105	.099	.107	.089	.106	.109	.092
555	.264	.189	.157	.110	.115	.110	.111	.094	.116	.119	.103

TABLE X (Continued)

Drop I-8

Depth (m)	5	20	54	82	100	190	668	1580	2300	2693
λ (nm)	Attenuation Coefficient $\alpha(m^{-1})$									
386	.181	.161	.329	.150	.122	.101	.069	.064	.059	.077
398	.173	.155	.315	.145	.115	.095	.064	.059	.053	.066
410	.165	.146	.303	.135	.107	.089	.055	.050	.050	.060
421	.162	.140	.288	.125	.100	.080	.052	.046	.042	.056
432	.159	.129	.277	.119	.092	.074	.047	.043	.038	.053
443	.152	.128	.269	.112	.088	.072	.044	.041	.035	.048
451	.151	.126	.261	.107	.083	.070	.043	.039	.035	.045
461	.148	.120	.256	.103	.078	.065	.042	.037	.034	.042
469	.145	.118	.248	.097	.074	.062	.040	.034	.030	.040
478	.145	.116	.244	.095	.071	.060	.040	.036	.030	.039
497	.153	.126	.257	.098	.077	.065	.048	.041	.036	.042
506	.158	.132	.262	.106	.084	.072	.053	.048	.044	.055
515	.160	.132	.266	.114	.089	.080	.060	.056	.052	.060
524	.163	.142	.264	.114	.095	.083	.065	.060	.054	.064
535	.165	.138	.265	.117	.094	.086	.069	.065	.056	.072
546	.172	.145	.271	.126	.102	.095	.078	.074	.066	.078
555	.184	.152	.280	.134	.111	.104	.086	.083	.077	.090

TABLE X (Continued)

Drop I-9

Depth (m)	5	70	121	283	1924	2673
λ (nm)	Attenuation Coefficient $\alpha(m^{-1})$					
386	.425	.172	.146	.090	.058	.074
398	.410	.164	.140	.084	.050	.066
410	.396	.154	.130	.078	.043	.058
421	.387	.143	.123	.075	.041	.054
432	.380	.135	.115	.070	.036	.050
443	.373	.132	.108	.066	.035	.048
451	.370	.126	.105	.062	.033	.046
461	.366	.122	.100	.058	.031	.043
469	.360	.117	.097	.056	.030	.041
478	.357	.116	.092	.055	.030	.040
486	.356	.112	.089	.054	.028	.039
497	.362	.118	.097	.060	.034	.044
506	.363	.126	.105	.069	.041	.054
524	.370	.130	.108	.076	.050	.060
535	.370	.134	.112	.079	.052	.064
546	.379	.144	.120	.087	.065	.074
555	.391	.156	.130	.100	.076	.086

TABLE X (Continued)

Drop I-10

Depth (m)	3	23	42	60	99	190	911	1498	2278	2602
λ (nm)	Attenuation Coefficient $\alpha(m^{-1})$									
386	.352	.244	.185	.244	.118	.084	.064	.058	.064	.068
398	.340	.231	.172	.237	.112	.078	.057	.052	.054	.060
410	.330	.222	.160	.220	.105	.071	.052	.047	.048	.054
421	.322	.214	.151	.209	.096	.066	.048	.043	.044	.050
432	.317	.206	.144	.200	.092	.062	.045	.040	.040	.046
443	.311	.200	.135	.191	.083	.055	.042	.036	.040	.042
451	.309	.200	.133	.186	.081	.055	.040	.036	.037	.042
461	.306	.196	.129	.180	.077	.052	.040	.035	.035	.040
469	.303	.192	.123	.176	.075	.049	.034	.033	.034	.040
478	.298	.186	.117	.168	.070	.045	.034	.030	.030	.036
486	.296	.190	.115	.169	.070	.045	.033	.030	.030	.034
497	.301	.193	.122	.177	.077	.050	.041	.037	.035	.042
506	.305	.200	.128	.181	.083	.058	.048	.044	.043	.048
524	.308	.200	.139	.190	.089	.066	.056	.052	.053	056
535	.310	.203	.142	.194	.092	.071	.062	.058	.058	.064
546	.321	.210	.148	.200	.102	.080	.071	.066	.068	.071
555	.336	.220	.157	.209	.111	.090	.083	.078	.077	.083

TABLE X (Continued)

Drop I-11

Depth (m)	3	9	15	51	110	166	381	497	578
λ (nm)	Attenuation Coefficient $\alpha(m^{-1})$								
386	-	-	.457	.182	.194	.160	.099	.210	.238
398	.472	.460	.442	.172	.188	.151	.092	.204	.230
410	.464	.452	.431	.164	.178	.142	.089	.200	.224
421	.450	.438	.420	.156	.166	.134	.080	.192	.216
432	-	.424	.411	.148	.158	.126	.076	.189	.204
443	-	.414	.405	.145	.151	.122	.072	.183	.198
451	.424	.410	.399	.139	.145	.114	.069	.177	.190
461	.419	.406	.393	.134	.142	.111	.065	.172	.186
469	.412	.398	.385	.129	.136	.105	.060	.167	.178
478	.406	.397	.380	.126	.132	.103	.060	.163	.176
486	.404	.394	.376	.122	.126	.100	.057	.157	.176
497	.407	.402	.383	.129	.130	.105	.065	.160	.180
506	.412	.408	.387	.135	.139	.111	.072	.168	.185
524	.423	.419	.394	.140	.144	.118	.082	.171	.188
535	.422	.419	.393	.144	.147	.122	.085	.171	.190
546	.421	.424	.394	.150	.150	.129	.094	.174	.194
555	.428	.431	.403	.158	.162	.139	.105	.190	.206

TABLE X (Continued)

Drop I-12

Depth (m)	86	192	293	480	586	673
λ (nm)	Attenuation Coefficient α (m^{-1})					
386	.122	.103	.111	.088	.130	.151
398	.115	.095	.106	.081	.121	.143
410	.109	.089	.100	.075	.117	.137
421	.104	.084	.095	.072	.110	.130
432	.096	.079	.087	.065	.103	.126
443	.091	.076	.086	.062	.101	.122
451	.091	.073	.084	.061	.099	.119
461	.088	.071	.083	.056	.095	.114
469	.083	.066	.076	.055	.092	.110
478	.078	.062	.071	.050	.088	.106
486	.076	.058	.069	.047	.085	.104
497	.083	.066	.074	.054	.090	.111
506	.090	.076	.083	.064	.099	.118
524	.095	.080	.090	.070	.106	.126
535	.099	.085	.094	.074	.110	.128
546	.112	.095	.106	.086	.122	.140
555	.123	.110	.117	.097	.134	.151

TABLE X (Continued)

Drop I-13

Depth (m)	150	270	360	400	700	1200	1342	1456	1550
λ (nm)	Attenuation Coefficient $\alpha(m^{-1})$								
386	.117	.129	.111	.128	.092	.095	.135	.100	.110
398	.108	.118	.102	.119	.084	.088	.128	.090	.099
410	.104	.112	.095	.114	.078	.083	.120	.086	.095
421	.095	.109	.090	.110	.075	.079	.117	.082	.086
432	.092	.104	.086	.105	.070	.077	.112	.077	.083
443	.086	.097	.083	.100	.065	.070	.108	.075	.077
451	.084	.095	.083	.100	.066	.071	.106	.072	.078
461	.080	.090	.077	.095	.064	.065	.106	.070	.076
469	.077	.089	.078	.093	.060	.063	.100	.068	.074
478	.074	.087	.075	.089	.055	.060	.096	.065	.070
486	.073	.083	.072	.086	.054	.057	.095	.062	.068
497	.078	.092	.077	.092	.060	.065	.104	.070	.074
506	.088	.099	.084	.099	.070	.074	.112	.077	.082
524	.093	.110	.095	.108	.080	.083	.120	.088	.099
535	.099	.114	.097	.112	.086	.089	.124	.092	.099
546	.108	.118	.105	.124	.095	.097	.132	.100	.108
555	.120	.129	.115	.130	.105	.108	.145	.112	.118

where attenuation has moderated. The deeper waters at 1200 meters and 1456 meters are relatively clear with a minimum attenuation of about 0.06 m^{-1} at the 485 nm wavelength. Mediterranean water intrudes into this region of clear water at a depth of 1342 meters. Although the level of the attenuation spectrum from the Mediterranean water is substantially higher than those of the adjacent Atlantic water, the spectral signatures are remarkedly very similar.

A comparison of the spectra recorded within 10 meters of the surface along the length of the track within the Mediterranean is presented in Figure 40. The major difference between spectra is in the amplitude of the signature which generally increases as we proceed west towards the Atlantic. There is some variation in spectral shape; the consistent change being the proportionally larger increase in attenuation in the shorter wavelength interval as the overall level of the spectra increase. Inconsistencies which arise with this general scheme are the transposition of the spectra of drops I-9 and I-10 and the rather high relative short wavelength attenuation of drop I-8. Perhaps local conditions, such as major weather changes which affect vertical mixing of surface layers are responsible for upsetting the general trends of these optical data.

VIII SUMMARY

Substantial data has been collected from diverse ocean areas under a variety of climatic and seasonal conditions from seven of the nine DOOM measurement cruises. Except for the final cruise in the Mediterranean Sea, all measurements were conducted in the North American basin and the adjacent waters of its coastal margin, the Caribbean Sea, and the Gulf of Mexico. Stations are shown in Figure 41.

The North Atlantic is traversed by the warm waters of the Gulf Stream which enter through the Strait of Florida, run northeastwardly along the coast to a position off the Virginia Capes, and then veer eastward toward Europe. The Gulf Stream separates the sub-tropical waters of the Sargasso Sea to the southeast from the cooler temperate waters of coastal North America to the Northwest. Ocean areas both to the north and south as well as in the Stream proper were sampled during several of the DOOM measurement cruises. Stations were located at various positions in the Gulf Stream opposite the Mid-Atlantic states in Cruises B, E, and H and in the strait east of the Florida coast in Cruise D. Measurements north of the Stream were confined to Cruises B and H and those in the Sargasso Sea to Cruises B, E, and H. Tropical waters were sampled during Cruise D in the Bahamas, Cruise F in the trench area north of Puerto Rico, and in Cruise G to the Caribbean south of Cuba. Coastal measurements were made in Cruises D and E off the coasts of Florida and Virginia respectively. The Mediterranean Sea cruise, I, included stations in both the eastern and western basins as well as stations at both the Atlantic and Mediterranean sides of the Strait of Gibraltar.

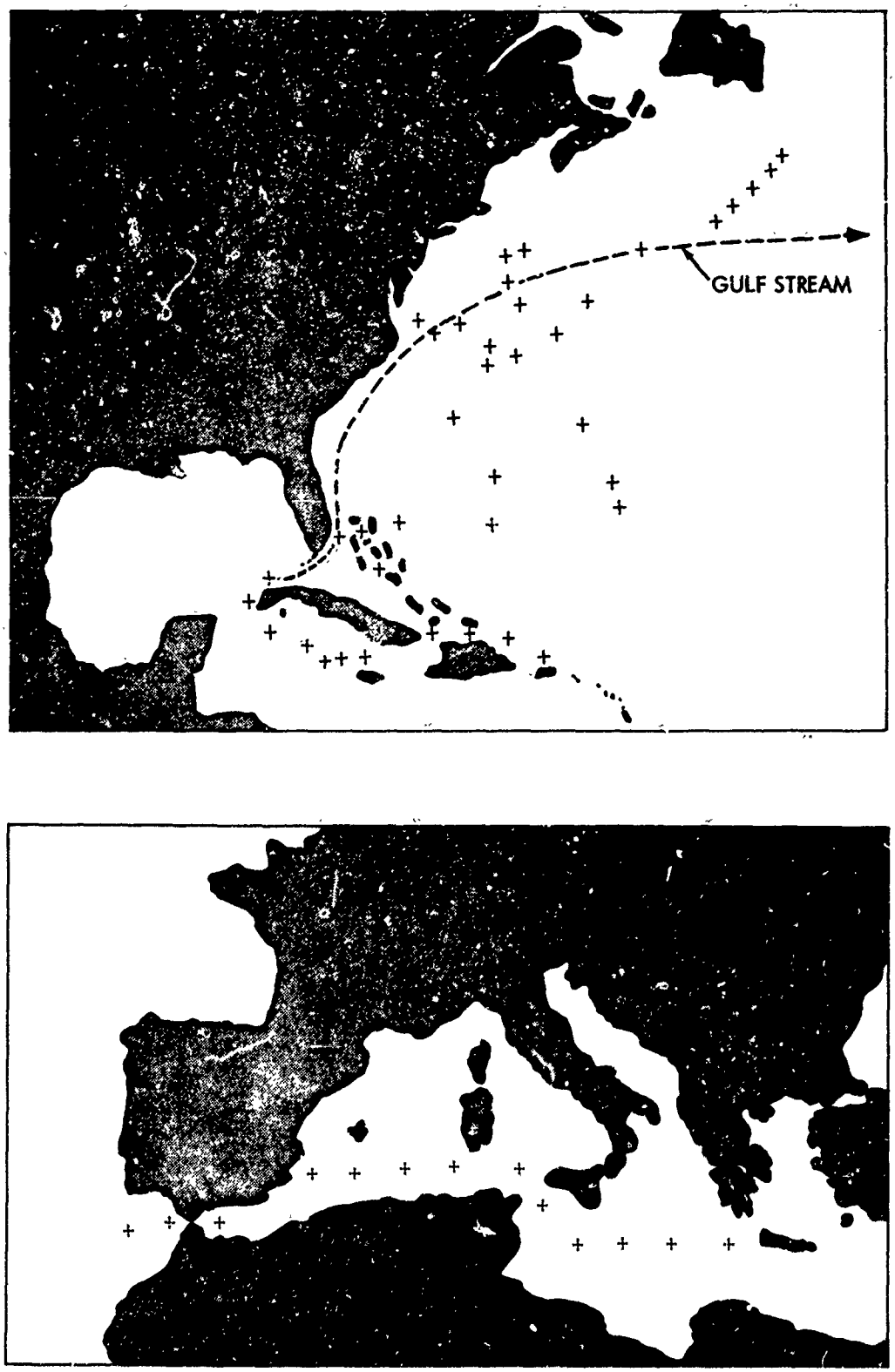

FIG. 41 DOOM STATIONS IN THE NORTHWESTERN ATLANTIC OCEAN AND MEDITERRANEAN SEA.

Optical parameters obviously vary with geographical location and water type, but they also change characteristically as a function of depth. In general, DOOM measurements were made at all depths from surface to bottom, so that the behavior of the attenuation profile at every point within the water column was identified.

The water column may be divided into three regions, the surface, intermediate, and bottom waters, each of which has particular optical features. Surface waters are characterized by relatively high attenuation due to primary production of living matter, principally the phytoplankton, within the euphotic zone. Attenuation is moderately uniform in the isothermal surface layer but then decreases rapidly at the primary thermocline. Near the top of the thermocline there is frequently a nepheloid layer which produces a peak in the attenuation profiles. Similarly changes or irregularities in the thermal structure will generally produce corresponding changes in attenuation. Below the thermocline is a water layer of high clarity which produces a minimum in the profile between 200 and 800 meters. Below this layer there is a slight increase in attenuation which produces a weak but rather broad maximum at around 1000 meters and nominally corresponds to the base of the secondary thermocline. Surface water features are well illustrated in the Cruise B data.

The intermediate water which lies just below the surface layers may extend downward for thousands of meters to the proximity of the bottom. It is characterized by nearly uniform optical properties and very low attenuation. In the absence of bottom currents this clear intermediate water does extend to the ocean floor. Deep currents tend to agitate bottom sediments and lead to turbidity layers formed by lateral transport of suspended particulate matter. The magnitude of this effect will depend on bottom topography and the nature of the currents and may range from a very minor rise in attenuation just a few meters off bottom to a several fold increase with major turbidity layers extending upward hundreds of meters.

Although there are common features within most deep ocean attenuation profiles, characteristics do vary greatly in both shape and magnitude due to the different oceanographic and meteorological conditions prevailing in various geographical ocean areas. Two profiles from different areas within the North American basin are compared in Figure 42. Station E-5 was located within the optically clear, sub-tropical waters of the Sargasso Sea while drop H-8 was in temperate waters at the northern extremity of the deep basin just south of the continental rise to the Grand Banks of Newfoundland. The waters at station E-5 were perhaps the clearest sampled in the DOOM program. The surface α of 0.08 m^{-1} is slightly lower than the typical α of 0.10 to 0.14 m^{-1} which is normal for sub-tropical latitudes. Similarly an α of 0.03 m^{-1} in the intermediate water column is on the low side of the nominal range from 0.03 to 0.05 m^{-1}. At the northern station H-8 surface α's fell beyond the dynamic range of the instrument which was in excess of 0.40 m^{-1} and α in the clear intermediate water dropped to a minimum value of only 0.08 m^{-1}.

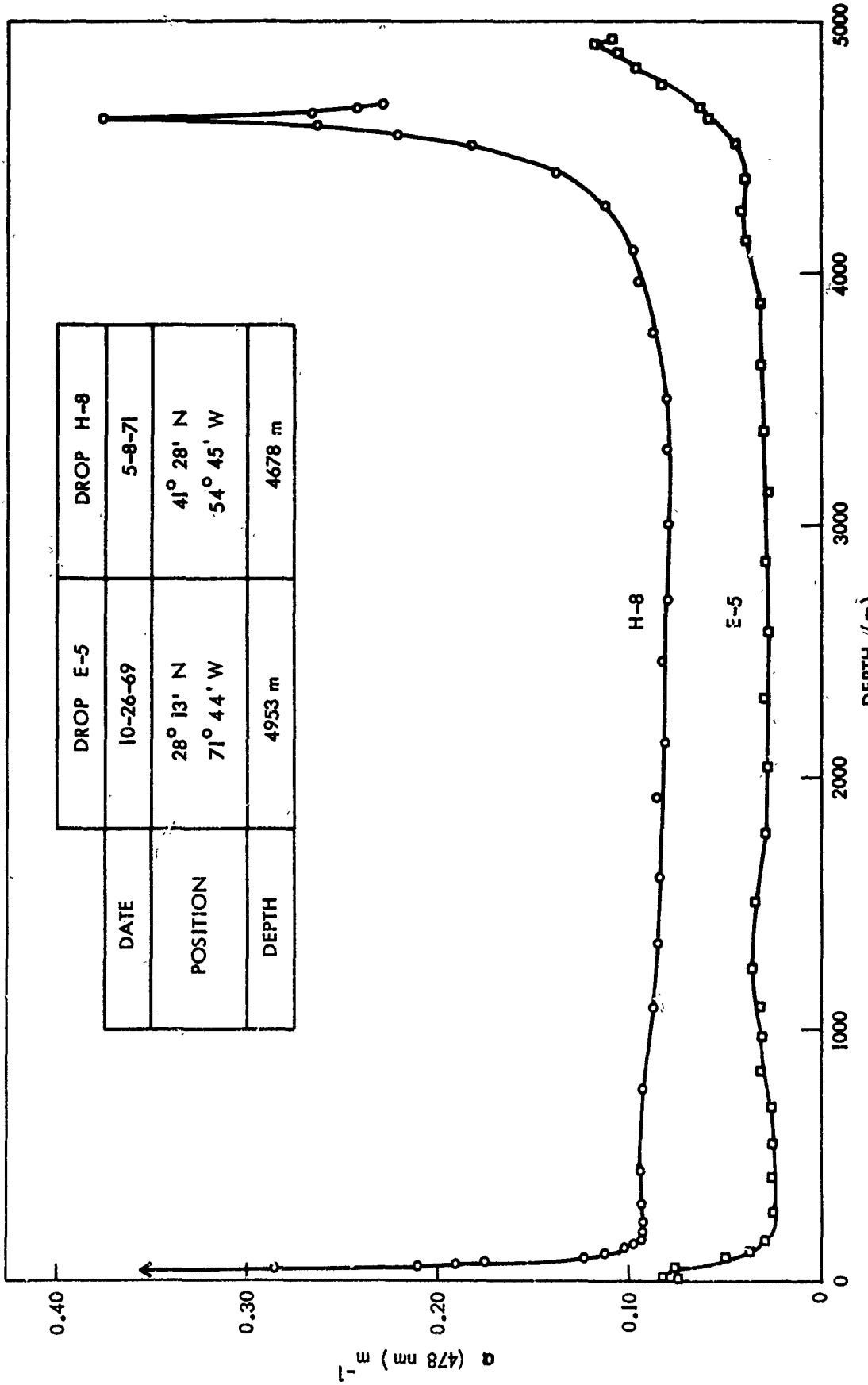

FIG. 42 COMPARATIVE ATTENUATION PROFILES FROM NORTHERN AND SOUTHERN LATITUDES WITHIN THE NORTH AMERICAN BASIN.

Attenuation in the surface layers at this northern station then is over four times that found in the Sargasso Sea and at intermediate depths is about twice that found in southern latitudes. In both profiles there is about a four fold increase in turbidity of the bottom waters above those of the intermediate water which begins some 1000 meters above the basin floor. In both cases maximum attenuation in the deep waters is not found adjacent to the bottom but in a layer slightly above the floor which in drops H-8 and E-5 are respectively about 70 and 20 meters off the bottom. This structured increase in turbidity is characteristic of the bottom waters of the North American basin and is attributed to lateral transport by deep ocean currents of suspended sediments from adjacent topographical heights.

Separating the different water types of the Sargasso Sea and the temperate North Atlantic are the dynamic waters of the Gulf Stream. East of Cape Hatteras the Stream is characterized by multiple currents and countercurrents, eddies, meanders, and lateral offshoots and influxes of adjacent waters which lead to a highly layered vertical water structure. Resulting optical profiles reflect this complexity and consist of a continuously changing structure of maxima and minima which generally can be correlated with gradients in temperature. This Gulf Stream phenomenon is well illustrated in Figures 4 and 5 from Cruise B.

In the semitropical waters of the Bahamas and the Caribbean Sea where primary production is relatively low, attenuation characteristics of the surface and intermediate layers are similar to those of the Sargasso Sea. Surface α, including the usually minor turbidity peaks, normally ranges from 0.10 to 0.15 m^{-1}. In the clear intermediate water α's fall between 0.04 and 0.06 m^{-1}. In many areas of the Bahamas and Caribbean, this intermediate water extends to or very nearly to the bottom. Exceptions are found in restricted channels such as the Yucatan and Florida Straits where deep currents produce an increase in levels of turbidity near the bottom.

Attenuation is generally high in coastal areas due to runoff of nutrients and particulate material from the land mass and from tidal disturbances in the shallows along the shore. An example of the coastal influence is illustrated in Figure 43 from Cruise E at a station just south of the Virginia Capes. Attenuation is fairly constant over the 28.5 meter depth and is perhaps two to three times higher than the adjacent "blue water" in the Atlantic.

The Mediterranean Sea is a nearly confined body of water in a warm arid climate where evaporation exceeds runoff so that replenishment is supplied from the surface waters of the Atlantic through the Strait of Gibraltar. Consequently physical properties, such as salinity and thermal profiles, differ substantially from those in the Atlantic. Surface water attenuation generally increased with proximity to Gibraltar. In the eastern Mediterranean basin surface α's ranged from 0.12 to 0.16 m^{-1} which is only slightly higher than in the subtropical Atlantic. In the western basin the more

complicated physical structure of the surface water leads to values of α from 0.15 to 0.30 m^{-1} and peaks in the large gradients in excess of 0.40 m^{-1}. Immediately east of Gibraltar in the Alboran Sea a surface α of 0.40 m^{-1} was recorded which is comparable to those of the North Atlantic. Intermediate waters within both the eastern and western basins generally extend to the bottom and their clarity, α from 0.03 to 0.05 m^{-1}, is comparable to the sub-tropical Atlantic. In the restricted waters of the Strait of Sicily where the two basins are separated by a shallow sill, interchange of water takes place at various depths which results in a structured water column of generally high attenuation. Minimum α's across the sill were about 0.10 m^{-1}.

There were two locales in the DOOM program where turbidity layers intruded into the clear intermediate water column. In the eastern Atlantic west of Gibraltar, the outflow of Mediterranean water mixes with the Atlantic in a unique fashion. This dense highly saline water spills across the sill, flows down the continental slope until it finds water of the same density, and then spreads laterally through the Atlantic. Since it has scoured the bottom in search of its predetermined depth, this layer has accumulated particulate material and hence is of higher turbidity then the intermediate Atlantic waters into which it intrudes. This Mediterranean water is clearly delineated as the bottom layer in Figure 34 and in Figure 35 as the turbidity layer centered slightly below 1300 meters.

The second case of a high turbidity layer at intermediate depths was over the Puerto Rico trench and is illustrated in Figures 13, 14, and 15 as the peak at around 5000 meters. This layer is attributed to lateral transport of high turbidity bottom water from the adjacent North American basin south over the area of the deep submarine trench.

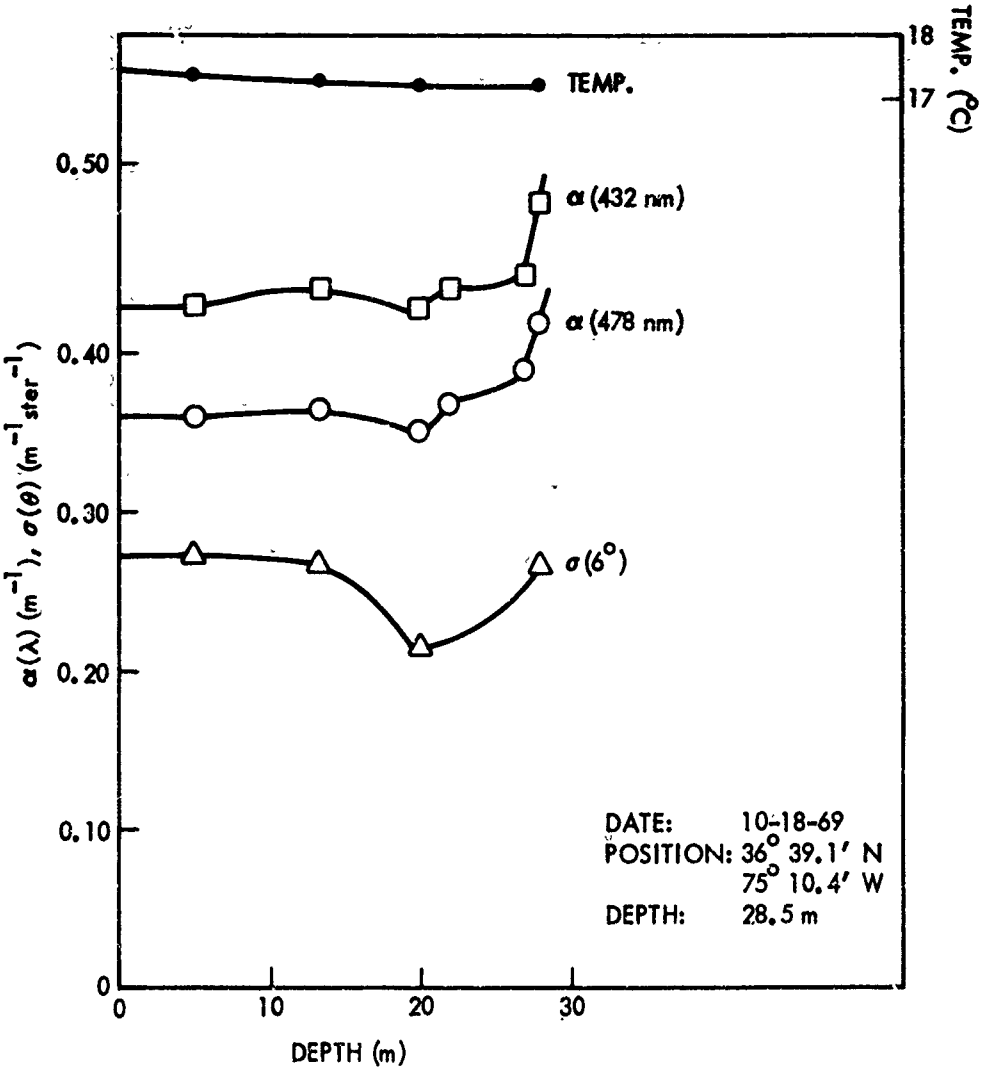

FIG. 43 OPTICAL ATTENUATION AND TEMPERATURE PROFILES OF COASTAL DROP E-1.

REFERENCES

1. Donald E. Matlack, "The Deep Ocean Optical Measurement (DOOM) Program," NOLTR 70-165, 18 January 1971.

2. Donald E. Matlack, "Deep Ocean Optical Measurement (DOOM) Report; Bahama Channels and Northwestern Atlantic Ocean," NOLTR 72-284, 20 November 1972.

3. Donald E. Matlack, "Deep Ocean Optical Measurement Program (DOOM)," Ocean'72, IEEE International Conference on Engineering in the Ocean Environment, September 1972.

APPENDIX A

Cruise G results are presented in abbreviated form in this appendix in order to expedite release of optical attenuation data which is somewhat reduced in quantity due to a variety of operational problems encountered during the cruise. Failure of oceanographic equipment as well as marginal operation of some DOOM subsystems combined with logistic problems to restrict the meaningful data collected. Data in this appendix will consist of optical attenuation profiles as a function depth.

The cruise schedule specified departure from Montego Bay, Jamaica, aboard the USNS LYNCH on 6 February 1971, operations to the Northwest over the Cayman trough until 11 February, and then a succession of daily stations while en route around the western end of Cuba to port at Key West, Florida, on 17 February. An on-schedule departure from Jamaica permitted an initial drop in deep water north of Montego Bay on the evening of 6 February. Pinger flooding aborted the attempt at placing the DOOM package near the bottom. Subsequent failure of back-up pingers during the next two drops again restricted depths of the casts and prompted a message to the Oceanographic Office in Washington requesting that functional on-the-shelf replacement units be air freighted to the island of Grand Cayman which lay along our track about two days hence. Upon receiving confirmation of the shipment, we steamed into port at Georgetown, Grand Cayman, on 10 February to pick up the pingers. The shipment was not at the airport nor did it arrive on the following day. In the meantime an ancient pinger of only moderate signal strength had been found in a storage hold and, with minor repairs, could be pressed into service. Since depth along the remainder of the track was not great, we decided to take a chance on the repaired pinger and set sail on the evening of 11 February. Five additional drops were completed en route to Key West, all of which were successfully placed near the bottom. The Cruise G track is presented in Figure A-1 and pertinent data on the nine stations are presented in Table A-I.

In addition to the pinger problems, difficulty was also experienced with the electrical cable between the instrument sphere and the pressure-temperature sensor. Opens developed intermittently in the electrical conductors which resulted in loss of the temperature and pressure signals. Temperature profiles are consequently restricted to XBT data which is useful to depths of only about 750 meters. Package depth determination in the shallow, pingerless casts is based solely on the length of wire played out. Package depths of the last five drops are calculated from combined data continuously recorded from the fathometer measurements, the received pinger traces, and the record of the length of wire out. This same electrical cable also contains a conductor to an external switch which permits activation of the system from outside the pressure sphere. An open developed in this conductor during drop G-6 as the package passed 335 meters which shut down the system for the rest of the cast.

TABLE A-1 PERTINENT DATA ON CRUISE G STATIONS

Station	Date	Time	Latitude North	Longitude West	Depth (m)	Package Depth (m)
G-1	2-6-71	2035	19° 07'	78° 05'	5230	4300
G-2	2-7-71	1952	19° 07'	79° 02'	6126	5280
G-3	2-8-71	1856	19° 08'	79° 46'	6490	790
G-4	2-9-71	1933	18° 43'	80° 35'	5190	850
G-5	2-12-71	2011	19° 30'	82° 34'	3070	3070
G-6	2-13-71	1926	20° 30'	84° 00'	4398	335
G-7	2-14-71	1957	21° 25'	85° 55'	1975	1974
G-8	2-15-71	1959	22° 48'	85° 16'	2118	2116
G-9	2-16-71	2003	23° 10'	84° 21'	2487	2484

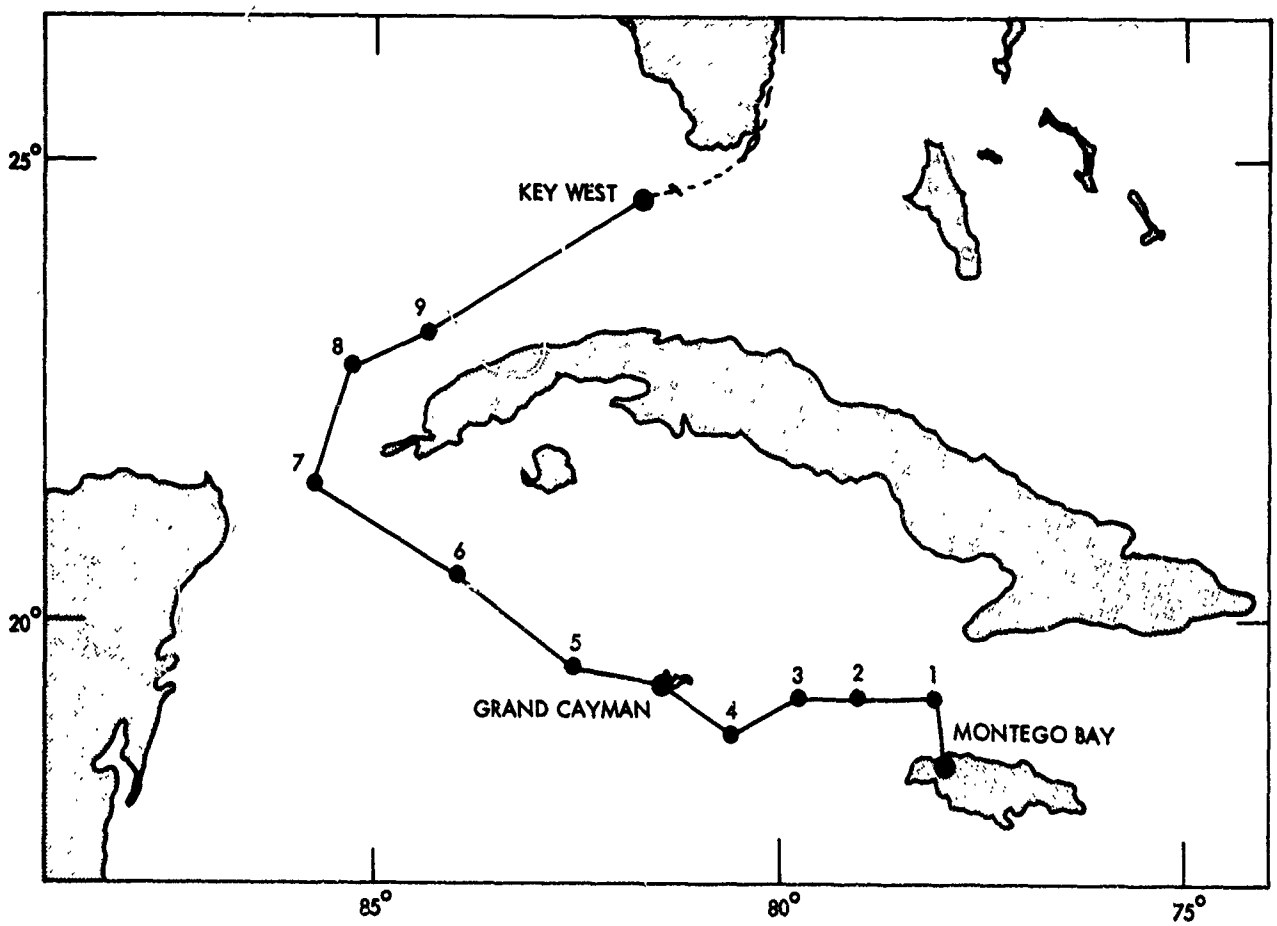

FIG. A-1 TRACK CHART OF CRUISE G

Satisfactory spectral attenuation data was recorded in all cases and in drops G-5, G-7, G-8, and G-9 measurement was successful to the very bottom. This data is presented for each drop as a profile of the attenuation coefficient α at a wavelength in the transmission window of 478 nanometers. Temperature profiles, derived from the XBT casts, are included. Operation of the scattering measurement section was marginal during the entire cruise, and it is not considered worthwhile to process the meager scattering data which was recorded.

Attenuation profiles, presented in Figures A-2 through A-10, are characteristic of those found in tropical Caribbean waters. In the isothermal surface layer attenuation is moderate, generally ranging between 0.10 and 0.12 m^{-1}, but then decreases rapidly at the thermocline to a minimum from 0.04 to 0.05 m^{-1} between 200 and 500 meters depth. The profile then climbs slightly forming a broad maximum between 600 and 1000 meters depth which corresponds nominally with the base of the primary thermocline. Attenuation then drops slowly and levels off close to 0.04 m^{-1} at around 2000 meters. In some cases, as in drop G-1, Figure A-2, there are large turbidity spikes associated with nepheloid layers in the surface waters. Levels of attenuation tended to increase slightly as we proceeded north from the Cayman basin through the Yucatan Straits to the stations northwest of Cuba. Surface α's rose to between 0.12 and 0.15 m^{-1} and deep water values dropped to only about 0.05 m^{-1}. The appreciable increase in α when approaching the bottom at depths below 1800 meters in drops G-7, G-8, and G-9 suggests a deep current flowing north through the strait into the Mexico basin.

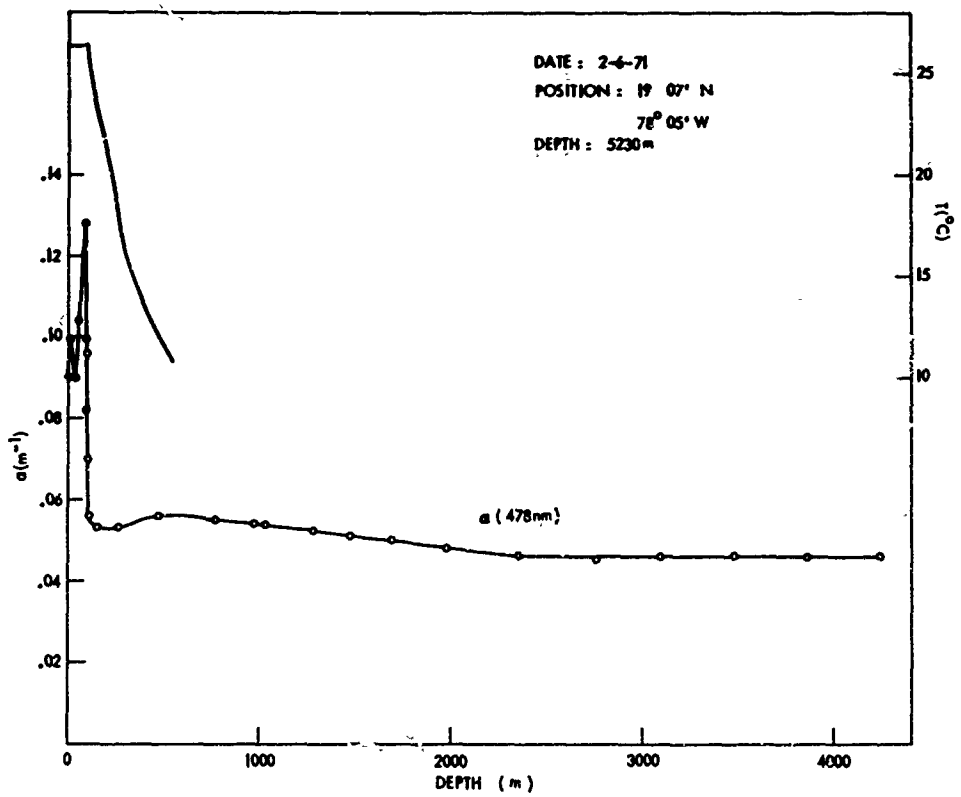

FIG. A-2 OPTICAL ATTENUATION AND TEMPERATURE PROFILES OF DROP G-1.

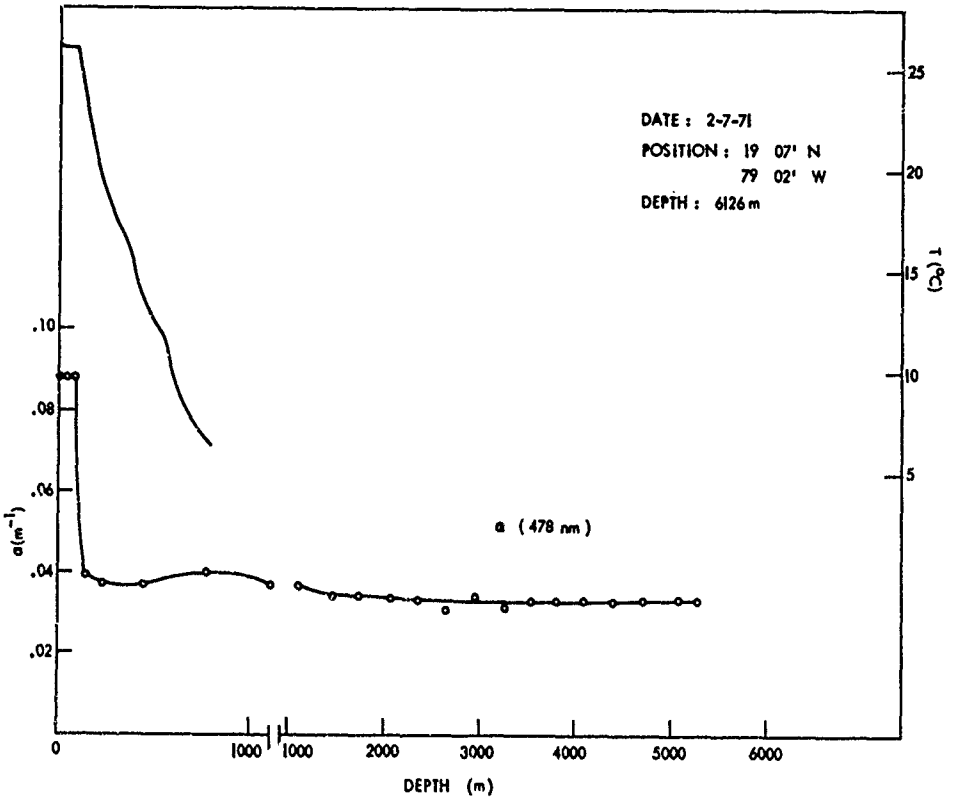

FIG. A-3 OPTICAL ATTENUATION AND TEMPERATURE PROFILES OF DROP G-2.

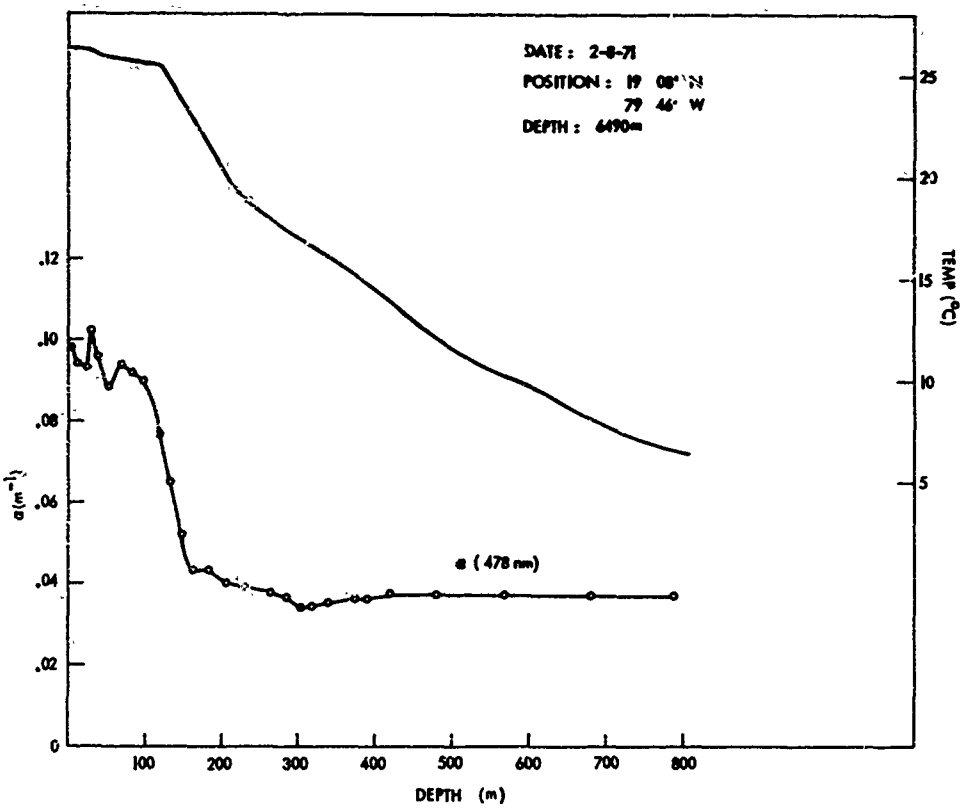

FIG. A-4 OPTICAL ATTENUATION AND TEMPERATURE PROFILES OF DROP G-3.

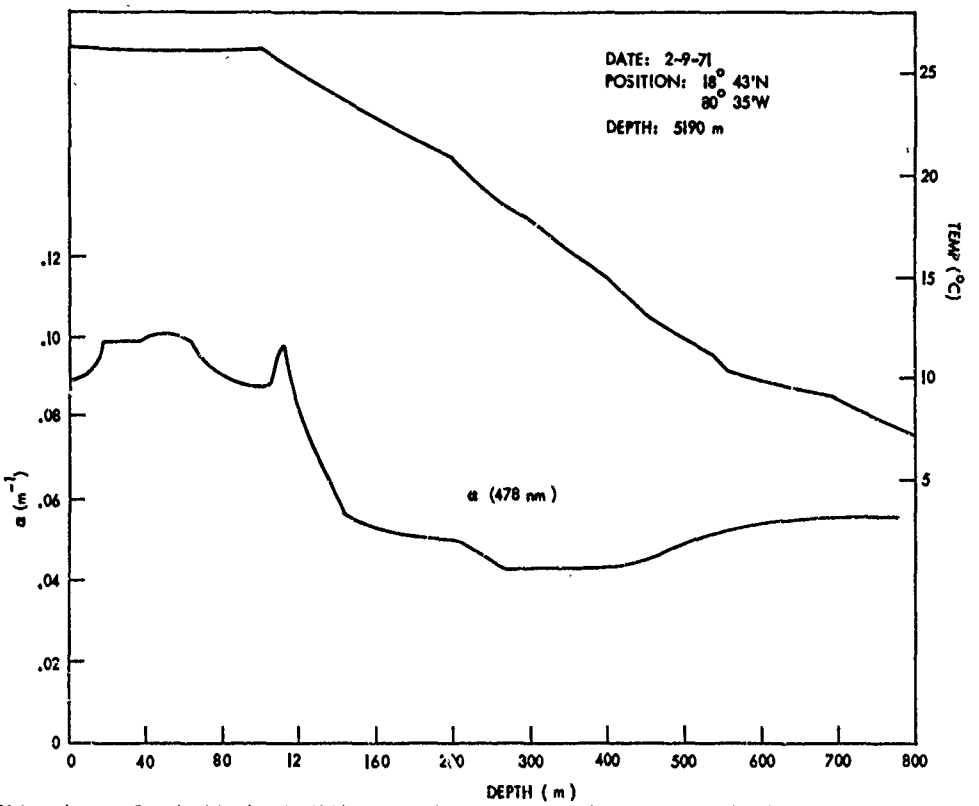

FIG. A-5 OPTICAL ATTENUATION AND TEMPERATURE PROFILES OF DROP G-4.

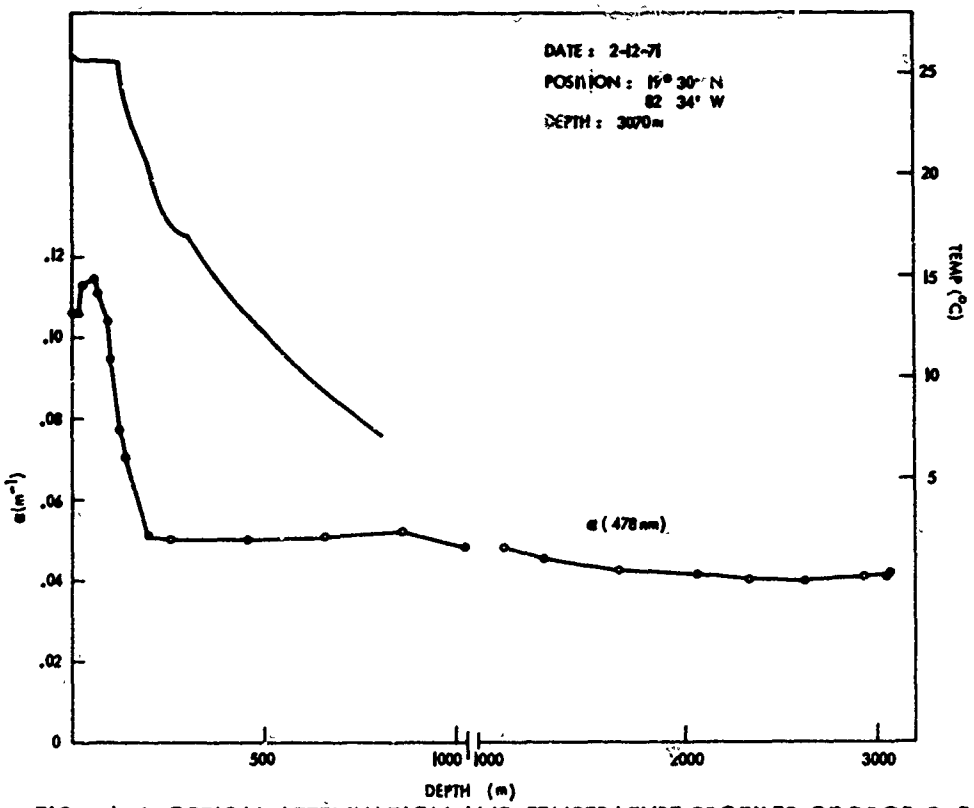

FIG. A-6 OPTICAL ATTENUATION AND TEMPERATURE PROFILES OF DROP G-5

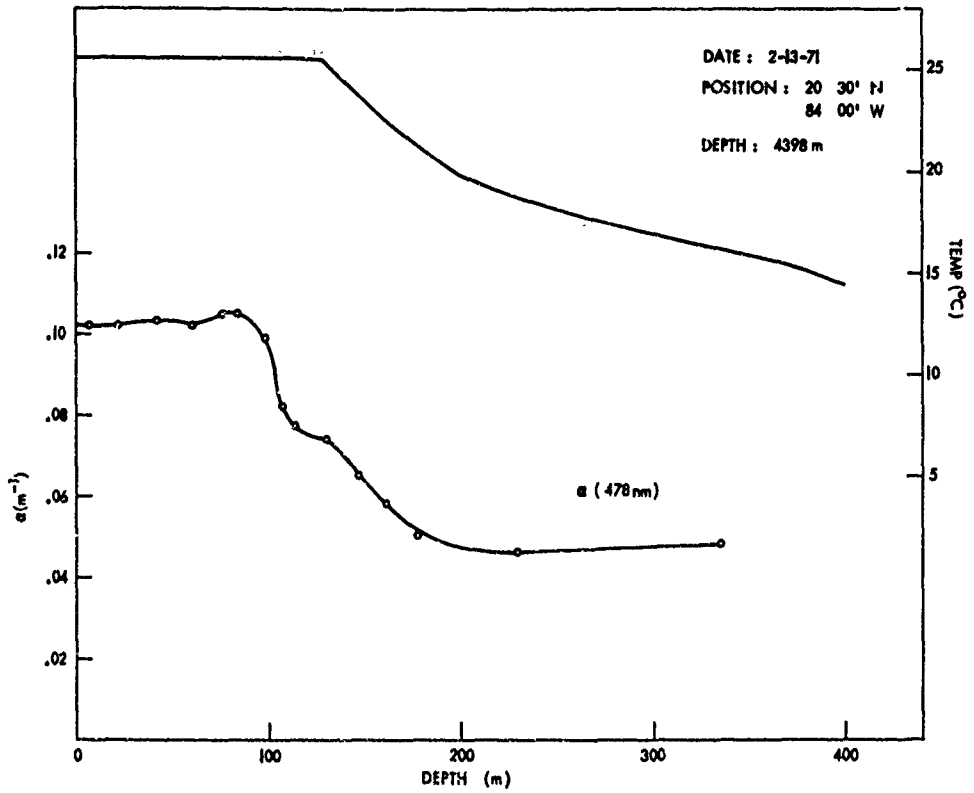

FIG. A-7 OPTICAL ATTENUATION AND TEMPERATURE PROFILES OF DROP G-6

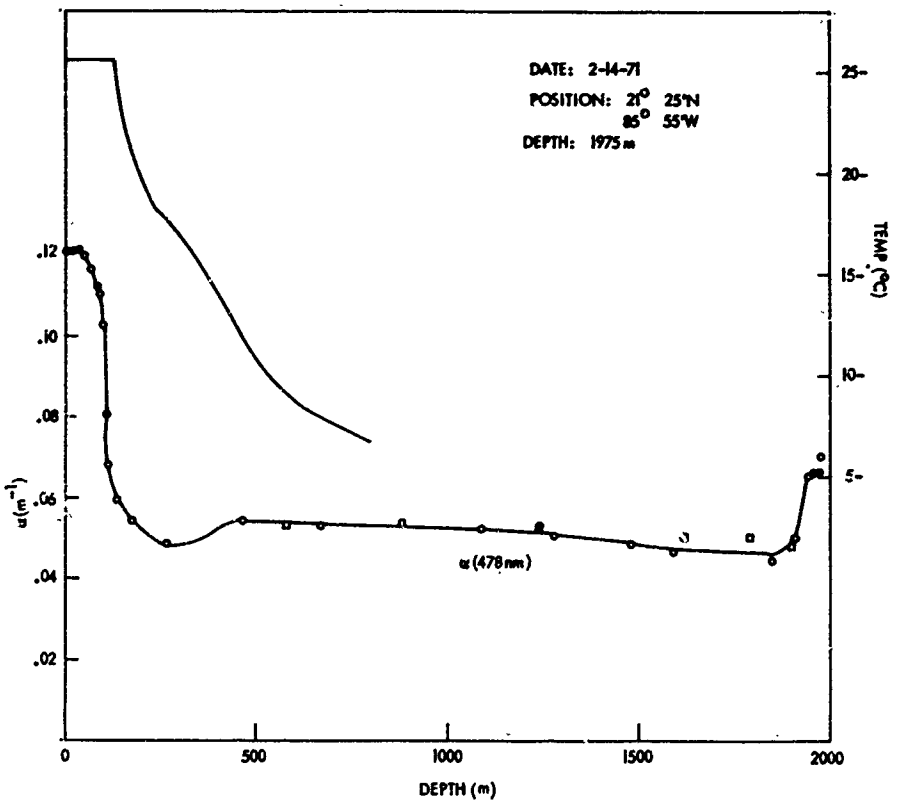

FIG. A-8 OPTICAL ATTENUATION AND TEMPERATURE PROFILES OF DROP G-7.

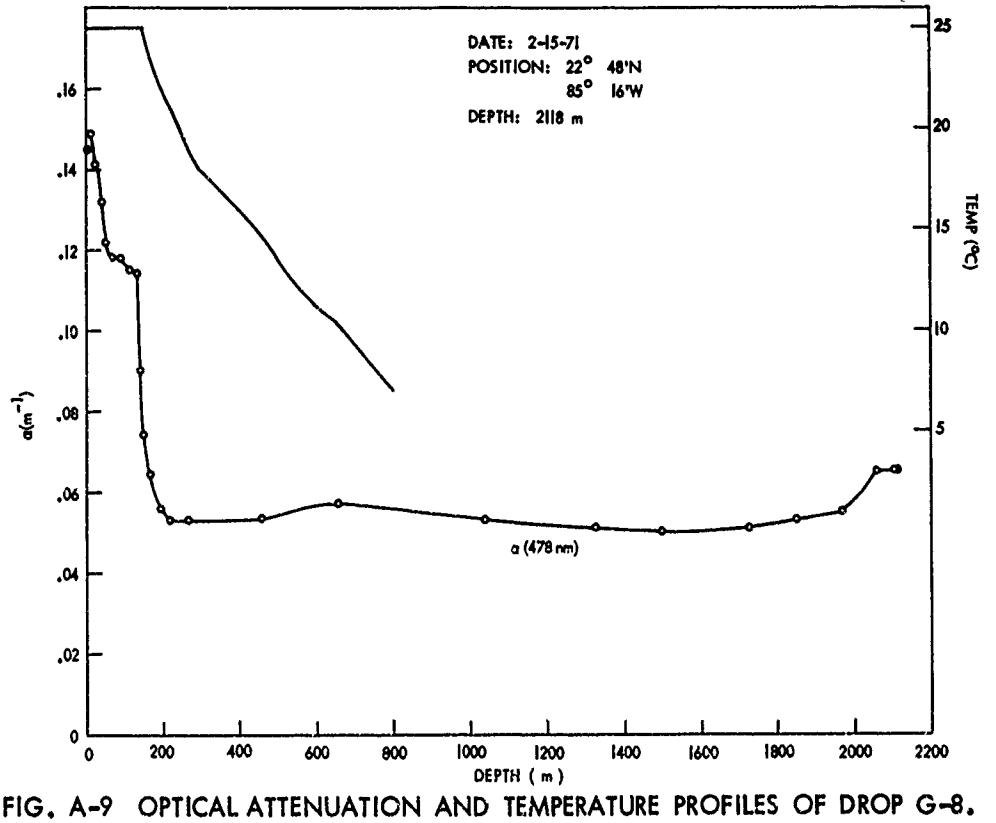

FIG. A-9 OPTICAL ATTENUATION AND TEMPERATURE PROFILES OF DROP G-8.

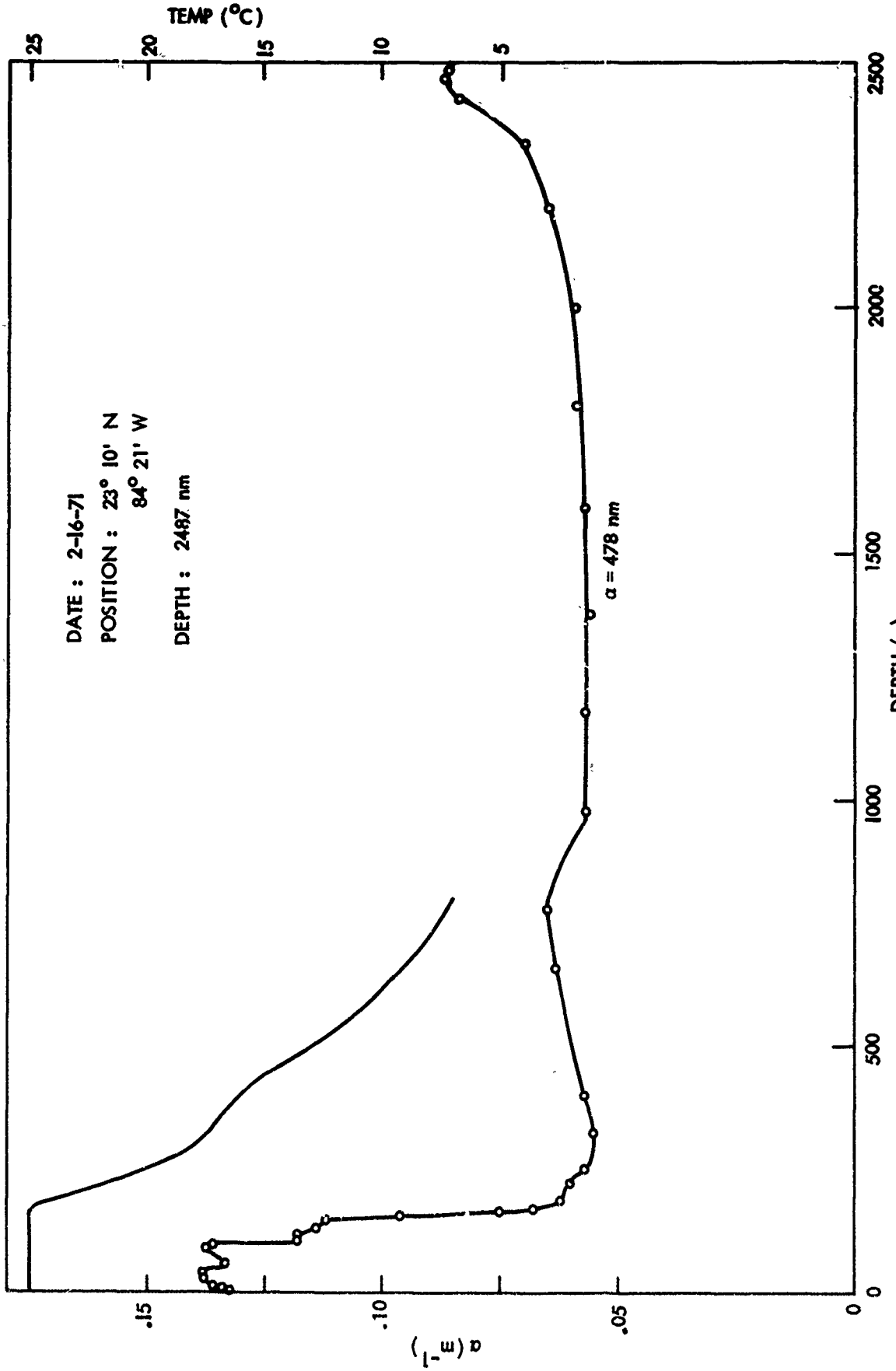

FIG. A-10 OPTICAL ATTENUATION AND TEMPERATURE PROFILES OF DROP 3-9.